

**NASA CONTRACTOR
REPORT**



NASA CR-2427

NASA CR-2427

**CASE FILE
COPY**

**UPPER-SURFACE BLOWING NACELLE
DESIGN STUDY FOR A SWEEP WING
AIRPLANE AT CRUISE CONDITIONS**

*by W. B. Gillette, L. W. Mohn,
H. G. Ridley, and T. C. Nark*

Prepared by

BOEING COMMERCIAL AIRPLANE COMPANY

Seattle, Wash. 98124

for Langley Research Center



NATIONAL AERONAUTICS AND SPACE ADMINISTRATION • WASHINGTON, D. C. • SEPTEMBER 1974

1. Report No. NASA CR-2427	2. Government Accession No.	3. Recipient's Catalog No.	
4. Title and Subtitle UPPER-SURFACE BLOWING NACELLE DESIGN STUDY FOR A SWEEP WING AIRPLANE AT CRUISE CONDITIONS		5. Report Date September 1974	6. Performing Organization Code
7. Author(s) W. B. Gillette, L. W. Mohn, H. G. Ridley, and T. C. Nark		8. Performing Organization Report No. D6-41763	
9. Performing Organization Name and Address Boeing Commercial Airplane Company P. O. Box 3707 Seattle, Washington 98124		10. Work Unit No.	
12. Sponsoring Agency Name and Address National Aeronautics and Space Administration Washington, D.C. 20546		11. Contract or Grant No. NAS1-12214	
		13. Type of Report and Period Covered Contractor Report	
		14. Sponsoring Agency Code	
15. Supplementary Notes FINAL REPORT			
16. Abstract <p>A study was made to design two types of overwing nacelles for an existing wing-body at a design condition of $M_{\infty} = 0.8$ and $C_L = 0.2$. Internal and external surface contours were developed for nacelles having either a D-shaped nozzle or a high-aspect-ratio nozzle for upper-surface blowing in the powered-lift mode of operation. The goal of the design was the development of external nacelle lines that would minimize high-speed aerodynamic interference effects. Each nacelle type was designed for both two- and four-engine airplanes using an iterative process of aerodynamic potential flow analysis. Incremental nacelle drag estimates were made for flow-through wind tunnel models of each configuration.</p>			
17. Key Words (Suggested by Author(s)) Nacelle design Upper-surface blowing Potential flow analysis Powered lift Over-wing nacelle		18. Distribution Statement Unclassified—unlimited STAR Category: 01	
19. Security Classif. (of this report) Unclassified	20. Security Classif. (of this page) Unclassified	21. No. of Pages 125	22. Price* \$4.50

*For sale by the National Technical Information Service, Springfield, Virginia 22151

CONTENTS

	Page
1.0 SUMMARY	1
2.0 INTRODUCTION	2
3.0 SYMBOLS	4
4.0 ENGINE SELECTION	7
4.1 Engine Cycle Selection	7
4.2 Engine Size	7
5.0 NACELLE DESIGN	9
5.1 D-Nozzle Nacelle Design	9
5.2 Spread Nozzle Nacelle Design	11
5.3 Application of Spread Nozzle Designs on Nonpowered-Lift Aircraft Configurations	13
6.0 AERODYNAMIC ANALYSIS	14
6.1 General Approach	14
6.2 Wing-Nacelle Surface Lofting	14
6.3 Subsonic Potential-Flow Analysis	15
6.4 Two-Engine D-Nozzle Configuration	17
6.5 Two-Engine Spread Nozzle Configuration	19
6.6 Four-Engine D-Nozzle Configuration	21
6.7 Cycle 2 Nacelle Geometry Modifications	22
6.8 Assessment of Wind Tunnel Scaling Effects	24
6.9 Estimated Drag Increment for Nacelles	24
7.0 SYSTEM STUDIES	29
7.1 Spread Nozzle Design and Performance	29
7.2 Nacelle Weight Studies	31
7.3 Variable Geometry	31
7.4 Thrust Reversers	32
8.0 CONCLUDING REMARKS	33
APPENDIX A—Design Study of Alternate Bypass Ratios	34
APPENDIX B—Four-Engine Spread Nozzle Nacelle Configuration Evaluation	35
REFERENCES	41
FIGURES	42

UPPER-SURFACE BLOWING NACELLE DESIGN STUDY FOR A SWEEP WING AIRPLANE AT CRUISE CONDITIONS

By W. B. Gillette, L. W. Mohn, H. G. Ridley, and T. C. Nark

1.0 SUMMARY

The design of nacelles for upper-surface blowing presents particular problems in the areas of high-speed aerodynamics and internal flow. A study has been made to develop external lines for two types of nacelles with the objective of reducing unfavorable flow-field interactions among the wing, body, and nacelles at the design condition ($M_\infty = 0.8$ $C_L = 0.2$). Both two- and four-engine arrangements were investigated using an existing wing-body design. The work also included a parametric performance study of engine exhaust nozzles for turbofan engines having bypass ratios of 2 to 12 and nozzle aspect ratios of 5 to 50. A design study of possible thrust reverser arrangements and variable geometry nozzles was made.

The engines were sized for a field length of approximately 610 m (2000 ft) and a bypass ratio of 10 was selected, consistent with the desired noise goal of 95 EPNdB at 153 m (500 ft) sideline distance. The two nacelle types studied are characterized by (1) D-shaped nozzles and (2) spread nozzles. The latter type nozzle was designed with an aspect ratio (width/height) of 10 for the two-engine airplane and 7 for the four-engine airplane.

Before the detailed aerodynamic design of the nacelles was begun, the general arrangement of each configuration was determined. These preliminary designs took into account various real-airplane considerations in addition to the basic aerodynamic and propulsion considerations. The primary design rule was to design the nacelle inboard contours along wing-body streamlines, and then let the nacelle outboard contours develop as required to provide the required nacelle internal volume. The spanwise location of these nacelles was selected to provide optimum coverage of the trailing edge flap by the exhaust flow.

Evaluations of the designs are made in light of theoretical aerodynamic analyses and corresponding Boeing experience. Theoretical pressure distributions on the wing and nacelle, configuration isobar plots, and wing C_q and load distribution were computed at $M_\infty = 0.7$ and indicate that, at that design condition, the nacelle geometries achieve the design goals. The levels and gradients of pressure calculated along the final nacelle surfaces are reasonably well behaved for both D-nozzle and spread nozzle nacelles.

Both two-engine configurations have wing isobars whose nacelle interference effects reveal no serious problems. Wing velocities are considerably higher in the four-engine D-nozzle case, although favorable wing isobar sweep is maintained. Experience at Boeing with four-engine over-wing designs indicates that at critical Mach numbers and beyond, the wing upper-surface shock between the two nacelles has less sweepback than would be indicated by the computed isobar pattern. If the critical Mach number of the wing-body configuration has some margin over the goal for this design ($M_{\infty} = 0.8$), the drag of the four-engine D-nozzle configuration may be acceptable. Minimization of the penalty in critical Mach number for addition of over-wing nacelles almost certainly requires local modification of the wing profile in the four-engine case. This is best accomplished empirically during developmental testing.

Incremental nacelle drag estimates were made for flow-through wind tunnel models of each of the four configurations. The effect of the nacelles on the wing-body polar shape is small for all but the four-engine spread nozzle case, and the increment of nacelle drag improves the configuration drag rise in all four cases.

A brief design study was made of alternate bypass ratios of 4 and 6, and it was found that this parameter has a significant effect on the maximum practical nozzle aspect ratio.

2.0 INTRODUCTION

Low noise is one of the most important requirements for public acceptance of new commercial aircraft. A significant reduction in aft turbomachinery noise is possible when the engines are shielded by the wing as in over-the-wing engine installations. Additionally, this concept can include upper-surface blowing in which the engine exhaust flow is blown tangentially over the upper wing surface. The use of upper-surface blowing has shown considerable promise as a powered-lift concept when used with a trailing edge flap which causes the engine exhaust to turn and follow the flap contour during the powered-lift mode of operation.

The design of nacelles for upper-surface blowing presents particular problems in the areas of high-speed aerodynamics and internal flow. The present study is concerned with the development of external lines for nacelles that will minimize unfavorable flow-field interactions between the wing, body, and nacelles at the cruise condition, and with the design of spread-exhaust nozzles to achieve good internal flow performance.

The first portion of the report concerns the aerodynamic design of two types of nacelles. One type, incorporating a D-shaped nozzle of modest aspect ratio, may require a variable geometry

device in order to keep the exhaust flow attached to the flap during powered-lift operation. The second type, referred to as the spread or high-aspect-ratio nozzle, provides a much thinner jet which flows over a significant portion of the span of the wing. Each nacelle type was designed for both two- and four-engine airplanes around an existing wing-body design. The designs evolved through an iterative process of aerodynamic analysis, using a generalized potential flow computer program.

Ground rules for this portion of the work were:

- Total airplane thrust 178 000 to 356 000 N (40 000 to 80 000 lb)
- Field length 610 to 915 m (2000 to 3000 ft)
- Noise goal 95 EPNdB at 153 m (500 ft)
- Cruise Mach number 0.80

The latter portion of the report gives the results of several system studies related to nacelles designed for upper-surface blowing. A parametric study of spread-exhaust nozzle design and performance is presented for nozzles having aspect ratios varying from 5 to 50, with engine bypass ratios in the range of 2 to 12. A detailed nacelle weight estimate is given for the nacelles derived in the aerodynamic analysis. Finally, conceptual layouts are shown for variable exhaust nozzle geometries that may be required to achieve jet spreading with D-shaped nozzles, and of the thrust reversers for over-the-wing engines.

During the course of the work, it became desirable to examine the impact of the bypass ratio on the maximum practical nozzle aspect ratio. The results of this work are shown in appendix A.

3.0 SYMBOLS

R	aspect ratio
A_{WD}	nozzle wetted area upstream of the convergent section, m^2 (ft^2)
A_D	nozzle cross-sectional area, upstream of the convergent section, m^2 (ft^2)
b	span, m (ft)
c	local wing chord, m (ft)
\bar{c}	S_{ref}/b , m (ft)
$C_{D_{P_{min}}}$	minimum level drag coefficient
C_{D_i}	drag coefficient for ideal elliptic induced drag
C_{ℓ}	sectional wing lift coefficient, $L'/q_{\infty}c$
C_L	lift coefficient, $L/q_{\infty}S_{ref}$
C_F	average skin friction coefficient
C_p	pressure coefficient, $(P - P_{\infty})/q_{\infty}$
C_v	nozzle velocity coefficient, $\frac{F}{m\sqrt{[2R\gamma/(\gamma-1)]T_T\left[1 - (P_{\infty}/P_T)^{\frac{\gamma-1}{\gamma}}\right]}}$
d_{hi}	inlet highlight diameter, m (ft)
D_{max}	nacelle external diameter at compressor entrance, m (ft)
F	nozzle thrust, N (lb)
L	total lift, N (lb)
L'	local lift per unit span, N/m (lb/ft)

m	nozzle mass flow, kg/sec (slugs/sec)
M_∞	flight Mach number (cruise or free stream)
M_{crit}	wing-body critical Mach number (occurs at $\Delta C_D = 0.0020$ above the C_D at $M = 0.7$ at constant C_L)
M_D	Mach number in the upstream portion of the nozzle
N	newton
p	local pressure, N/m^2 (lb/ft ²)
p_∞	atmospheric pressure, N/m^2 (lb/ft ²)
P_T	nozzle total pressure, N/m^2 (lb/ft ²)
q_∞	dynamic pressure, N/m^2 (lb/ft ²)
R	universal gas constant, $m^2/sec^2 \text{ } ^\circ K$ (ft ² /sec ² $^\circ R$)
S_{ref}	reference wing area, m^2 (ft ²)
T_T	nozzle total temperature, $^\circ K$ ($^\circ R$)
V_{hi}	average velocity at inlet highlight, m/sec (ft/sec)
V_∞	flight velocity (cruise or free stream), m/sec (ft/sec)
WBL	wing buttock line
α	angle of attack, deg
γ	ratio of specific heats
ΔC_{DM}	variation in drag coefficient due to transonic flow effects
ΔC_{DP}	variation in drag coefficient due to lift, excluding elliptic induced drag

$\Delta C_{D\pi}$	interference drag term based on nacelle frontal area
ΔP_T	loss in nozzle total pressure, N/m^2 (lb/ft ²)
η	fraction of wing semispan

4.0 ENGINE SELECTION

4.1 ENGINE CYCLE SELECTION

The engine cycle selection was based primarily on noise considerations. The sideline noise objective was 95 EPNdB at 153 m (500 ft). A detailed airplane design study was beyond the scope of this work; the results of STOL aircraft studies given in references 1 and 2 were used as a basis for selection of both the engine cycle and engine size required. It was shown there that mixed jet velocities of approximately 215 m/sec (700 ft/sec) are necessary with externally blown flap configurations in order to meet the noise objectives. Somewhat higher velocities may be acceptable with upper-surface blowing.

Quiet clean STOL experimental engine (QCSEE) studies made by Allison and the General Electric Company were examined to determine if a scaled version of one of these engines would be suitable for use in this work. All of the Allison engines were of relatively high bypass ratio (15 and greater) and would not permit mixing of the primary and fan streams. This feature is particularly desirable for upper-surface blowing designs. One of the GE engines (GE19/F2C3) was attractive; however, the bypass ratio of 8.3 resulted in an average jet velocity of 244 m/sec (800 ft/sec). This velocity was judged to be higher than acceptable.

A Boeing engine performance program was used to generate performance for a family of mixed flow turboflow engines having bypass ratios of 2, 4, 6, 8, 10, and 12. The maximum turbine inlet temperature was fixed at 1560°K (2800°R), consistent with the values recommended in the Allison study, based on noise considerations. Figure 1 shows the mixed jet velocity and fan pressure ratio as a function of the design bypass ratio at sea level, takeoff thrust, on a 29° C (84° F) day. As can be seen, an engine with a bypass ratio of 10 will achieve the desired jet velocity; therefore, this was the ratio selected.

4.2 ENGINE SIZE

The range of field lengths to be considered was 610 to 915 m (2000 to 3000 ft). Analysis of the data of references 1 and 2 showed that the land areas subjected to maximum noise would be reduced by 25% if the lower value were selected. Therefore, the field length was set at 610 m (2000 ft) for the four-engine designs. It was desired that the total thrust be equal for the two-engine and four-engine designs, and thus the field length of the two-engine airplanes will be somewhat greater because of the reduced engine-failure performance.

Some results of the references 1 and 2 parametric studies are reproduced in figure 2. Since it was desired that the total airplane thrust for this study be in the range 178 000 to 356 000 N (40 000 to 80 000 lb) values of thrust/weight ratio and wing loading were selected as noted on figure 2. These values correspond to a thrust of 162 000 N (36 320 lb) per engine for the two-engine airplane, the values being reduced by one-half for the four-engine airplane. Wind tunnel testing is proposed on a model having a wing area of 0.189 m^2 (2.0316 ft^2). Thus the model scale will be 0.035.

An engine outline drawing for the two-engine airplane is shown on figure 3.

5.0 NACELLE DESIGN

The principal emphasis of this contract was the design of nacelle geometries that would have acceptable high-speed performance characteristics. This goal was responsible for the detailed shape and curvature of each configuration. The general arrangement of the configurations was established by a set of requirements that recognized aerodynamic, propulsion, stability and control, weight, structural, reliability, accessibility, and manufacturing considerations. In each case, a general arrangement was found that best met the requirements before the detailed aerodynamic design of the nacelle began. The two types of nacelles, the D-nozzle and the spread nozzle, are fundamentally different when viewed from the standpoint of these general considerations. Therefore, they will be discussed separately below.

5.1 D-NOZZLE NACELLE DESIGN

Since, in the plan view, the exit nozzle width is about the same as the nacelle width, the configuration selection for the D-nozzle nacelle is straightforward. The nacelle itself will not produce large changes to the stability and control characteristics, as it is essentially an axisymmetric body. The effect on low-speed performance will also be slight since only a small portion of the wing leading edge is affected by the nacelle. Accessibility and maintenance requirements dictate that the engine rear turbine flange be forward of the front spar, so that the engine can be easily lowered for removal. The engine height relative to the local wing chord plane must be such that the engine flow can be turned over the front spar in a distance at least three times the vertical displacement, and that the external crown line boattail angle does not exceed a maximum of 12° . (See, e.g., fig. 6.)

Since the specific contours being designed are for a flow-through nacelle model, perfect simulation of all of the aircraft nacelle external lines is not possible. Consequently, the model nacelle external lines aft of a plane corresponding to the front of the engine are scaled exactly, and the lines forward of that plane were modified to ensure that the inlet spillage would not cause a premature drag rise.

The inlet highlight diameter was selected to provide subsonic flow both internally and externally at a free-stream Mach number of 0.8. The minimum internal area is at the nozzle exit, hence the nozzle exit area and nozzle exit static pressure determine the inlet flow. The inlet will satisfactorily accommodate the nozzle flow whether the nozzle exit flow is sonic or at the free-stream velocity. Table 1 shows values of average Mach number for a free-stream Mach number of 0.8. The nacelle internal area distribution for the two-engine D-nozzle configuration is shown in figure 4. The area distribution for the four-engine D-nozzle configuration is similar, but smaller in total area.

TABLE 1.—INLET AND EXIT CONDITIONS

Average Mach number for $M_{\infty} = 0.8$			$\frac{V_{hi}}{V_{\infty}}$	$\frac{d_{hi}}{D_{max}(b)}$
At nozzle exit	At inlet highlight	At inlet throat (a)		
0.80	0.50	0.57	0.64	0.84
1.00	0.52	0.60	0.67	0.84

^aBased on the highlight/throat area ratio = 1.10 (model only)

^b D_{max} does not include the streamline contouring bump in the lower quadrant.

The design goal for achieving satisfactory high-speed performance is that any disturbance of the wing flow field by the nacelle should be in a favorable direction. Specifically, the nacelle must not cause any isobar unsweeping, but may be allowed to cause increased isobar sweep. If the nacelle inboard contour follows a wing-body streamsheet, the nacelle will be “invisible” to the wing flow inboard of the nacelle, and the isobar sweep and the resulting shock sweep at cruise will be similar to that for the wing body. Also, placing the nacelle contour on a streamsheet tends to prevent a stagnation condition at the nacelle exit, which would interfere with the normal supersonic flow development on the wing. If the nacelle were instead made symmetric in the plan view, the inboard wing flow would feel the nacelle curvature and the wing isobars would unsweep as they approached the nacelle. The wing shock would thus have less sweep and higher drag. Clearly, the design goal is to have the nacelle inboard contour lying along a sheet of wing-body streamlines. It should be pointed out that the shape of the wing-body streamsheet becomes more distorted with increased sweep and with more peaky wing leading edge pressures, since both effects cause greater spanwise flow turning at the wing leading edge. In this respect, the wing sweep specified for this contract (31°) does not lend itself to an easy aerodynamic over-wing nacelle design. In the detailed configuration development of section 6.0, it will be seen that the nacelle inboard contours exhibit a “bump” on the lower quadrant forward of the wing leading edge.

If the nacelle inboard contour follows a wing streamsheet, then the nacelle outboard contour cannot, since the nacelle has thickness. The nacelle outboard contour will present a boattail to the wing flow, and the resulting stagnation condition at the nacelle exit on the outboard side will terminate the supersonic flow over the wing at that point, causing a shock to form in the wing flow. This wing shock will form with a sweep higher than the wing-alone shock, as it moves outboard to join the wing-body shock pattern. The resulting lamda-type shock pattern is desirable from a high-speed drag point of view.

The two-engine D-nozzle nacelles were located spanwise so that the exhaust flow would cover the flap to its inboard edge, while at the same time keeping the nacelle about a diameter away from

the fuselage. The resulting configuration is given in figure 5 and represents the starting point for the detailed aerodynamic design process.

In the case of the four-engine D-nozzle design, the inboard nacelles were positioned in a way similar to the two-engine D-nozzle. The outboard nacelles were positioned to have as small a gap in the flap blowing as possible, while maintaining a separation of about one diameter between the inboard and outboard nacelles. A characteristic four-engine D-nozzle nacelle is presented in figure 6. The aerodynamic design is more complicated than for the two-engine case, in that the inboard contour of the outboard nacelle must be designed along a streamsheet which includes the influence of the inboard nacelle as well as the wing.

5.2 SPREAD NOZZLE NACELLE DESIGN

The configuration selection for a spread nozzle nacelle is not as simple as for the D-nozzle nacelle. In the plan view of the spread nozzle, as the internal contours expand, they must be contained in an external contour that minimizes adverse aerodynamic effects. Two basic configuration concepts were considered, as shown in figure 7. Both spread nozzle approaches use an aerodynamic strake to cover the internal duct. The first, featuring a symmetric nozzle, is preferable from internal flow considerations, but its expected cruise shock pattern is likely to produce early drag rise. The second, featuring an offset nozzle, satisfies the inboard streamsheet rule applied to the D-nozzle nacelle design and, for this reason, should have the favorable cruise shock pattern shown. Therefore, the offset concept was selected for the spread nozzle designs.

The sweep of the strake that shields the internal duct is of importance to the aerodynamic characteristics of the spread nozzle nacelle configurations. At nozzle aspect ratios only slightly larger than that of the D-nozzle nacelles, the strake will have very large sweep and will begin vortex shedding at a relatively low angle of attack. This vortex shedding will likely produce nonlinearities in the pitching moment and is thus an undesirable situation. At nozzle aspect ratios in the range from 7 to 10, the strake sweep angle is reduced, and by proper selection of the strake section, the appearance of a vortex should be prevented at cruise angles of attack and may also be avoided at low-speed angles of attack. As the nozzle aspect ratio further increases, the strake begins to be merely a wing extension, but the internal duct contours become unacceptable on the outboard side. Because of these considerations, the nozzle aspect ratio of 10 was chosen for the two-engine spread nozzle configuration. For reasons given later, the nozzle aspect ratio of 7 was selected for the four-engine spread nozzle configuration.

The preliminary lines for the two-engine nacelle configuration are given in figure 8. This figure shows that the inboard nacelle contour is on a streamsheet, with the nacelle located spanwise so

that the exhaust flow should cover the wing flap from its inboard edge, subject to the limitation that the nacelle be one diameter from the fuselage. This figure also indicates the streamwise section used for the strake. The airfoil selected was the NACA 66₃-418, chosen for its flat upper-surface pressure distribution and forward camber. The airfoil was placed on the strake to preserve the original wingspan load distribution and to provide suitable sweep of the crest of the strake. Use of a 66-series airfoil is allowed by the low section lift coefficient ($C_l < 0.2$), and the nonpeaky pressure distribution should delay vortex formation to a higher angle of attack than would a section with a peaky pressure distribution. A half-model-scale wooden model of the fuselage and wing was constructed so that the lines of the spread nacelle could be seen in three dimensions. A photograph of this model with the clay nacelle is provided as figure 9. The internal area distribution is given in figure 10.

Consideration was also given to sweeping the nozzle exit plane along a wing isobar line which would have certain aerodynamic advantages and would improve noise shielding benefits. It would, however, require turning vanes inside the nozzle to achieve streamwise internal exit flow, since the flow would otherwise tend to have a direction perpendicular to the nozzle exit plane. This turning-vane concept could not be included in the present work because of the large amount of additional effort required to ensure a low-loss vane design. Therefore, the exit plane was left unswept.

Preliminary layouts of a four-engine spread nozzle configuration indicated that a nozzle aspect ratio of 10 was too large to be practical. The reason was that the center of pressure for the powered lift would be too far outboard for lateral control with an engine out. The choice of 7 for the nozzle aspect ratio was found to be more suitable. The basic nacelle lines for one nacelle are presented in figure 11. This nacelle was developed by the same process as was the two-engine spread nozzle nacelle.

Considerable difficulty was encountered, however, in finding a suitable arrangement for four of these nacelles. A set of rules was established, and seven configuration variations were considered. The details of the configuration evaluation are presented as appendix B. The best configuration that satisfies the rules of the evaluation is shown in figure 12. This rather unusual arrangement uses two nacelles developed similarly to the two-engine spread nozzle nacelles, with a NACA 66₃-418 section applied to the strake of the outboard nacelle and to the web between the inboard and outboard nacelles. This web is designed to have low pressure gradients and peaks, thus relieving the contour and channel flow problems between the nacelles. This configuration and the others considered in appendix B have been defined merely to investigate high-speed cruise aerodynamic effects. It is most likely that other aerodynamic design considerations such as static stability margins and flow at moderately high angles of attack will rule out the four-engine spread nozzle nacelle configuration as a practical airplane design concept.

5.3 APPLICATION OF SPREAD NOZZLE DESIGNS ON NONPOWERED-LIFT AIRCRAFT CONFIGURATIONS

The main reason for using over-wing spread nozzles other than for upper surface blowing powered-lift applications is to achieve some noise alleviation as the result of wing shielding. The shielding effect varies with nozzle aspect ratio, with the higher aspect ratio providing increased benefits. As the nozzle aspect ratio increases, the jet becomes thinner, increasing the wing shielding effect and decreasing the length of primary jet core because of increased mixing surface area between the fan and primary flows. On the other hand, as the nozzle aspect ratio increases, the aerodynamic problems of drag level, drag rise, and stability effects become more difficult to eliminate. The proper trade between a high nozzle aspect ratio for noise benefits and a low nozzle aspect ratio for good aerodynamic characteristics and high nozzle efficiency will be determined by the mission of the particular aircraft.

6.0 AERODYNAMIC ANALYSIS

6.1 GENERAL APPROACH

This section describes the technical approach that was followed and the results that were achieved in meeting the design and analysis objectives set forth in section 5.0. The preliminary nacelle designs as shown in figures 5, 6, 8, and 12 are taken as the initial data in the task of aerodynamic analysis. Before discussing the actual analysis of the various nacelle configurations, a description will be given of the preliminary task of determining a smooth loft of the wing and nacelle surfaces. This discussion of the lofting procedure will lead to a description of the three-dimensional potential flow computational method used in this study in which the wing-body-nacelle surfaces are represented by networks of small flat panels. The capabilities of this method will be discussed in general and as they apply to the design problem of this contract. The calculated aerodynamic data will then be presented and their implications discussed. Second cycle modifications to the nacelle designs will be described. The final subsections will discuss the influence of the nacelle configurations on wind tunnel scaling effects and the estimated drag increment due to nacelles at off-design Mach numbers and lift coefficients.

Subsection 5.2 and appendix B describe some of the difficulties that must be overcome in achieving a successful four-engine spread nozzle nacelle configuration design. The basic design concepts espoused in the two-engine spread nozzle over-wing nacelle configuration need to be evaluated in the wind tunnel before undertaking design iterations on a four-engine spread nozzle configuration. The risk involved in the basic two-engine spread nozzle design is sufficiently high to conclude that the corresponding four-engine design does not warrant aerodynamic refinement.

6.2 WING-NACELLE SURFACE LOFTING

Upon completion of the preliminary design of a given nacelle configuration, the internal and external surfaces of the nacelle were lofted numerically using a Boeing-developed computer program. The preliminary nacelle contours were thereby converted to smooth continuous surfaces whose numerical definition in terms of cubic splines was saved on tape for subsequent interrogations and modifications. In the same way, the wing geometry provided by NASA was lofted. Although the aerodynamic analysis could have been prepared directly from the preliminary nacelle contours, there were several advantages in creating the numerical wing and nacelle lofts:

- 1) The intersection of a nacelle with the wing upper and lower surfaces could be determined accurately and conveniently. This was especially important in determining the nacelle internal duct shape as it passed onto the wing upper surface.

- 2) The wing or nacelle geometry could be determined at any desired place on the surface. For example, nacelle cross-section shapes could be extracted at stations in between the defining nacelle cross sections.
- 3) Much of the three-dimensional surface panel geometry used to represent the nacelle in the aerodynamic analysis could be generated automatically (see, e.g., figure 35).
- 4) The output from the numerical loft of a nacelle would be in a form convenient for presentation as final nacelle lines at the completion of the contract (loft lines in plan and side views and cross-sectional defining members). (See, e.g., figures 33 and 34.) This geometry would be available in coordinate form as well as machine-generated model-scale plots.

The computer program used in developing these surface lofts is called the geometry control system (GCS). It produces smooth numerical surface definitions for wing-like surfaces and fuselage-nacelle-type surfaces, with up to second-derivative continuity. GCS combines the capabilities of surface generation, modification, and extraction for complete three-dimensional geometry evaluation. Data may be extracted from a GCS definition for numerical control machining of a model.

Based on section definitions provided by NASA for the wing and fuselage, smooth surface definitions were generated and saved by the GCS program. Twenty streamwise sections defined the wing and 20 body sections normal to the centerline determined the fuselage.

In a typical loft of an internal or external nacelle surface, 15 cross sections normal to the nacelle centerline were input. The nacelle centerline was not parallel to the body centerline, since the nacelles were normally canted nose-inboard and down so as to align with the local flow approaching the inlet. It was convenient to use a local nacelle coordinate system in developing the geometry of each nacelle. Therefore, this local coordinate system was related to the wing-body reference coordinate system by a general three-dimensional rotation and translation. The exit plane of each nacelle was canted downward slightly toward the wing upper surface.

6.3 SUBSONIC POTENTIAL-FLOW ANALYSIS

Analysis and optimization of the nacelle configurations developed in the preliminary design study was accomplished using the generalized potential-flow computer program TEA-230 (refs. 3 and 4). This method uses panel distributions of source and vortex (or doublet) singularities to represent the surface geometry and lifting elements of arbitrary three-dimensional configurations.

The solution consists of local pressure coefficients for all surface panels, flow conditions at specified points in the external flow field, and streamline tracing through desired points. Compressible subsonic flow problems are solved through application of the Gothert rule. The surface panel representation and lifting system panels can be plotted automatically in four views, to help in preliminary verification of the geometry and as a visual aid in locating panels corresponding to the output data. Samples of these plots are included in the following sections.

The initial step of the design process was to analyze the wing-body model based on geometric data provided by NASA, as described in the previous section. Aerodynamic data is presented in figures 13 through 16 for a free-stream Mach number of 0.7. The lift curve calculated for the configuration (fig. 13) exhibits the same slope but a considerably higher level than the corresponding wind tunnel lift curve provided by NASA. This difference in level is not surprising in view of the neglect of the boundary layer in the potential flow calculation. The rather severe C_p gradients on both the upper and lower surfaces of the aft wing (fig. 14) would promote a relatively thick boundary layer, whose decambering effect on the wing is consistent with the difference between theoretical and wind tunnel lift levels.

Based on these lift curve comparisons, a design angle of attack of 0° was selected, since this provided the desired design lift level of about $C_L = 0.2$ at $M_\infty = 0.8$ in the wind tunnel. Experience with the potential flow method and its accounting of compressibility effects led to the following design condition at the same α for the theoretical analyses:

$$M_\infty = 0.7, \alpha = 0^\circ, C_L = 0.265.$$

The lower Mach number selected reflects the fact that the more extensive transonic flow characteristics at $M_\infty = 0.8$ cannot be simulated in the potential flow calculation. Although there will be locally supersonic flow regions on the configuration in the wind tunnel at $M_\infty = 0.7$ as well, they will be much more limited in extent. Gothert's rule compressibility corrections are therefore adequate in the theoretical solution at $M_\infty = 0.7$. The most serious differences between theoretical and experimental wing pressure distributions at high free-stream Mach numbers will occur on the aft portion of the wing, not on the forward portion of the wing. Furthermore, as the Mach number is increased from $M_\infty = 0.7$, the analysis condition, to $M_\infty = 0.8$, the cruise condition, the wing streamlines will remain essentially unchanged in the plan view. They will of course change shape considerably in the side view as expansion to high transonic flow occurs, but the critical contours of the upper-surface-blowing nacelles are in the plan view, not the side view. Therefore, the use of plan view wing streamlines generated analytically at $M_\infty = 0.7$ is valid for the design of nacelle contours to provide suitable aerodynamic characteristics at $M_\infty = 0.8$.

Aerodynamic pressures and forces were also calculated in the wing-body solution for $\alpha = -2^\circ$, -1° , -0.5° , 0.5° , 1° , 1.5° , 2° , 4° , and 8° . This same α -series and design point were used for all wing-body-nacelle configurations analyzed during the contract.

The inboard upper wing surface isobar pattern for the wing-body configuration is shown in figure 15 for the design condition. Figure 16 shows the triangular wing span load distribution and the corresponding sectional lift distribution. Streamline data for the wing-body analysis were saved for future calculations of streamlines in the regions where the nacelles will be located. As an example, figure 17 shows a D-nozzle exit around which several initial points are specified for streamline tracing in a forward direction.

6.4 TWO-ENGINE D-NOZZLE CONFIGURATION

The next three subsections will present geometric and aerodynamic data for the three wing-body-nacelle configurations which were aerodynamically refined in the TEA-230 method. Nacelle pressure data will be presented along the following near-streamwise panel columns (internal and/or external surfaces):

- Along a panel column following (approximately) the crown line of the nacelle.
- Along a panel column following (approximately) the keel line of the nacelle.
- Along the inboard and outboard extremes of the nacelle. These are often called the "maximum half-breadth" lines, but this term is not strictly applicable here, because of the distorted shapes of some of the nacelle cross sections. Nevertheless, these panel columns will be taken to follow approximately the 3 o'clock and 9 o'clock positions in the front view, and pass aft to the wing and include the nacelle panels just above the wing upper surface.

Wing pressures adjacent to the nacelles will also be presented. It will be helpful to the reader to refer to the wing-nacelle plan view plot for each configuration when studying the various C_p plots.

Figure 18 shows the plan view reference plot for the two-engine D-nozzle nacelle. Figures 19 through 21 show the panel representations of the nacelle in several views, including the source panel singularities on the external and internal nacelle surfaces and adjacent wing surface, and the nacelle lifting system panels which lie along the nacelle camberline. These plots are originally made to model scale (or larger) on a Gerber machine plotter. Various networks of panels are defined on the surface, and different ink colors are used by the plotter for each network for better clarity.

The configuration lift curve, wing span load distribution, and wing sectional lift distribution are contrasted in figures 22 and 23 with the corresponding wing-body data. Inclusion of the nacelle in the analysis does not change the total lift at the design condition, but the lift curve slope is increased by about 5% for the angles of attack shown. The wing span loading could be expected to deteriorate slightly since the span loading for the wing-body was greatest over the region where the nacelle is being added. However, figure 23 shows a slight improvement in the load and C_D distributions, in at least two respects: the loading has become more elliptic so that no induced drag penalty is anticipated; and the moderate increase in wing C_D outboard of the nacelle may encourage separation on the wing just outboard of the nacelle first (when separation ultimately occurs). In the latter respect, it is desirable from the standpoint of airplane pitch-up that wing separation is initiated in the midspan region. Furthermore, separation of the inboard part of the wing flow is undesirable because of the adverse effect on the engine exhaust flow.

Figures 24 and 25 show the effect of the nacelle on wing pressures just inboard and just outboard of the nacelle (wing buttock line 4.2 and 9.4 in figure 18). Figures 26 through 29 display nacelle pressure distributions along the four extrema described at the beginning of this subsection. Notice that both internal and external surface C_p values are shown. Taken together, these six figures imply a reasonably good nacelle design, but indicate areas of potential improvement for cycle 2.

The internal nacelle flow is well behaved, based on the C_p distributions exhibited in these figures. The external nacelle C_p distributions indicate that only minor local recontouring is required to arrive at final, cycle 2 nacelle lines. Areas on the external surface to be examined for possible cycle 2 improvements include:

- 1) Keel line, at body station 12.5. The excessive "dip" in C_p here is probably due to a slight error in the panel representation of the surface at that point.
- 2) Outboard maximum half-breadth (MHB), aft of body station 20. The double peak in C_p should be smoothed by modifying the surface curvature on the nacelle. The first peak is caused from the aft nacelle bump and the second peak represents the influence of the flow over the wing leading edge. Figure 25 shows that the level of C_p on the adjacent wing leading edge has increased more than is desirable.
- 3) Inboard MHB, aft of wing leading edge (fig. 28). The C_p level should recover steadily following the peak due to the wing leading edge. The variation of C_p exhibited in figure 28 implies a boattail angle, whereas the design was meant to follow a streamline. The same conclusion is reached in considering the velocity drop on the inboard part of the wing near the nacelle exit station (fig. 24). These features can be improved with cycle 2 modifications.

Levels and gradients of C_p on the wing and nacelle are illustrated in the isobar plot of figure 30 (top view). Based on Boeing wind tunnel experience, this isobar pattern exhibits features associated with successful over-wing nacelle designs. On the wing inboard of the nacelle, the isobar pattern implies that the wing shock will be parallel to the wing leading edge, since all isobars more negative than $C_p = -0.25$ are well swept. Outboard of the nacelle exit, the isobars from $C_p = -0.25$ to $C_p = -0.40$ suggest that the wing shock will be bifurcated, becoming a single shock on the outboard wing. As indicated in section 5.0, this lambda-type shock pattern is desirable for high-speed drag reduction. Finally, the isobars across the top of the nacelle are of sufficiently low C_p to give confidence that no nacelle shock will be present at this design condition.

Figure 31 is included simply to show another useful capability of the TEA-230 program. Plots of velocity vectors at the panel midpoints illustrate the magnitude and direction of the flow, and are useful in locating irregularities in an aerodynamic solution.

6.5 TWO-ENGINE SPREAD NOZZLE CONFIGURATION

The plan view reference plot for this nacelle configuration is presented in figure 32. In order to achieve as much surface detail as possible with the panel representation of the configuration, two separate potential flow analyses were made: nacelle internal duct alone, and nacelle external surface with wing and fuselage. Attempting to combine these cases would have exceeded the limit of total configuration singularities in the TEA-230 method. Another reason for the two-step analysis was to be certain that the internal duct geometry was acceptable aerodynamically before finalizing the external nacelle lines.

In the first analysis, a detailed solution was obtained for the flow through the nacelle. Figures 33 and 34 show the final loft lines and cross sections for the internal surface, as a sample of the results of the GCS method described in subsection 6.2. Figure 35 shows the corresponding panel representation of the internal surface. Notice that the external surface inlet lip is also present. A special type of vortex panel singularity was used in this analysis, providing the lifting surface as well as the internal surface representation. A disadvantage of this approach in TEA-230 is that the compressibility option is not available. Thus, the pressure data determined for the internal surface represent an incompressible flow solution, but the results will be just as useful in evaluating the design.

In the second potential-flow solution, the external surface of the nacelle, as paneled in figures 36 and 37 was integrated with the wing-body and analyzed compressibly ($M_\infty = 0.7$). The usual surface source panel and vortex lifting system singularities were used here, together with a simulation of the inlet and exit flows by specifying the mass flow across "barriers" inside the inlet

and inside the nozzle exit. These specified mass flows were based on actual velocities from the nacelle internal duct solution.

The effect of the nacelle on the configuration lift curve (fig. 38) is quite similar to the D-nozzle case. The wing span load and sectional lift distributions in figure 39 show that the nacelle strake carries too much load at its outboard end, and a cycle 2 modification is required (see subsection 6.7). The lift contribution of the internal nacelle flow is indicated separately, since this will be present on the flow-through wind tunnel model, but not on a full-scale airplane. This internal lift represents a penalty in span-load distribution for the model, but it does not penalize the external isobar pattern.

Figure 40 shows that the presence of the nacelle has moderately increased the pressures on the adjacent wing upper surfaces. The lower wing surface inboard of the nacelle is more of a problem area, and this channel between the fuselage and the inboard nacelle will be recontoured in cycle 2 to reduce these velocities.

The pressure distributions along the crown line, keel line, and inboard and outboard sides of the nacelle are plotted in figures 41 through 44. The internal surface incompressible C_p values are seen to be acceptable with the possible exception of the long adverse gradient along the outboard side of the nacelle (fig. 44), between body stations 19 and 24 (see fig. 32). A simple comparison of these pressure gradients with the gradient on the lower aft surface of an airfoil, corrected for compressibility effects, indicates that the boundary layer should negotiate this gradient without separation. However, the peak in C_p between body stations 17 and 20 should be reduced in the cycle 2 modification by introducing a more gentle contour in this region (see fig. 32). The external surface pressures along these same four nacelle lines are similar in nature to those of the two-engine D-nozzle nacelle, and present no serious problem areas. Figure 45 shows external surface pressure distributions along approximately streamwise panel columns on the outboard strake of the nacelle (see fig. 37). These distributions look much as expected except that the C_p level on the upper surface becomes a little too negative. The desirable features are: (1) the down-load on the nose provides a margin for pitchup, and a near-zero contribution to lift; and (2) a shock will probably develop on this strake about the same time as on the wing, but with a higher sweep angle.

The wing-nacelle isobar plot of figure 46 also shows encouraging aspects of the nacelle design. Again, the probable sweep of the strake shock based on the isobars is seen to be much greater than the sweep of the wing shock. In addition, comparison with figure 30 shows that the spread nozzle design produced less interference with the wing isobars than did the D-nozzle nacelle.

6.6 FOUR-ENGINE D-NOZZLE CONFIGURATION

Figure 47 shows the plan view reference plot for the four-engine D-nozzle configuration. This design was also developed in two steps, which involved two separate potential flow analyses. The first step was to design the inboard nacelle and analyze the flow about the wing-body-inboard nacelle configuration, without an outboard nacelle. The inboard contour of the outboard nacelle was then designed on the basis of streamlines from this first flow solution and the complete configuration was analyzed in step 2.

Figure 48 shows a streamline traced forward from a point on the wing upper surface and near the inboard corner of the nozzle exit on the outboard nacelle. The solid streamline is from the case with wing-body alone and the dashed streamline originating at the same point was determined from the case with inboard nacelle only. Thus, the effect of the inboard nacelle is to increase the downwash and sidewash at the station where the inboard contour of the outboard nacelle is to be designed (about wing buttock line 10.0).

In the step 2 analysis of the complete four-engine configuration, the opportunity was taken to introduce certain cycle 2 geometry improvements to the nacelles. Figure 49 illustrates some of these changes on the inboard nacelle, but this redesign and its effects will be discussed later.

Although a complete set of data is not included here, it should be noted that the pressure distribution over the wing and nacelle for the step 1 solution with inboard nacelle only was very similar to that of the two-engine D-nozzle solution, with less wing-nacelle interference. Data for this case are included in figures 50 and 56 through 58.

In the panel representation of the complete four-engine configuration, the nacelle inlet and exit flows were again simulated, rather than include complete source paneling of both nacelle internal surfaces. As before, this simulation was done to keep the total configuration singularities under the limit of the method while achieving maximum detail of the nacelle and wing surfaces.

Figure 50 shows a lift curve for the complete four-engine configuration which is comparable to the two-engine D- and spread-nozzle lift curves: the lift coefficient at $\alpha = 0^\circ$ is increased slightly and the lift curve slope is increased about 5% by integration of the nacelles onto the wing. The wing load distribution shown in figure 51 has again become more elliptic, a desirable feature, but the C_q distribution has increased excessively in level. A shock is expected in the channel between the nacelles on the wing upper surface, based on the data presented here. Such a shock is probably difficult to avoid for a configuration of this type (upper-surface blowing) with such a small nacelle spacing. However, it is hoped that this channel shock will exhibit some sweep. More will be said

about this in the discussion below about the configuration isobar pattern. This channel region is especially vulnerable to separation problems and pitchup at higher angles of attack (see appendix B).

The wing pressure distributions just inboard and just outboard of the two nacelles are illustrated in figure 52 (see also fig. 47). These four pressure distributions form a family of similar shapes, so it can be reasoned that if the wing flow is acceptable along one of these stations, it will be acceptable at all four stations. Both upper and lower surface velocities show increases at all stations relative to the wing-body data.

The pressure distributions along the two nacelles are presented in figures 53 through 58. The keel line distributions are not included since they do not present any aerodynamic problems and are generally well behaved. The distributions of C_p along the crown line and the inboard and outboard sides of the nacelle are qualitatively similar to the corresponding C_p values on the two-engine D-nozzle nacelle. The presence of the second nacelle is felt most at about body station 21. Refer to figures 47, 54, and 58. Further discussion of the C_p distributions on the two nacelles will be contained in the next section.

Figure 59 illustrates the isobar pattern on the upper surface of the wing and nacelles. The isobars on the outboard part of the wing were not determined all the way to the tip, but are expected to be relatively undisturbed. The pressure distribution over the two nacelles is well behaved and similar in nature to that of the two-engine D-nozzle nacelle (fig. 30). On the forward part of the wing, the isobar sweep outboard of the nacelles is continued inboard between the nacelles and on the wing inboard of the nacelles. In the channel between the nacelles, this favorable sweep is an encouraging aspect of the design, although the isobars are expected to become distorted and unswept at higher Mach numbers in the wind tunnel. The sweep of the inboard forward isobars has unexpectedly deteriorated slightly as compared to the two-engine D-nozzle case. The $C_p = -0.25$ isobar between the nacelles and the $C_p = -0.3$ isobar just outboard of the outboard nacelle suggest that a wing shock could emanate from both corners of the exit.

6.7 CYCLE 2 NACELLE GEOMETRY MODIFICATIONS

In the previous discussions of the theoretical analyses of the three nacelle configurations, areas of the nacelle designs that would benefit from local recontouring were indicated. As measured by these aerodynamic analyses, the cycle 1 nacelle geometries achieved the design goals quite successfully. Only a few areas of the nacelle surface contours were felt to require a change, and these cycle 2 modifications and their effect on the aerodynamic characteristics are discussed below.

Certain improvements in the nacelle and wing C_p distribution were believed to be attainable through geometry changes, based on the results of the two-engine D-nozzle analysis. These cycle 2 modifications were actually introduced in the design of the four-engine D-nozzle configuration. Based on the similarity of the two- and four-engine D-nozzle designs, this approach precluded separate second-cycle analyses of both the two-engine and four-engine configurations. The step 1 analysis of the latter configuration with inboard nacelle alone did not incorporate the cycle 2 changes, but the step 2 analysis of the complete configuration included modified inboard nacelle lines and corresponding inputs to the design of the outboard nacelle. The changes to the outside contours of the inboard nacelle are shown in the plan view of figure 49. The revised inboard contour attempts to eliminate the boattail angle felt by the flow over the inboard part of the wing and reverses the sense of the curvature. Since the inboard side of the exit is moved with this change, the outboard side of the exit is moved correspondingly, to preserve the exit shape. The outboard recontour proceeds forward, reducing the curvature ahead of the wing leading edge and filling out the contour over the forward half of the nacelle. A modification of a similar magnitude was also made to the nacelle crown line (not shown here), by moving the point of maximum height forward. The keel line geometry was not modified.

The results of these nacelle modifications can be evaluated by comparing cycle 1 D-nozzle C_p data (figs. 24 through 29 and dashed lines of figs. 56 through 58) with corresponding cycle 2 D-nozzle data (solid lines in figs. 53 through 58 together with fig. 52). The data comparisons must be made while taking into account the more negative C_p levels characteristic of the four-engine configuration as opposed to the two-engine cases. On the outboard nacelle, it can be concluded that the cycle 2 geometry inputs improved the C_p distributions significantly along the crown line and along the outboard side of the nacelle. In the latter C_p distribution of figure 29, the "double bump" characteristic approaching the wing leading edge has been greatly relieved in figure 55, by the curvature reduction in this region of the nacelle. The cycle 2 pressure distribution along the inboard side of the outboard nacelle is similar to the cycle 1 results, except for the addition of a pressure "bump" at body station 21 which reflects the presence of the adjacent nacelle.

The evaluation of the cycle 2 modifications to the inboard nacelle is similar to the above. The geometry changes have improved the shapes of the C_p distributions along the crown line and along the outboard side of the nacelle (figs. 56 and 58). Along the inboard side of the inboard nacelle, the distribution can be considered improved in the sense that the nacelle pressures look more like the adjacent wing pressures (fig. 57). The set of cycle 2 geometry changes described above was incorporated in a corresponding way into the cycle 1 two-engine D-nozzle nacelle lines (see fig. 18).

One area of the two-engine spread nozzle design which was felt to require cycle 2 geometry modifications on the basis of the cycle 1 analysis is the outboard contour of the internal duct surface, as indicated in subsection 6.5. The type of cycle 2 geometry change called for is indicated

in figure 32. A cycle 2 modification was also made to the strake of the spread nozzle nacelle. The change was to give the strake negative twist on its outboard part, to correct the undesired span load distribution shown in figure 39. The required twist change was deduced from the linearity of section lift, as determined from the potential-flow solution for the cycle 1 geometry. A final area of modification for cycle 2 is the lower inboard side of the nacelle under the wing. The excessive velocity on the wing lower surface can be reduced by recontouring the nacelle surface forming this channel. These minor changes to the configuration were not judged to be extensive enough to justify a cycle 2 potential flow analysis of the spread nozzle configuration. The predicted improvement in C_p associated with the former modification is indicated in figure 44. The span load distribution expected to result from the cycle 2 modification to the strake is indicated in figure 39.

6.8 ASSESSMENT OF WIND TUNNEL SCALING EFFECTS

Boeing wind tunnel experience has shown that improperly contoured overwing nozzle nacelle installations demonstrate large, definite flow breakdowns. Vortex formation in the inboard wing-nacelle intersections is likely to be very strong. Upper surface wing shock systems, in addition to being strong, are determined primarily as a consequence of nacelle geometry. For the poorly contoured nacelle, these flow characteristics are not likely to be altered by changes in Reynolds number.

For properly contoured installations, Boeing experience indicates that interference pressure gradients are much milder, and consequently the flow characteristics likely will be more conventionally related to Reynolds number. If the contouring is properly done, then conventional wing-body scaling rules should apply regardless of the nacelle configuration or nacelle location. The possibility of unusual scaling increases as the nozzle aspect ratio is increased beyond 2 or 3 because of the increased possibility of vortex-dominated flows.

6.9 ESTIMATED DRAG INCREMENT FOR NACELLES

Before presenting estimates of the drag increments for the four nacelle configurations, the drag prediction procedure must be defined. Figure 60 shows the partitioning of drag for a general configuration as it will be used in this analysis. The basic drag level, invariant with Mach number or lift, is denoted $CD_{P_{min}}$. This term is comprised of skin friction, supersonic effects due to thickness, body closure and upsweep, nacelle inlet shape and diameter ratio, and other similar terms. The lift-dependent portion of the drag polar is divided into two parts. The induced drag (denoted as CD_i) is assumed to be that for elliptic loading, and the remaining portion is termed ΔCD_p . This latter term includes effects due to viscous interaction with pressure development,

nonelliptic induced drag, corner interference, and drag due to camber shape. The arbitrary division of the lift-dependent drag into an ideal induced drag and a term for all the other lift-dependent drag is done as an aide to extracting the ΔC_{DP} from wind tunnel data. This term can be very precise for a given class of geometries when experimental data is available. In summary, the drag is given by:

$$C_D = C_{DP_{\min}} + \Delta C_{DP} + C_{D_i} \quad (1)$$

where

$C_{DP_{\min}}$ is estimated from experimental data; is not a function of C_L

ΔC_{DP} is estimated from experimental data; is a function of C_L

C_{D_i} equals $C_L^2/\pi AR$.

This expression accounts for the subcritical, or Mach independent, polar shape. An additional term, ΔC_{DM} , adds the effect of Mach number to the drag polar buildup. The ΔC_{DM} term is a function of C_L as well. It may add drag, as in the case of a wing-body, or in the case of overwing nacelles, may decrease the drag, due to an area ruling effect. The expression for total drag becomes

$$C_D = C_{DP_{\min}} + \Delta C_{DP} + C_{D_i} + \Delta C_{DM} \quad (2)$$

When a new component is added to an existing configuration, that component will add to each of the terms of equation (2):

$$C_D = \left(C_{DP_{\min}} + \Delta C_{DP_{\min}} \right) + \Delta C_{DP} + \Delta (\Delta C_{DP}) + C_{D_i} + \Delta C_{DM} + \Delta (\Delta C_{DM})$$

or

$$C_D = \left(C_{DP_{\min}} + \Delta C_{DP} + C_{D_i} + \Delta C_{DM} \right)_{\text{baseline}} + \Delta \left(C_{DP_{\min}} + \Delta C_{DP} + \Delta C_{DM} \right)_{\text{component}} \quad (3)$$

This is illustrated as figure 61. The use of equation (3) allows the additional drag of a component to be determined and added to an existing geometry. In the case of this contract, the incremental drag due to nacelles will be estimated, so that the effect on the wing-body drag can be determined when the wing-body drag polar is known.

The drag of each of the component terms of equation (3) will be described below. The general procedure is based on the Boeing in-house drag method, with use of Boeing background in overwing nacelle testing for some of the information. All drag estimates will be for the flow-through nacelle wind tunnel model, at a test condition Reynolds number of 11.5×10^6 per m (3.5×10^6 per ft), and the nacelles are assumed to be tripped at 10% of local chord.

Nacelle Drag Increment $\Delta C_{D_{P_{min}}}$

The basic drag level is composed of the sum of the nacelle external and internal drag, minus the estimated drag of the wing covered by the nacelle. The external drag includes the effects of inlet velocity ratio, nacelle fineness ratio and an experimentally observed interference term, $\Delta C_{D_{\pi}}$. The internal drag is assumed to be constant, and includes the corrections in Reynolds number and dynamic pressure q that occur inside the nacelle. Table 2 gives the estimated ΔC_D for each of these components for the four nacelle configurations of this report.

TABLE 2.— $\Delta C_{D_{P_{min}}}$ FOR EACH NACELLE CONFIGURATION

Nacelle configuration	External ΔC_D				Internal ΔC_D	ΔC_D of wing	Nacelle $\Delta C_{D_{P_{min}}}$
	Skin friction	Inlet velocity ratio	Fineness ratio	Interference			
Two-engine D-nozzle	0.00302	0.00040	0.00044	0.00156	0.00158	-0.00050	0.00650
Four-engine D-nozzle	0.00336	0.00044	0.00048	0.00156	0.00176	-0.00104	0.00656
Two-engine spread nozzle	0.00566	0.00043	0.00031	0.00110	0.00246	-0.00218	0.00778
Four-engine spread nozzle	0.00618	0.00050	0.00054	0.00156	0.00358	-0.00274	0.00962

Nacelle Drag Increment $\Delta(\Delta C_{D_P})$

The variation in nacelle drag with lift coefficient is based entirely on Boeing in-house test results. The estimates for the four configurations are shown in table 3.

TABLE 3. $-\Delta(\Delta C_{Dp})$ FOR EACH NACELLE CONFIGURATION

Nacelle configuration	$\Delta(\Delta C_{Dp})$			
	$C_L = 0$	$C_L = 0.2$	$C_L = 0.4$	$C_L = 0.5$
Two-engine D-nozzle	0.0004	0	0.0003	0.0008
Four-engine D-nozzle	0.0006	0	0.0005	0.0013
Two-engine spread nozzle	0.0005	0	0.0004	0.0010
Four-engine spread nozzle	0.0008	0	0.0006	0.0015

Nacelle Drag Increment $\Delta(\Delta C_{DM})$

The variation in nacelle drag with Mach number is given in table 4. This also is derived from Boeing in-house test results, and shows the favorable local area ruling that some nacelle configurations provide.

TABLE 4. $-\Delta(\Delta C_{DM})$ FOR EACH NACELLE CONFIGURATION

Nacelle configuration	$\Delta(\Delta C_{DM})$		
	$M \leq M_{crit} - 0.04$	$M = M_{crit}$	$M = M_{crit} + 0.02$
Two-engine D-nozzle	0	-0.00156	-0.00312
Four-engine D-nozzle	0	-0.00078	-0.00156
Two-engine spread nozzle	0	-0.00110	-0.00220
Four-engine spread nozzle	0	-0.00078	-0.00156

The drag components have been shown separately, so that the magnitude of each could be appreciated. The components are summed together in table 5, and are shown at $C_L = 0.2$ and 0.4 on figure 62. This sum represents the estimated total effect of each nacelle configuration on the reference wing-body drag polar.

TABLE 5.— $\Delta C_{D_{NACELLE}}$ FOR EACH NACELLE CONFIGURATION

Nacelle configuration	C_L	$\Delta C_{D_{nacelle}}$		
		$M \leq M_{crit} - 0.04$	$M = M_{crit}$	$M = M_{crit} + 0.2$
Two-engine D-nozzle	0	0.00690	0.00534	0.00378
	0.2	0.00650	0.00494	0.00338
	0.4	0.00680	0.00524	0.00368
	0.5	0.00730	0.00574	0.00418
Four-engine D-nozzle	0	0.00716	0.00638	0.00560
	0.2	0.00656	0.00578	0.00500
	0.4	0.00706	0.00628	0.00550
	0.5	0.00786	0.00708	0.00630
Two-engine spread nozzle	0	0.00828	0.00718	0.00608
	0.2	0.00778	0.00668	0.00558
	0.4	0.00818	0.00708	0.00598
	0.5	0.00878	0.00768	0.00658
Four-engine spread nozzle	0	0.01042	0.00964	0.00886
	0.2	0.00962	0.00884	0.00806
	0.4	0.01022	0.00944	0.00866
	0.5	0.01112	0.01034	0.00956

7.0 SYSTEM STUDIES

7.1 SPREAD NOZZLE DESIGN AND PERFORMANCE

A parametric study of spread nozzle internal performance was made. This study investigated the effects of bypass ratio and nozzle aspect ratio on net thrust at zero speed, 51 m/sec (100 kn), and 0.8 free-stream Mach number. The estimated performance of the specific nozzles developed for the wind tunnel models is also given.

The initial problem involved determining the approximate geometry of spread nozzles as a function of the bypass ratio and nozzle aspect ratio (fig. 63). Preliminary calculations based on a simplified form of the radial equilibrium equation suggested that the radii of curvature assumed would lead to reasonable pressure gradients through the nozzle although no boundary layer calculations were made to verify this. The fact that the required nozzle length is influenced by the bypass ratio was unexpected and it results from the characteristic that the higher bypass ratio engines require a larger nozzle area relative to the fan frontal area.

The nozzle velocity coefficient was then calculated at the critical pressure ratio (fig. 64). The nozzle velocity coefficient is defined as the ratio of the actual thrust to the isentropic thrust per unit flow. No allowance was included for wing scrubbing losses. The velocity coefficient reflects the following losses:

- 1) Friction loss in the constant area portion of the nozzle

$$\frac{\Delta P_T}{P_T} = C_F \frac{\gamma}{2} M_D^2 \frac{A_{WD}}{A_D}$$

where:

C_F was taken as 0.0032

and at critical pressure ratio:

$$\Delta C_v = 0.715 \frac{\Delta P_T}{P_T}$$

2) Vertical and spanwise turning of the flow

$$\frac{\Delta P_T}{P_T} = 0.054 \left(\frac{\Delta}{\ell} \right)^2$$

where:

Δ = displacement of the flow centroid
through the turn

ℓ = length of the turn

3) Friction loss through the convergent portion of the nozzle

$$\Delta C_v = 1.15 \times 0.005 \times \left(\frac{\text{nozzle exit perimeter}}{\text{perimeter of equal-area circular nozzle}} \right)$$

The velocity coefficient at pressure ratios other than critical was determined from figure 65. Below the critical pressure ratio, it was assumed that the loss in nozzle total pressure varied linearly with dynamic pressure at the nozzle exit. Other assumptions were tested. However, these did not correlate with experimental data as well. Above critical pressure ratio, the percentage pressure loss is constant; but as the nozzle pressure continues to increase, underexpansion losses cause the velocity coefficient to decrease. Most exhaust nozzles will not exhibit the discontinuity shown on figure 65 because uniform choking does not occur precisely at the critical pressure ratio.

The percentage loss in net thrust is equal to the loss in nozzle velocity coefficient $(1 - C_v)$ multiplied by the ratio of engine gross to net thrust shown on figure 66. Figure 67 shows the resulting net thrust loss at three flight conditions. It should be noted that the thrust loss is shown relative to a conventional engine installation having a nozzle velocity coefficient of 0.99 at critical pressure ratio.

The net thrust loss was also calculated for the particular nozzles proposed for the wind tunnel models. The results of this work, shown on table 6, agree reasonably well with the parametric analysis.

TABLE 6.—NET THRUST LOSS OF D-NOZZLES AND SPREAD NOZZLES^a

Altitude	Speed	Loss in net thrust, %			Flight condition
		Nozzle aspect ratio			
		D	7	10	
Sea level	0	0.3	1.1	1.6	Start of takeoff
Sea level	51 m/sec (100 knots)	0.4	1.3	1.9	Liftoff
9150 m (30 000 ft)	$M_\infty = 0.8$	0.9	3.3	5.1	Cruise

^aRelative to a conventional nozzle having a velocity coefficient of 0.99 at critical pressure ratio

7.2 NACELLE WEIGHT STUDIES

Weights were estimated for the D-nozzle and spread nozzle nacelles in the two-engine airplane, using parametric and statistical procedures. No weight allowance was made for variable geometry exhaust nozzles.

The results are shown in table 7. Nacelle weights include peripheral acoustic treatment in the engine inlet only. The estimated weights assume conventional nacelle structure with material selection governed by loads and temperature environment. No allowance was made for hot spots in the fan duct (upstream of the turbine exit plane) due to possible recirculation of the primary flow into the fan duct during reverse operation. The thrust reverser scheme assumed is that shown on figures 70 and 71.

7.3 VARIABLE GEOMETRY

The D-nozzle may not provide effective upper-wing-surface blowing without the use of a variable geometry device. The scheme developed (fig. 68) would divert a portion of the exhaust flow through two doors in the side walls of the nozzle, permitting the flow to spread over a greater area at low speeds.

The spread nozzles will require internal braces, with struts or fences, in order to maintain contour at engine operating pressures. With these nozzles, additional spreading of the flow could be achieved by adding hinged flaps to the nozzle supports as shown on figure 69.

TABLE 7.—NACELLE AND ENGINE WEIGHT SUMMARY, TWO-ENGINE AIRPLANE

Components	Weight per engine installation			
	D-nozzle		10/1 aspect ratio nozzle	
	N	(lb)	N	(lb)
Inlet cowl	4 048	(910)	4 048	(910)
Fan cowl	534	(120)	534	(120)
Core cowl	1 379	(310)	1 379	(310)
Side cowl	2 447	(550)	2 669	(600)
Strut shell	4 582	(1 030)	5 471	(1 230)
Primary nozzle	267	(60)	267	(60)
Primary nozzle plug	133	(30)	133	(30)
Engine mounts	801	(180)	801	(180)
Ramp (nozzle)	1 779	(400)	2 847	(640)
Lower nacelle fairing	845	(190)	1 334	(300)
Wing heat shield	667	(150)	667	(150)
Nacelle, support beams (in wing)	1 868	(420)	1 868	(420)
Aft outer nozzle	3 069	(690)	11 121	(2 500)
Total, nacelle and strut	22 419	(5 040)	33 139	(7 450)
Thrust reverser	4 893	(1 100)	4 893	(1 100)
Engine (Boeing estimate)	26 467	(5 950)	26 467	(5 950)
Systems	3 914	(880)	3 914	(880)
Total installed weight on wing	57 693	(12 970)	68 413	(15 380)

7.4 THRUST REVERSERS

Preliminary engineering studies were made to define the thrust reverser for the two-engine D-nozzles and spread nozzles. The resulting thrust reverser layouts (figs. 70 and 71) reflect a conventional approach, with cascades and blocker doors for the fan stream only. The primary stream provides only about 13% of the total thrust and approximately half of this will be spoiled because of the overexpansion. It is estimated that the thrust reverser arrangements shown would provide approximately 37% reverse thrust at speeds above 20.6 m/sec (40 kn). The weight of the thrust reverser is noted on the nacelle and engine weight summary (table 7).

8.0 CONCLUDING REMARKS

The success of the nacelle designs of this contract has been interpreted in section 6.0 in terms of: (1) theoretical potential flow analyses of the configurations, and (2) Boeing theoretical and experimental experience with over-wing nacelle configurations.

In spite of a number of potential problem areas characteristic of spread nozzle and four-engine over-wing nacelle configurations for upper-surface blowing (see appendix B), the present designs are believed to be a good compromise between high-speed aerodynamic considerations and the other ground rules of this study. The aerodynamic analyses suggest favorable shock sweeps in most of the crucial areas on the wing and nacelles.

The critical transonic flow interference effects that will be present in the channel between the nacelles in the four-engine D-nozzle case cannot be predicted by the potential flow method. As the Mach number increases in the wind tunnel, an unswept shock may develop on the wing upper surface between the nacelles. Boeing experience has shown that the critical Mach number of such a configuration can be increased significantly by empirical modifications to the wing upper surface contour in this region. If the critical Mach number of the wing-body has some margin over the goal for this design ($M_{\infty} = 0.8$), the drag of the four-engine D-nozzle design presented here is expected to be acceptable.

In both the two-engine D and spread nozzle configuration designs, local contours that represent potential problem areas in the wind tunnel are not as critical as in the case of the four-engine design. Based on the favorable wing-nacelle isobar characteristics, the acceptable wing load distributions, and the reasonable C_p levels and gradients in the theoretical analyses, these configurations are expected to meet design goals in the wind tunnel.

If the aerodynamic performance of the present two-engine spread nozzle design is successful in the wind tunnel, it is recommended that a four-engine spread nozzle design of the type developed in this contract (fig. 12) be further analyzed and tested.

Boeing Commercial Airplane Company

P.O. Box 3707

Seattle, Washington 98124, May 1, 1974.

APPENDIX A

DESIGN STUDY OF ALTERNATE BYPASS RATIOS

Based on noise considerations, a bypass ratio of 10 was selected for the detailed nacelle design study. However, the bypass ratio was found to have a significant effect on the options available for nacelle configuration for a fixed thrust. The nozzle areas of the lower bypass engines are smaller relative to the fan frontal area than the higher bypass engines as shown in table 8. This reduction in area has a favorable effect on the design.

The ratio of the required nozzle width to the basic nacelle width is shown as a function of the nozzle aspect ratio and bypass ratio on figure 72. Lines of constant nozzle width and constant nozzle height are shown which pass through the two- and four-engine design points. It can be seen that the nozzle for the lower bypass engines can be selected to provide the jet thickness (nozzle height) of the present designs with considerably less nozzle width.

A brief design study was made to determine approximate nacelle lines for engines having a bypass ratio of 4 and 6. Both two- and four-engine airplanes were considered. The results of this study are shown on figures 73 through 76.

TABLE 8.—EFFECT OF BYPASS RATIO

Bypass ratio	$\left(\frac{\text{Nozzle area}}{\text{Fan frontal area}} \right)$
4	0.574
6	0.644
8	0.708
10	0.767
12	0.824

APPENDIX B

FOUR-ENGINE SPREAD NOZZLE NACELLE CONFIGURATION EVALUATION

The selection of a good four-engine spread nozzle nacelle configuration requires the resolution of a number of dilemmas. In an attempt to make this process systematic, a set of rules was postulated and a merit-demerit scoring process was established. This system was then used to evaluate a number of configuration alternates. The details of this examination are presented in this appendix.

RULES

The following rules for the four-engine spread nozzle nacelle configuration evaluation were postulated:

- 1) The nacelle exits will be unswept, not on a wing spanline.
- 2) The nacelles will have common inlet geometry, forward nacelle, and exit shapes.
- 3) The engine bypass ratio will be common with the other configurations in this study.
- 4) The nacelle inboard contours will lie on a streamsheet.

Rule 1 is given for the reason discussed in the text for the two-engine spread nozzle nacelle design, namely that the effort necessary to design the internal turning vanes for the swept nozzle was too great to be done during this study. Rule 2 is a manufacturing and cost consideration. Rule 3 is established by the time limit of this study, in that the engine bypass ratio was to be selected early in the study and held constant for all configurations. Rule 4 is considered absolutely necessary for successful aerodynamic integration of the nacelle and wing.

SCORING

A *merit-demerit* scoring system was established, giving up to three merits or demerits in several categories for each configuration. The merits or demerits were assigned only when a configuration differed from an average condition for all the configurations.

A configuration could receive *merits* in the following categories:

- *Continuous flap blowing*—the best condition is considered to be continuous flap blowing without a gap between the nacelle exhaust flows.
- *Outboard wing stall protection*—certain configurations tend to reduce outboard wing stall due to inboard engine failure, by being arranged to prevent the unblown inboard engine flow from getting underneath the outboard blown flow and lifting it off the upper-surface blowing (USB) flap.
- *Parts commonality*—some configurations have more commonality of parts.
- *USB lift centroid inboard*—configurations having the lift centroid of the USB flaps further inboard have reduced engine-out rolling moments.
- *Improved isobars*—certain configurations produce wing-nacelle isobars more likely to have acceptable high-speed performance.
- *Reduced wetted area*—configurations with reduced wetted area were credited for this advantage.

A configuration could receive *demerits* in the following categories:

- *Internal duct losses*—a penalty was assessed against configurations having poor internal duct shapes.
- *Adjacent engine stall*—certain configurations tend to produce adjacent engine stall because of the proximity of the two inlets.
- *Engine burst damage*—the potential for adjacent engine damage due to engine burst was considered.
- *Critical wing-nacelle intersections*—the intersection between the wing leading edge and the nacelle inboard contour is very critical for the overwing nacelle. The severity of the local nacelle contouring required is reduced by decreased wing sweep or decreased wing leading edge peak pressures.

- *Channel with high α separation*—as the wing angle of attack is increased, the wing leading edge pressures become more peaky, causing a more abrupt local change to the streamline flow at the wing-nacelle intersection. The presence of a small channel between the nacelles would aggravate the situation, leading to probable flow separation in the channel.
- *Excess wetted area*—configurations with more wetted area than normal were penalized for the resultant weight disadvantages.

Configuration A

The first configuration considered is shown in figure 77, and is a siamese arrangement. All rules are satisfied, but a total score of 0 was found:

Merits		Demerits	
● Continuous flap blowing	2	● Internal duct losses	-2
● Outboard wing stall protection	2	● Adjacent engine stall	-2
● USB lift centroid inboard	2	● Engine burst damage	-1
		● Critical wing-nacelle intersections	-1
	+6		-6
Score: 0			

Configuration B

The second configuration splits the siamese nacelle into separate nacelles, placed about a nacelle diameter apart as shown in figure 78. A total score of 0 was also found for this arrangement:

Merits		Demerits	
● Outboard wing stall protection	1	● Internal duct losses	-1
● Parts commonality	2	● Critical wing-nacelle intersections	-2
● USB lift centroid inboard	1	● Channel with high α separation	-1
	+4		-4
Score: 0			

Configuration C

The next arrangement (fig. 79) moves the outboard nacelle toward the inboard nacelle. The small channel between the nacelles aggravates the flow in that region, so a wing leading edge extension is shown, and would be contoured to reduce the severity of the outboard nacelle contouring. A total score of 2 was found:

Merits		Demerits	
● Continuous flap blowing	2	● Internal duct losses	-1
● Outboard wing stall protection	1	● Critical wing-nacelle intersections	-2
● Parts commonality	2	● Channel with high α separation	-2
● USB lift centroid inboard	<u>2</u>		<u>-5</u>
	7		
Score: 2			

Configuration D

The final step in the configuration arrangement series is to eliminate the channel entirely by putting a large leading edge extension between the nacelles (fig. 80). This section would have a NACA 66-series airfoil, to reduce the pressure gradients and provide a favorable pressure gradient allowed by the very low section lift required at cruise. A score of 4 was achieved by this arrangement, and since it satisfies all the rules, is recommended as the candidate four-engine spread nozzle nacelle configuration.

Merits		Demerits	
● Continuous flap blowing	2	● Internal duct losses	-1
● Outboard wing stall protection	2	● Critical wing-nacelle interference	-1
● Parts commonality	1	● Excess wetted area	-1
● USB lift centroid inboard	<u>2</u>		<u>-3</u>
	7		
Score: 4			

Alternate Configuration 1

Several configurations were also examined to explore possible gains that could be made by relaxing some of the rules. Alternate configuration 1 as shown in figure 81 gives the arrangement resulting from relaxing rule 1. A fence is shown to reduce the risk of outboard wing separation, and a wing leading edge extension is provided to improve the channel flow. A score of 3 was counted for this configuration.

Merits	Demerits
<ul style="list-style-type: none"> ● Continuous flap blowing 2 ● Outboard wing stall protection 1 ● USB lift centroid inboard 2 ● Parts commonality 2 ● Improved isobars 2 	<ul style="list-style-type: none"> ● Internal duct losses (turning vanes) -2 ● Critical wing-nacelle intersections -2 ● Channel with high α separation -2
<hr style="width: 50%; margin-left: auto; margin-right: 0;"/> 9	<hr style="width: 50%; margin-left: auto; margin-right: 0;"/> -6
Score: 3	

Alternate Configuration 2

This configuration relaxes rule 2, and mixes a D-nozzle nacelle inboard with a spread nozzle nacelle outboard (fig. 82). The fence and wing leading edge extension from configuration 1 are retained. A score of 4 was recorded, giving this configuration the same score as configuration D.

Merits	Demerits
<ul style="list-style-type: none"> ● Continuous flap blowing 2 ● Outboard wing stall protection 1 ● Parts commonality 1 ● USB lift centroid inboard 3 ● Reduced wetted area 1 	<ul style="list-style-type: none"> ● Critical wing-nacelle intersections -2 ● Channel with high α separation -2
<hr style="width: 50%; margin-left: auto; margin-right: 0;"/> 8	<hr style="width: 50%; margin-left: auto; margin-right: 0;"/> -4
Score: 4	

Alternate Configuration 3

The last configuration considered is shown as figure 83 and combines the more desirable features of alternate configurations 1 and 2, by relaxing both rules 1 and 2. The score for this configuration was 5, only one point above that recorded for configuration D.

Merits	Demerits
<ul style="list-style-type: none"> ● Continuous flap blowing 2 ● Parts commonality 1 ● Outboard wing stall protection 1 ● USB lift centroid inboard 3 ● Improved isobars 1 ● Reduced wetted area 1 	<ul style="list-style-type: none"> ● Internal duct losses (turning vanes) -1 ● Critical wing-nacelle intersections -2 ● Channel with high α separation -1
<hr style="width: 50%; margin-left: auto;"/> 9	<hr style="width: 50%; margin-left: auto;"/> -4
Score: 5	

REFERENCES

1. Rochte, L. S.: Study of Quiet Turbofan STOL Aircraft for Short Haul Transportation. NASA CR-114607, 1973.
2. Higgins, T. P.: Quiet Turbofan STOL Aircraft for Short Haul Transportation. NASA CR-114612, 1973.
3. Rubbert, P. E.; and Saaris, G. R.: Review and Evaluation of a Three-Dimensional Lifting Potential Flow Analysis Method for Arbitrary Configurations. Paper presented at AIAA 10th Aerospace Sciences Meeting, San Diego, California, January 1972.
4. Rubbert, P. E., et al: A General Method for Determining the Aerodynamic Characteristics of Fan-in-Wing Configurations. Volume 1, Theory and Application. Technical report 67-61A, USAAVLABS, 1967.

29°C (84°F) sea level static takeoff thrust

Polytropic efficiency	Fan	0.871
	Low pressure compressor	0.944
	High pressure compressor	0.902
Adiabatic efficiency	High pressure turbine	0.886
	Low pressure turbine	0.908
Turbine inlet temperature	1560° K (2800° R)	
Overall pressure ratio	25	

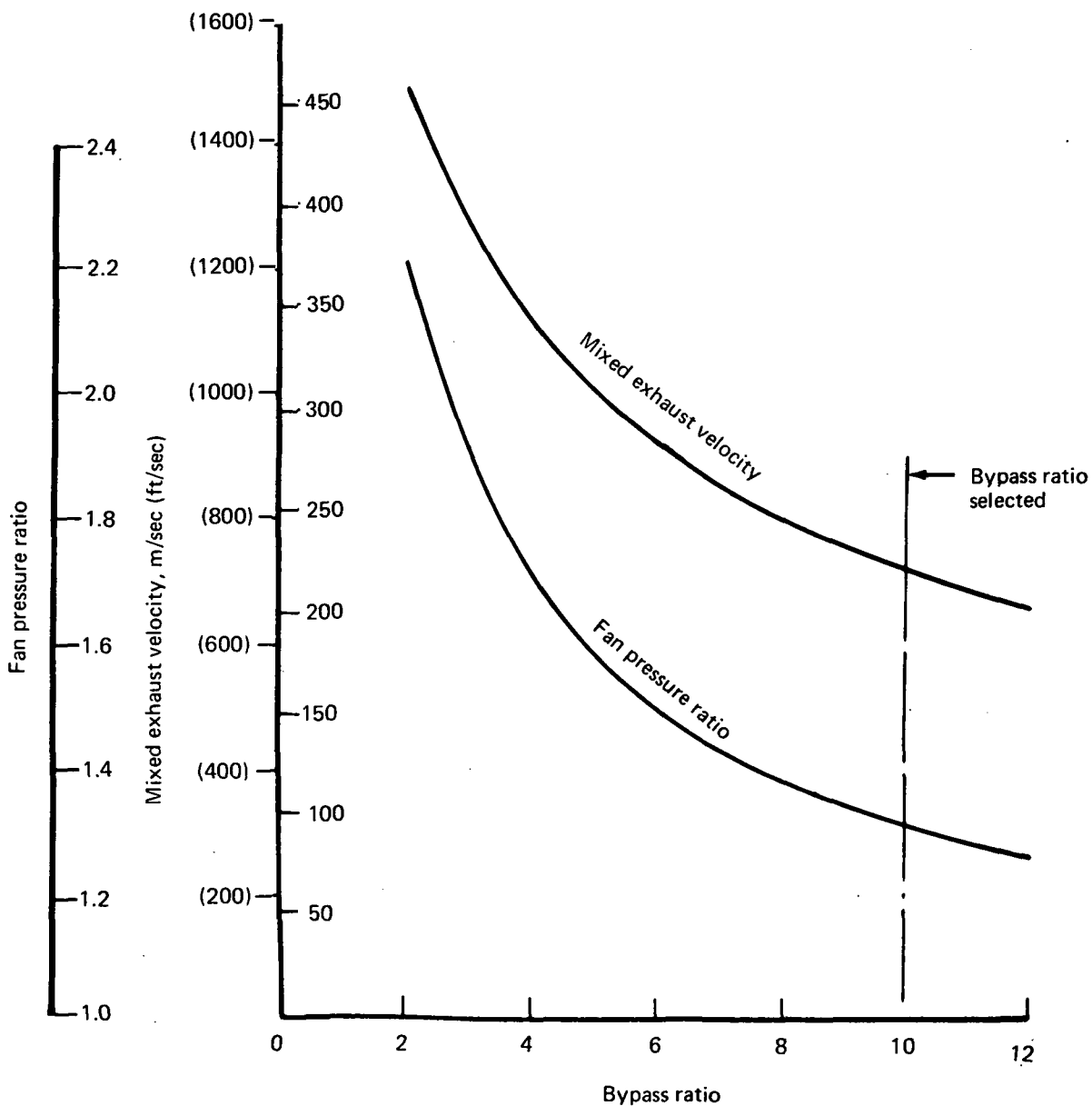


FIGURE 1.—MIXED EXHAUST VELOCITY STUDY, TURBOFAN ENGINES

Field length 610 m (2000 ft)
 Range 926 km (500 nmi)
 Altitude 9150 m (30 000 ft)
 Four engines with upper surface blowing

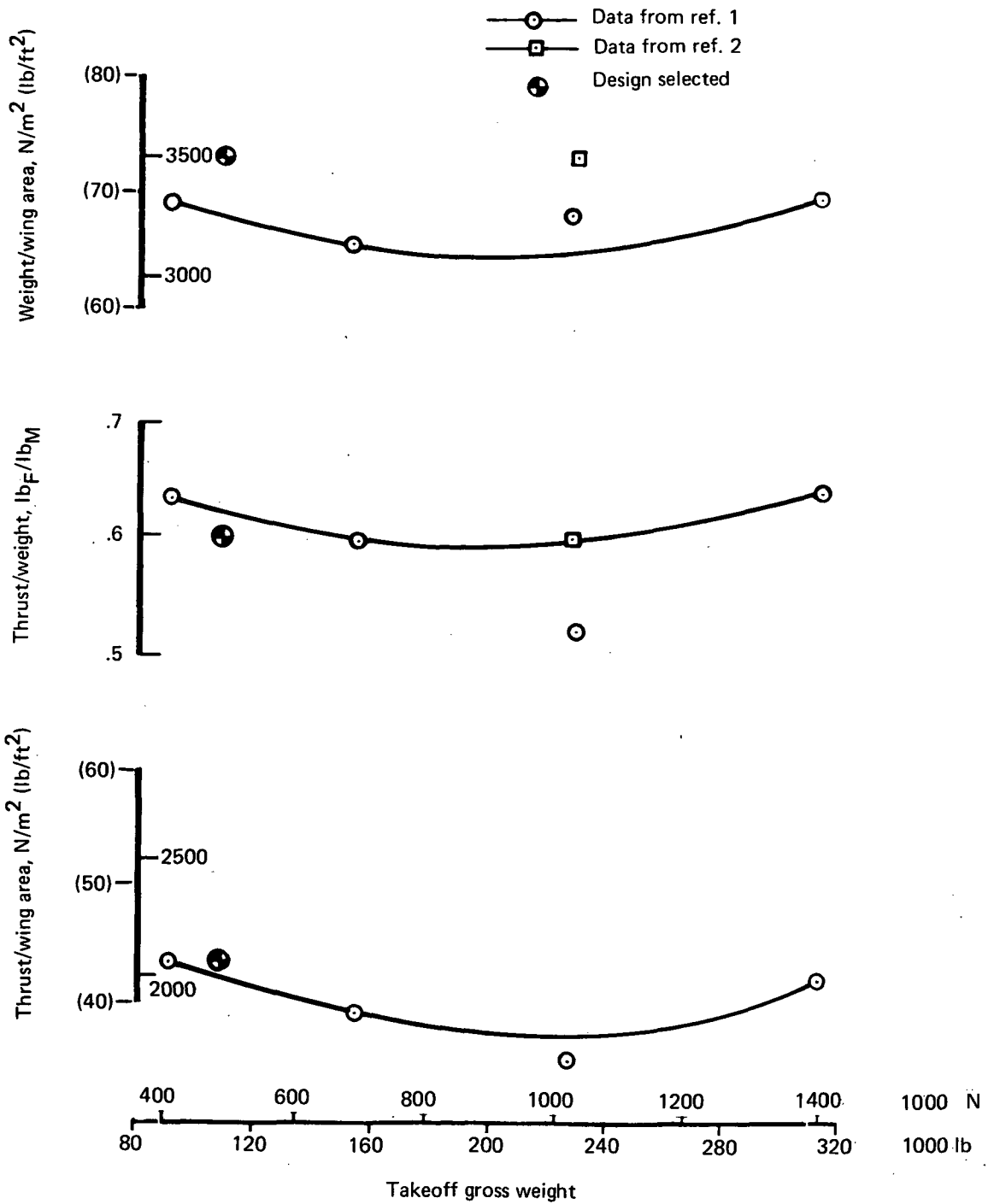


FIGURE 2.—BASIS FOR SELECTION OF ENGINE THRUST

Uninstalled sea level static thrust = 161 560 N (36 320 lb)
Engine airflow = 735 kg/sec (50.4 slugs/sec)
Fan pressure ratio = 1.32
Bypass ratio = 10

Divide all dimensions by $\sqrt{2}$ to obtain engine
dimensions of four-engine airplane

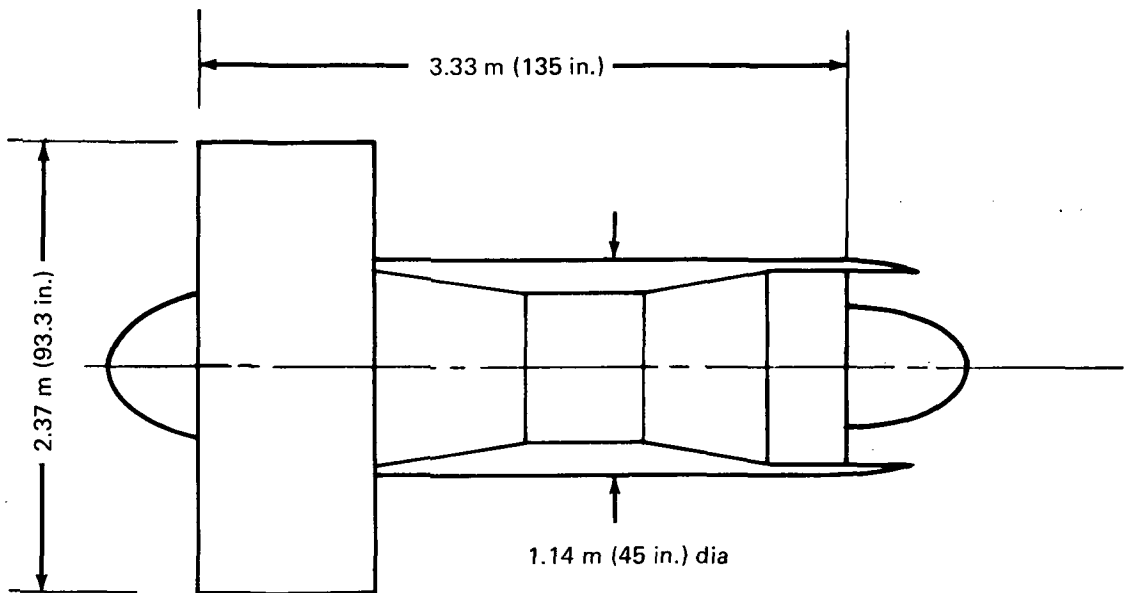


FIGURE 3.—ENGINE OUTLINE, TWO-ENGINE AIRPLANE

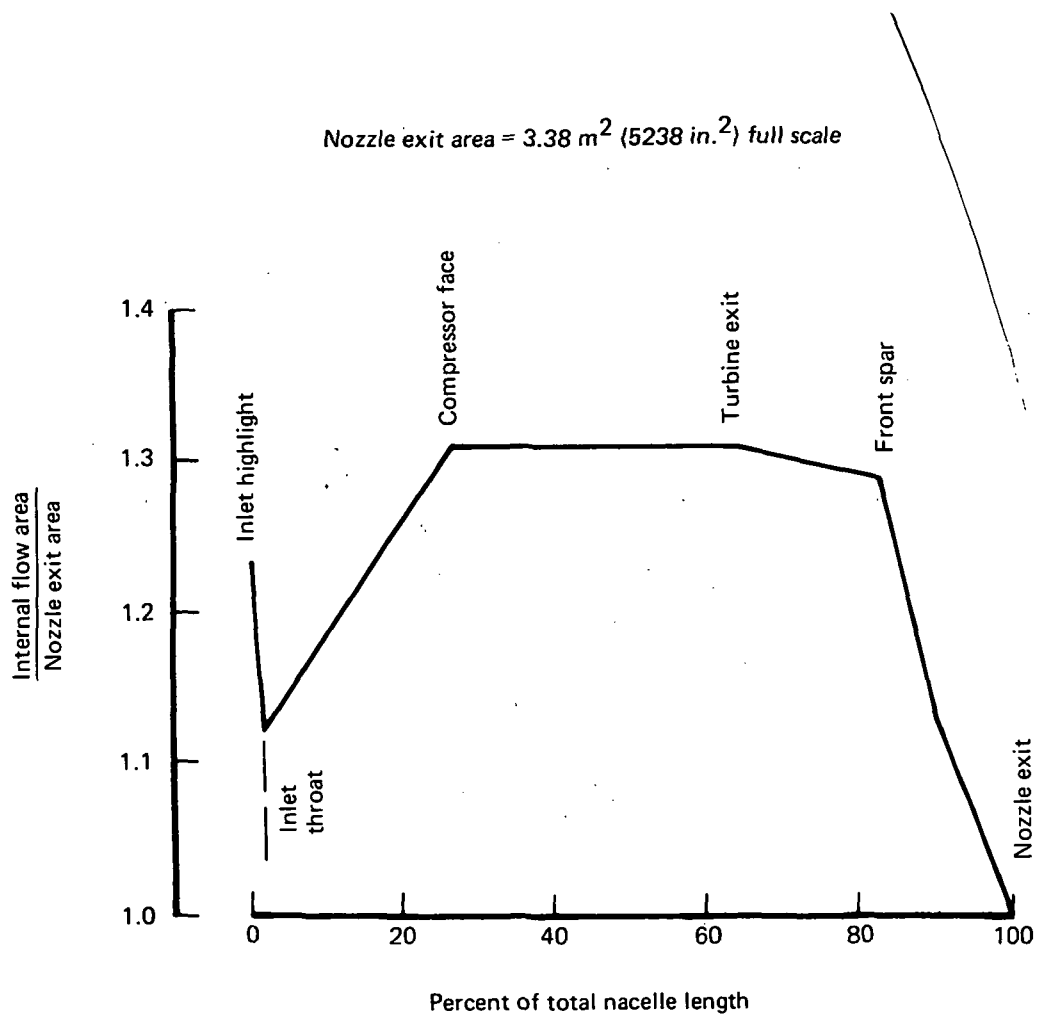


FIGURE 4.—NACELLE-INTERNAL AREA DISTRIBUTION, TWO-ENGINE D-NOZZLE CONFIGURATION

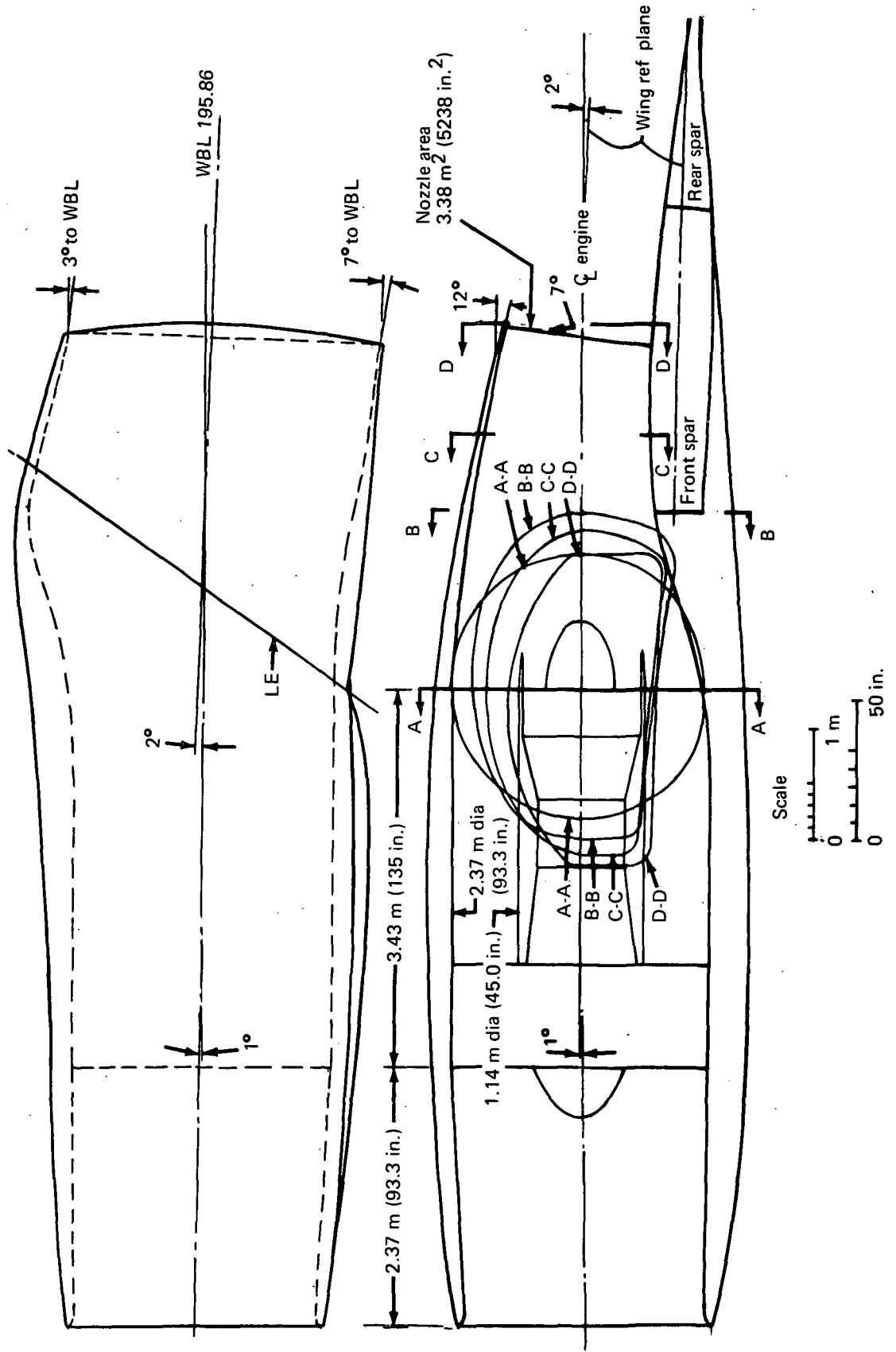


FIGURE 5.—D-NOZZLE NACELLE FOR TWO-ENGINE AIRPLANE

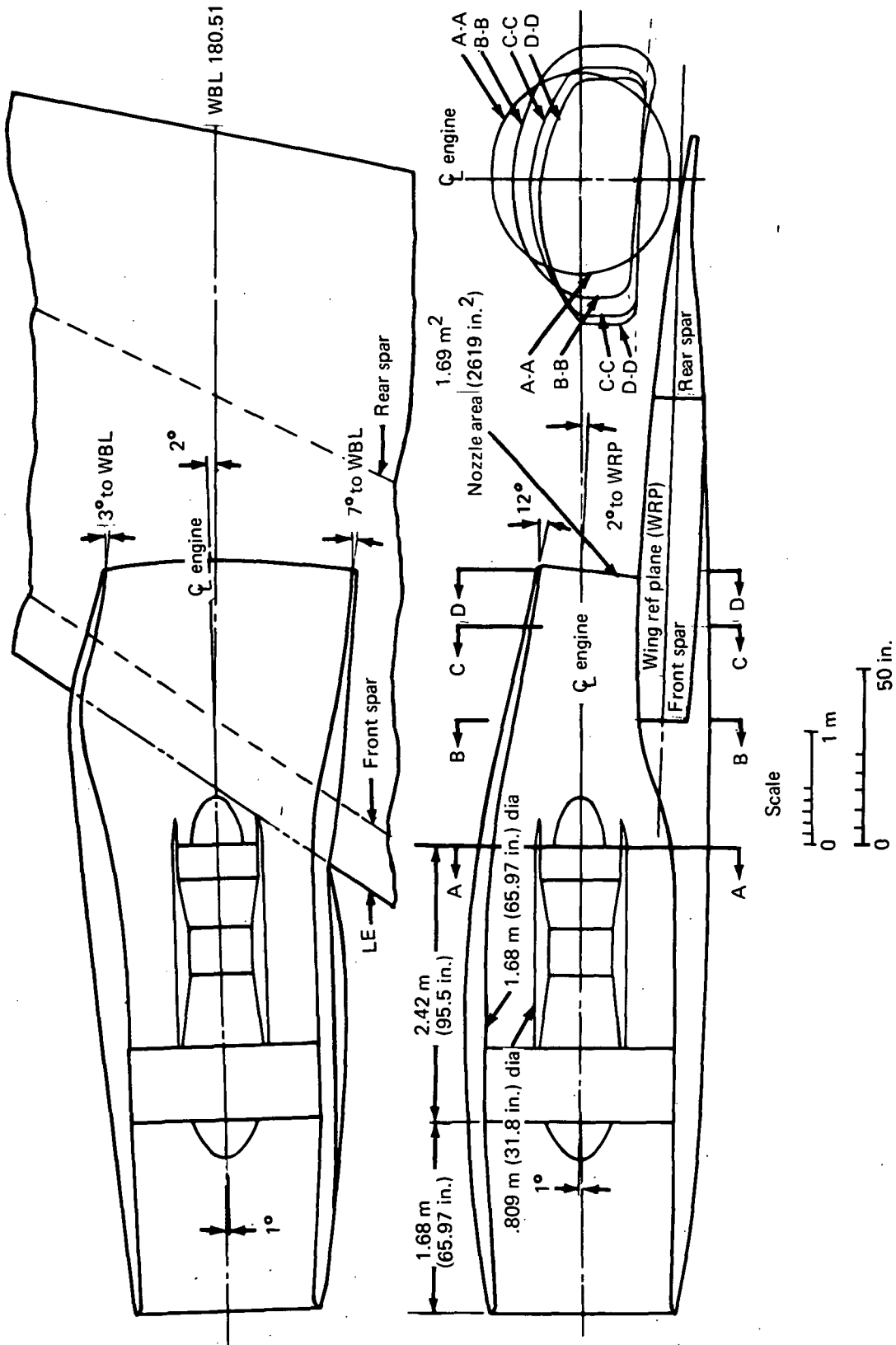
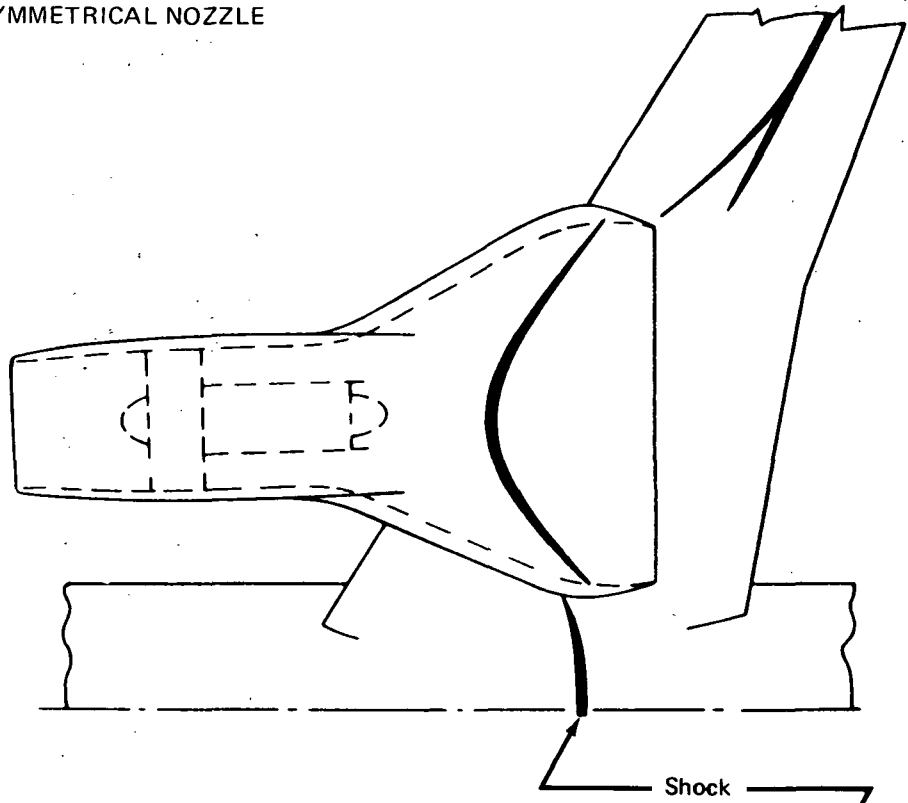


FIGURE 6.-D-NOZZLE NACELLE (INBOARD ENGINE) FOR FOUR-ENGINE AIRPLANE

SYMMETRICAL NOZZLE



OFFSET NOZZLE

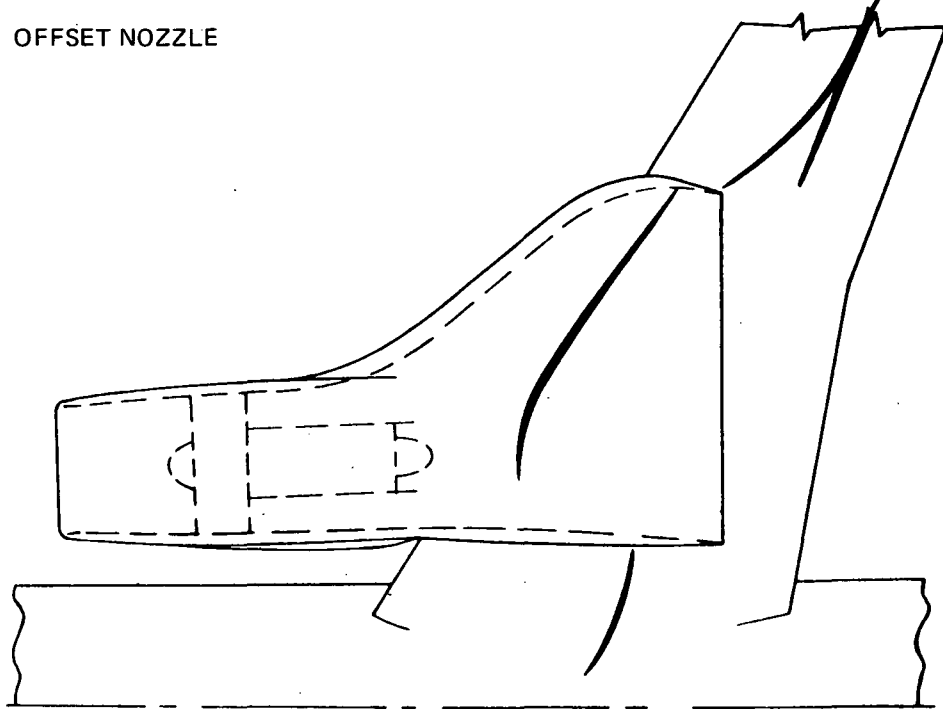


FIGURE 7.—PROBABLE CRUISE SHOCK PATTERNS ON SPREAD NOZZLE NACELLE CONFIGURATIONS

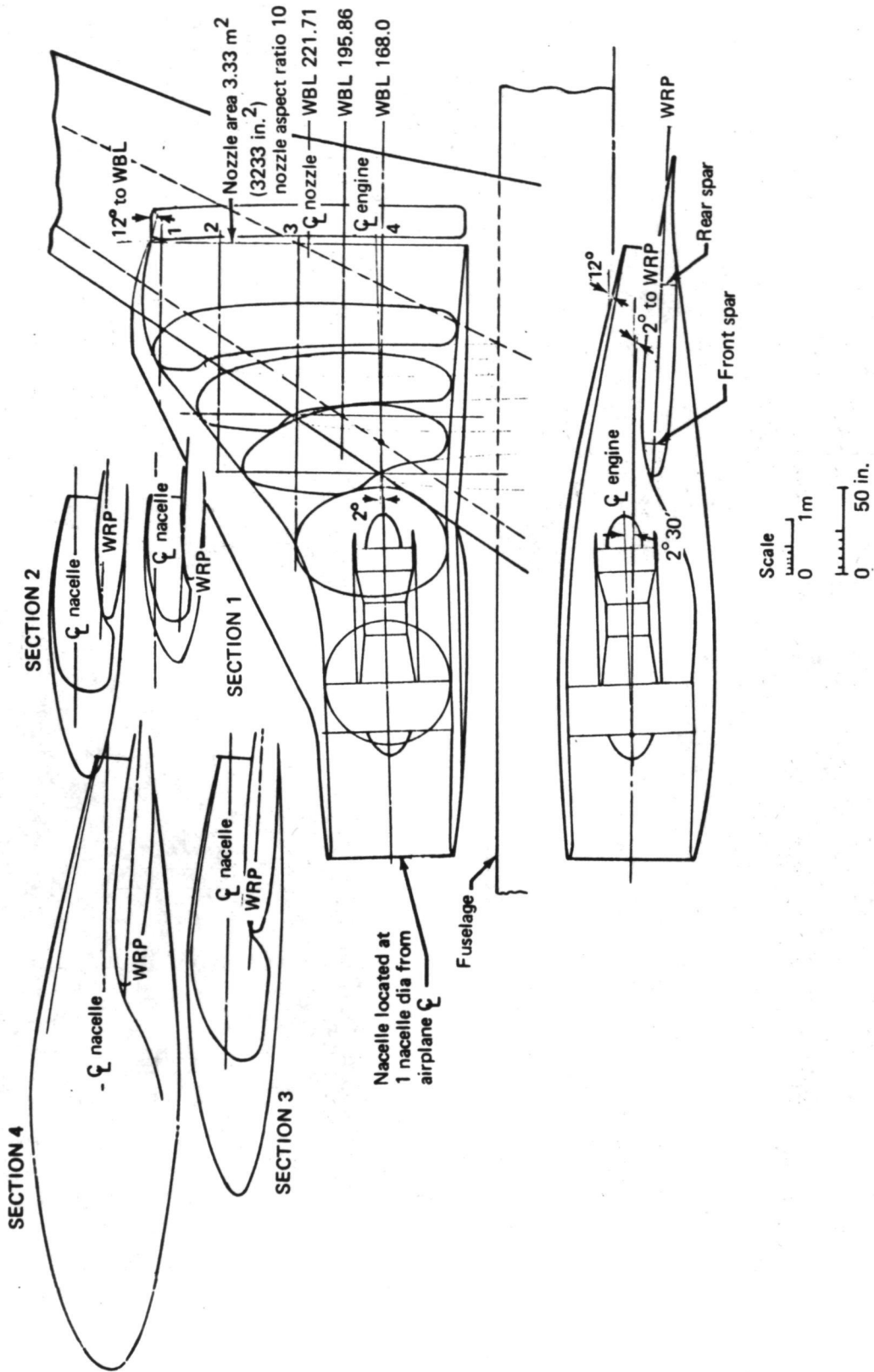


FIGURE 8.—SPREAD NOZZLE NACELLE FOR TWO-ENGINE AIRPLANE

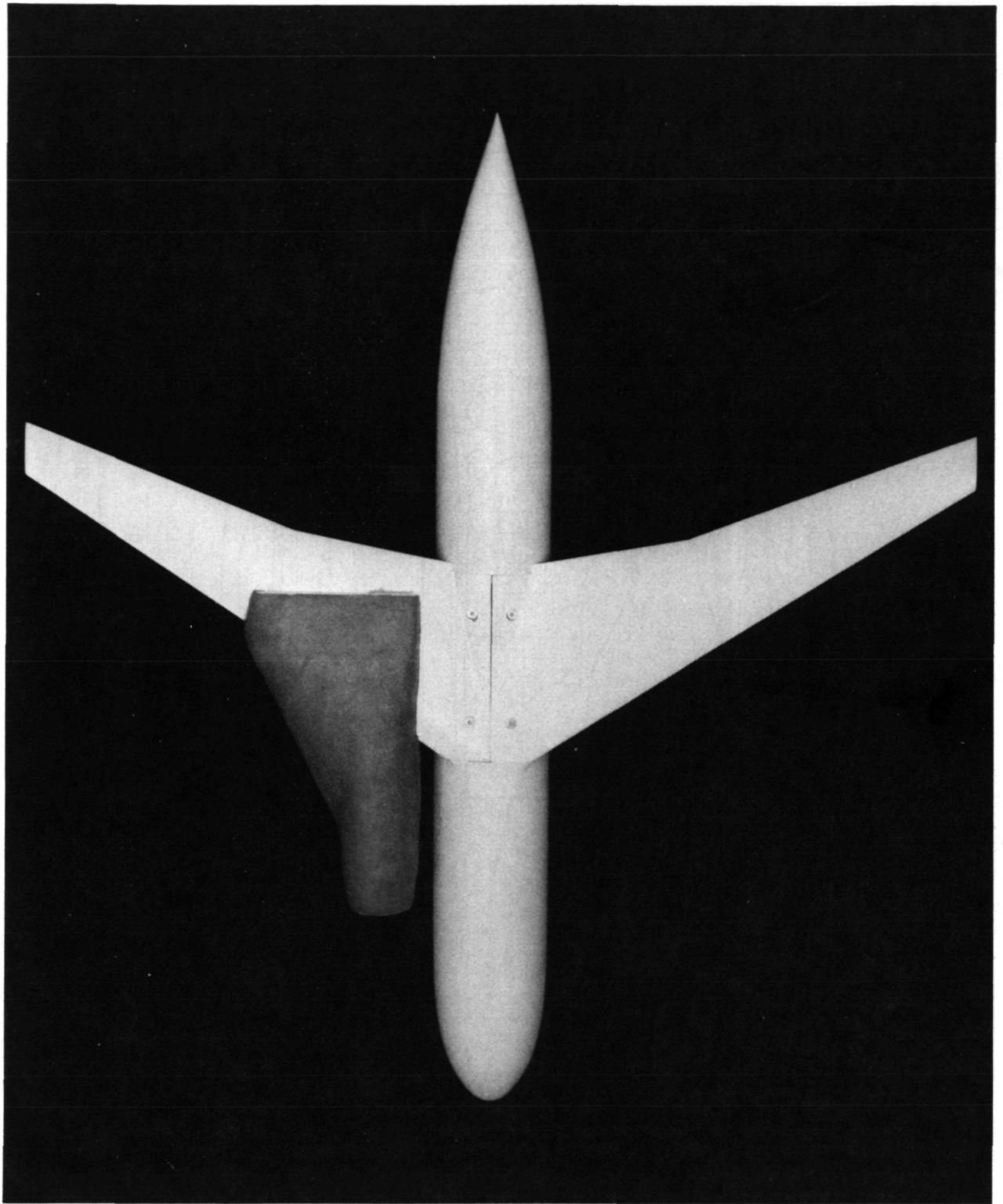


FIGURE 9.—WOODEN VISUALIZATION MODEL WITH CLAY-MOLDED SPREAD NOZZLE NACELLE

Nozzle exit area = 3.38 m² (5238 in.²)

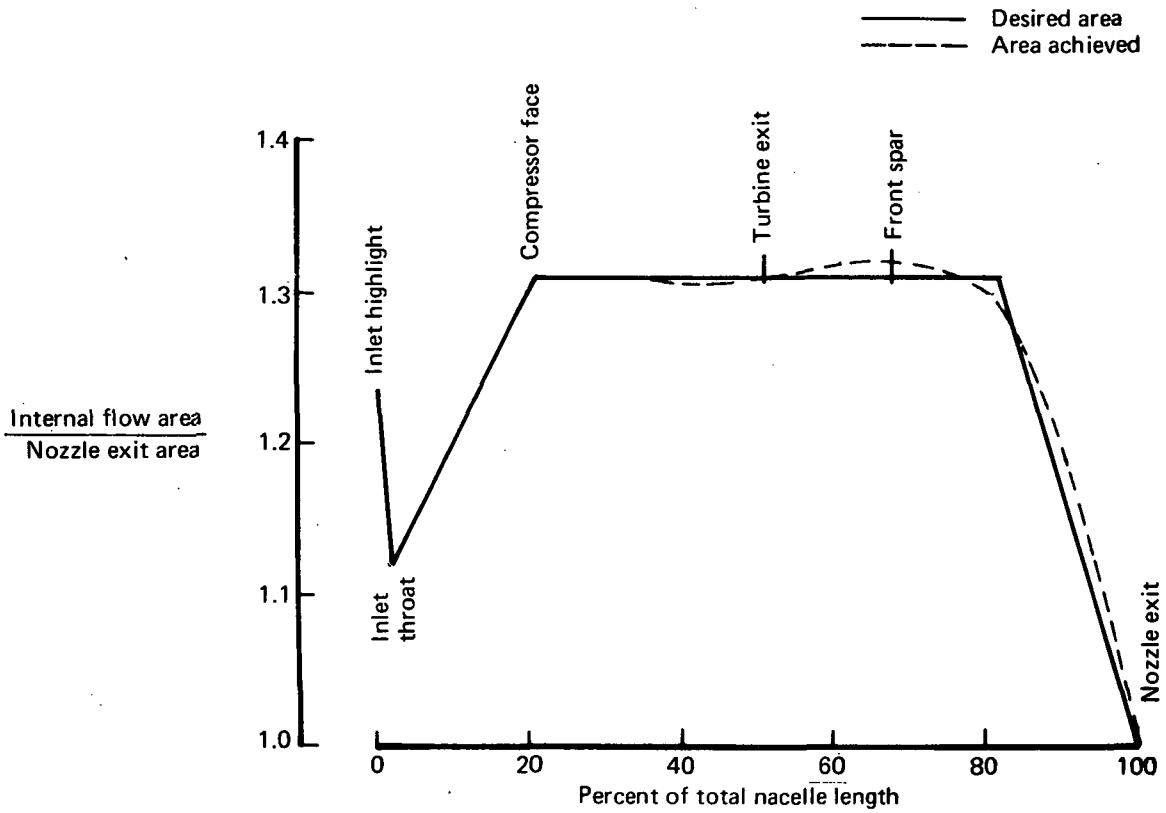


FIGURE 10.—NACELLE INTERNAL AREA DISTRIBUTION, TWO-ENGINE SPREAD NOZZLE

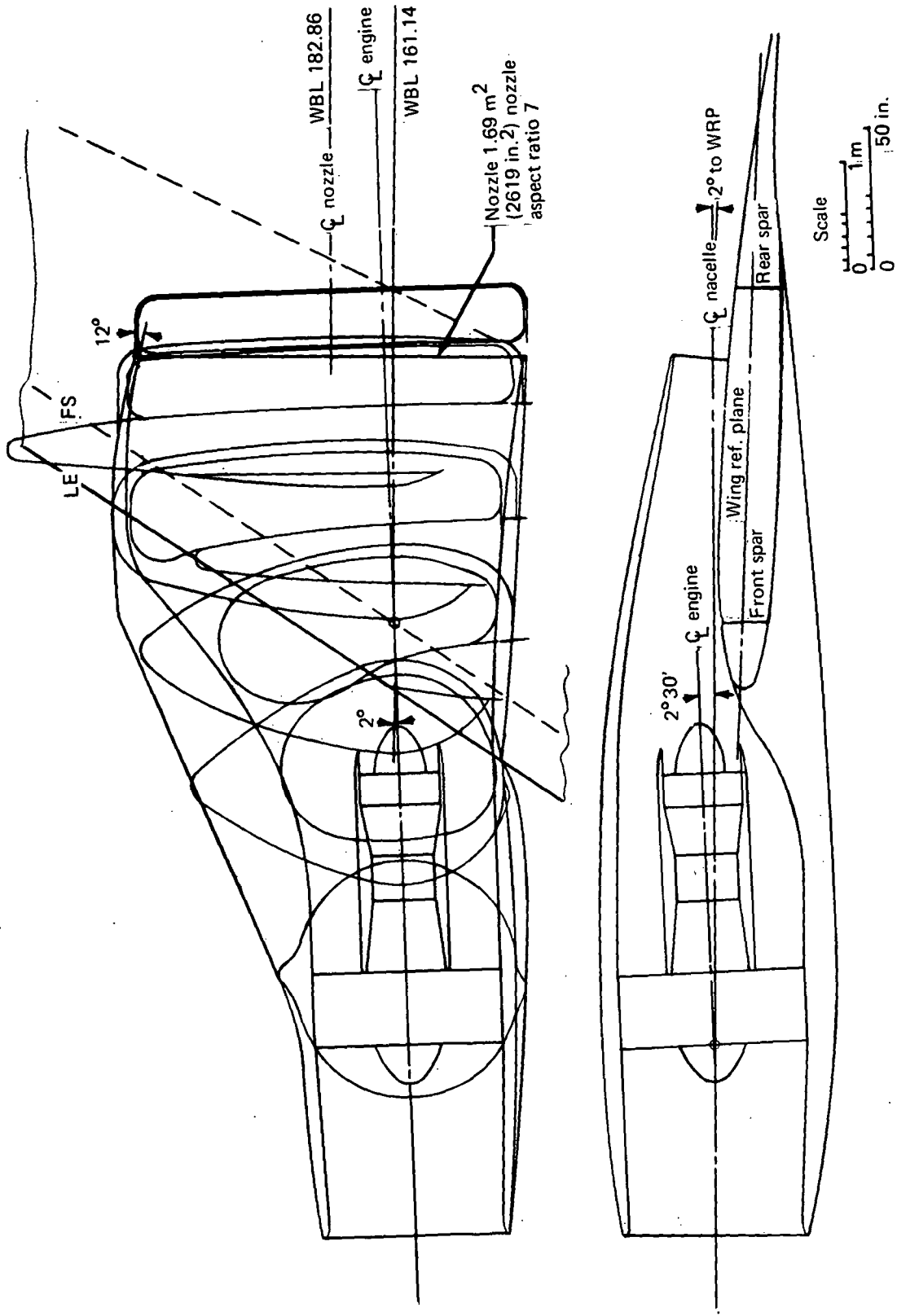


FIGURE 11.—SPREAD NOZZLE NACELLE (INBOARD ENGINE) FOR FOUR-ENGINE AIRPLANE

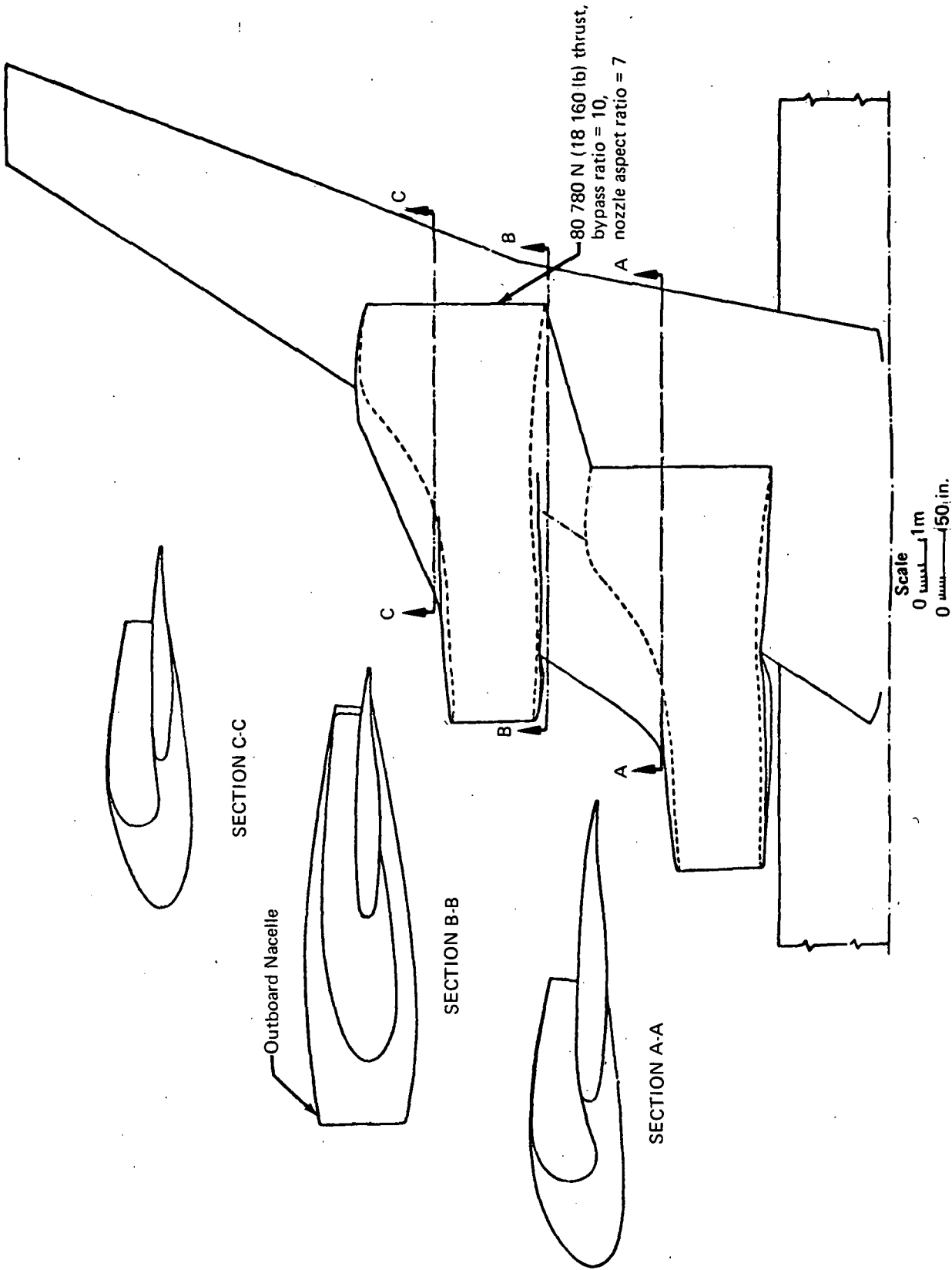


FIGURE 12.--SPREAD NOZZLE NACELLES FOR FOUR-ENGINE AIRPLANE

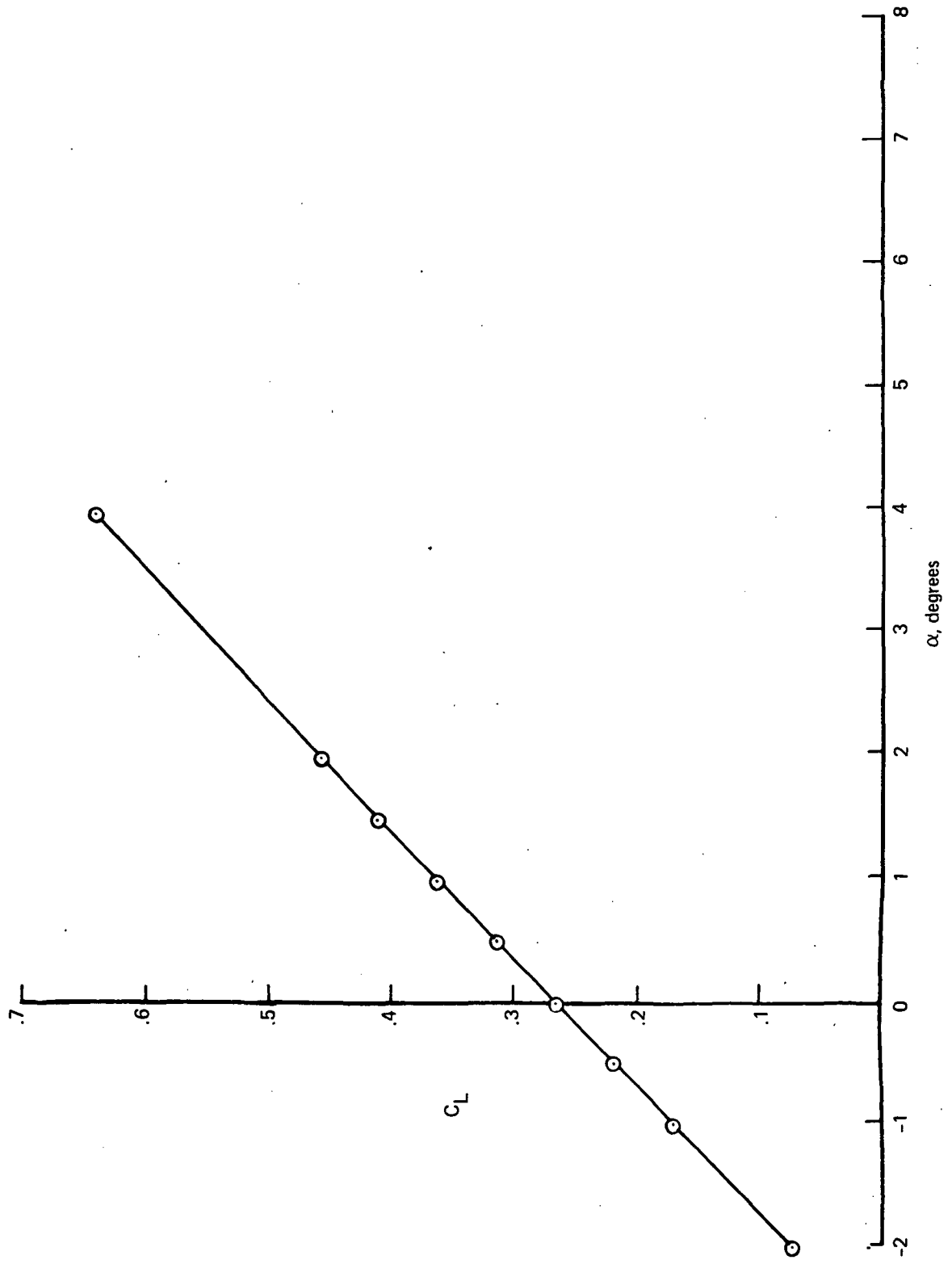


FIGURE 13.—LIFT CURVE, WING-BODY ALONE, POTENTIAL FLOW ANALYSIS, $M_\infty = 0.7$

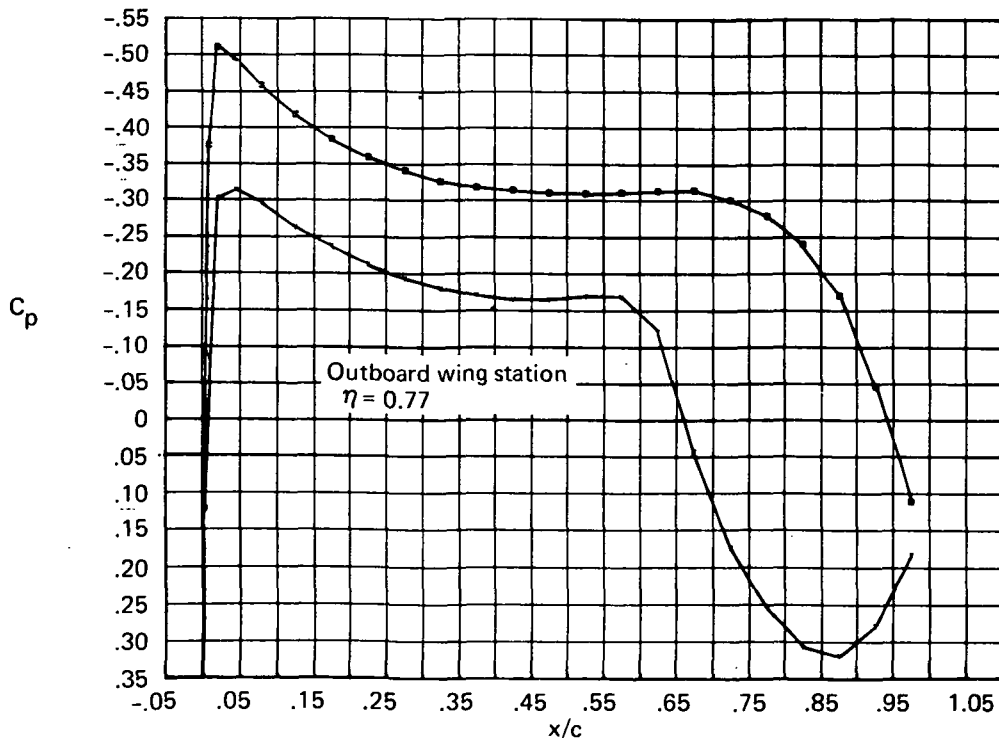
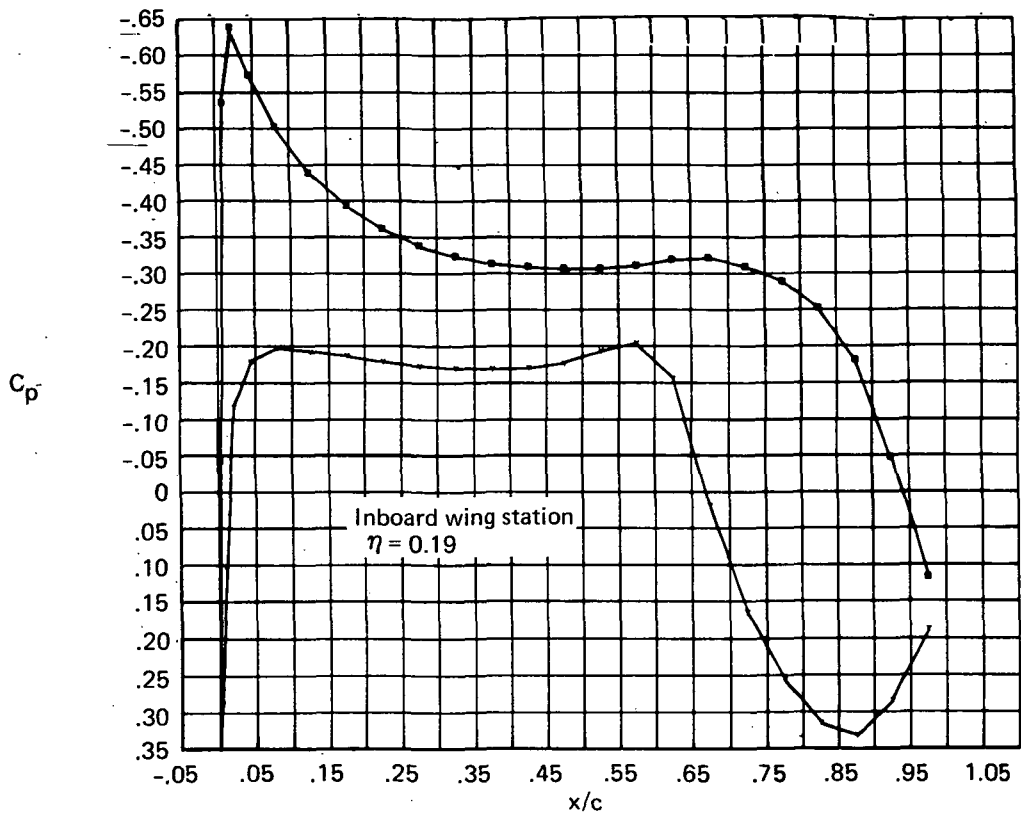


FIGURE 14.—STREAMWISE C_p DISTRIBUTIONS, POTENTIAL FLOW ANALYSIS,
 $\alpha = 0^\circ$, $M_\infty = 0.7$, WING-BODY CONFIGURATION

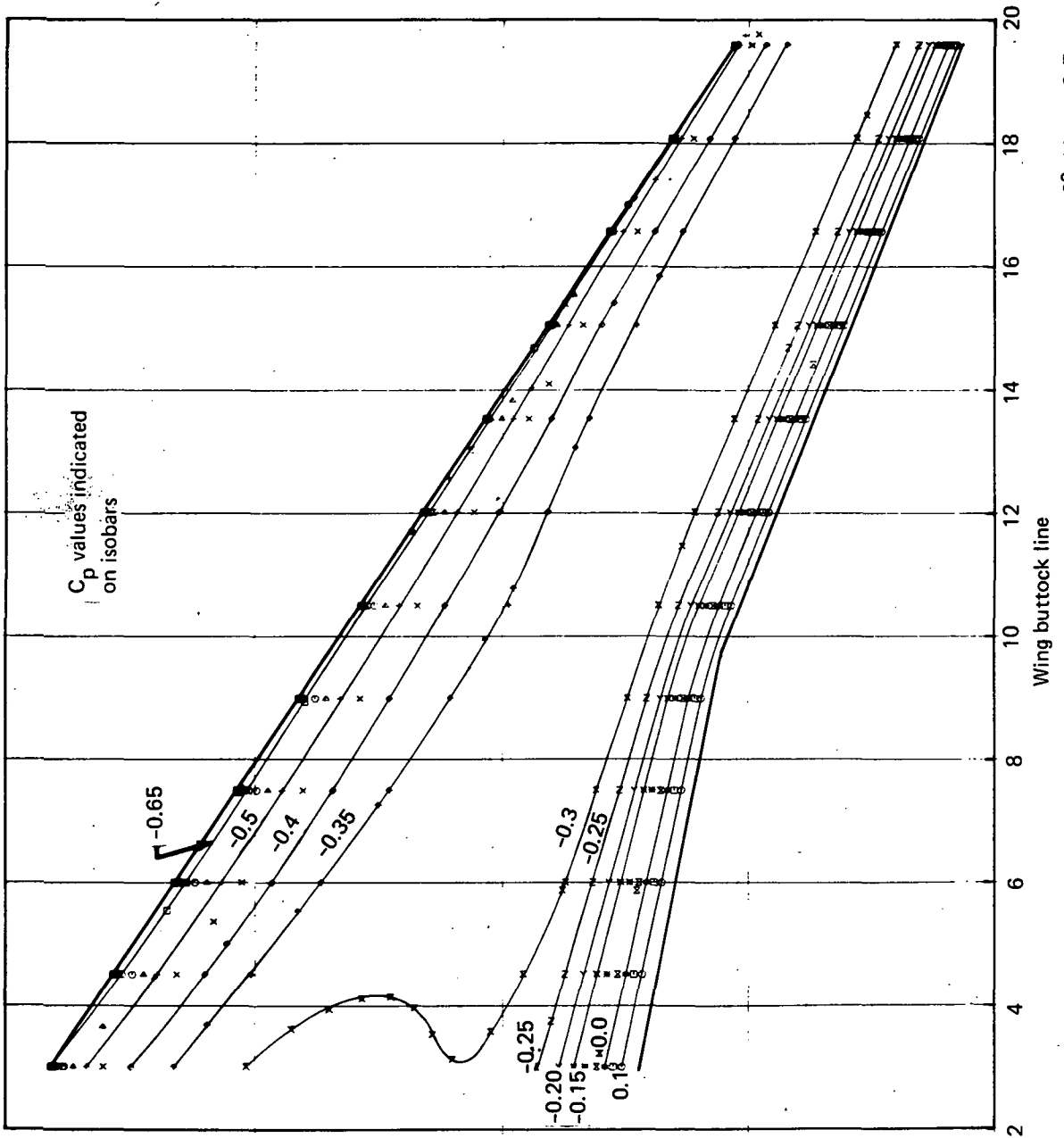


FIGURE 15.—UPPER SURFACE ISOBARS FROM ANALYSIS OF WING-BODY, $\alpha=0^\circ$, $M_\infty=0.7$

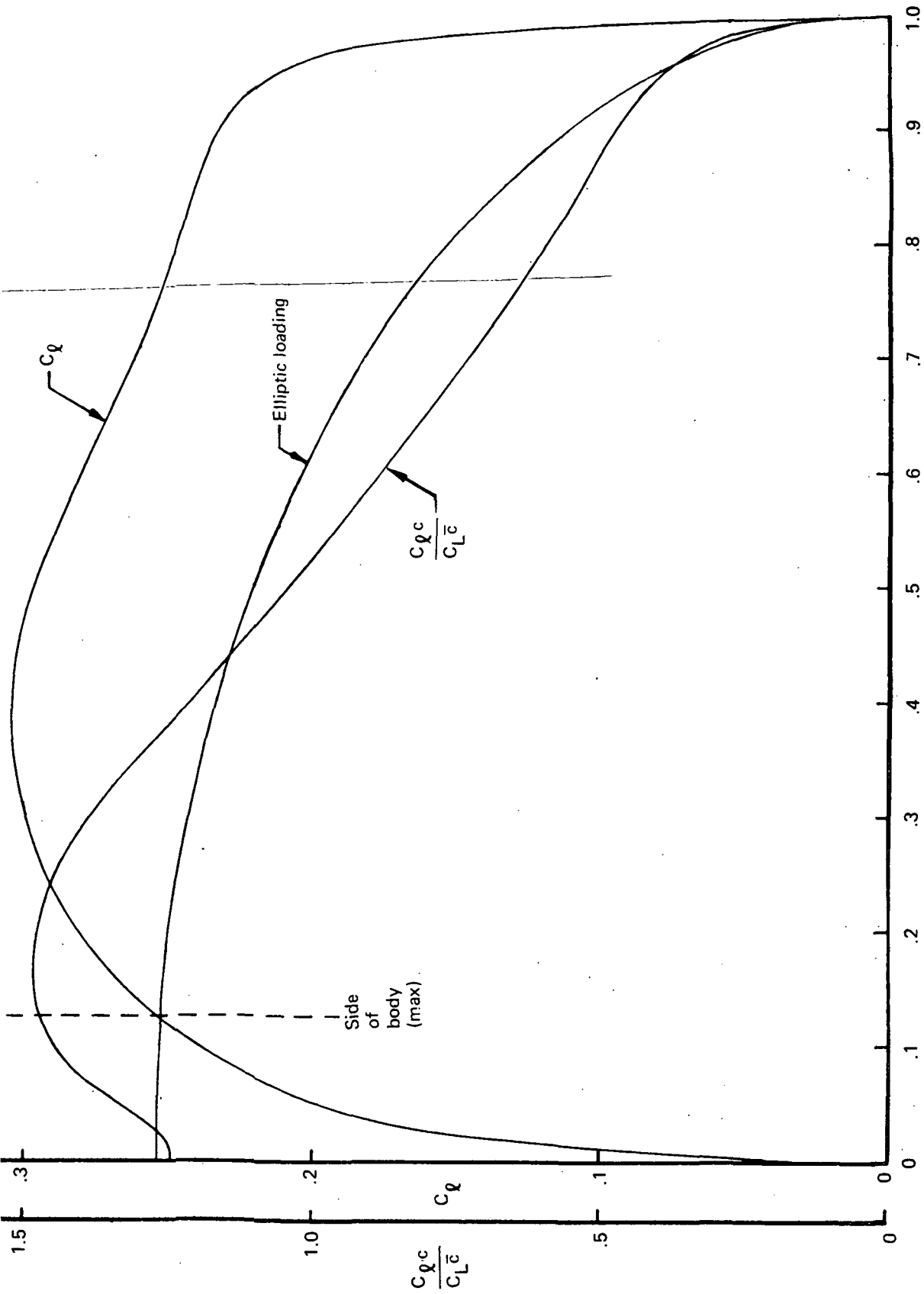


FIGURE 16.—SPAN LOAD AND SECTIONAL LIFT DISTRIBUTIONS, WING-BODY, $\alpha = 0^\circ$, $M_\infty = 0.7$

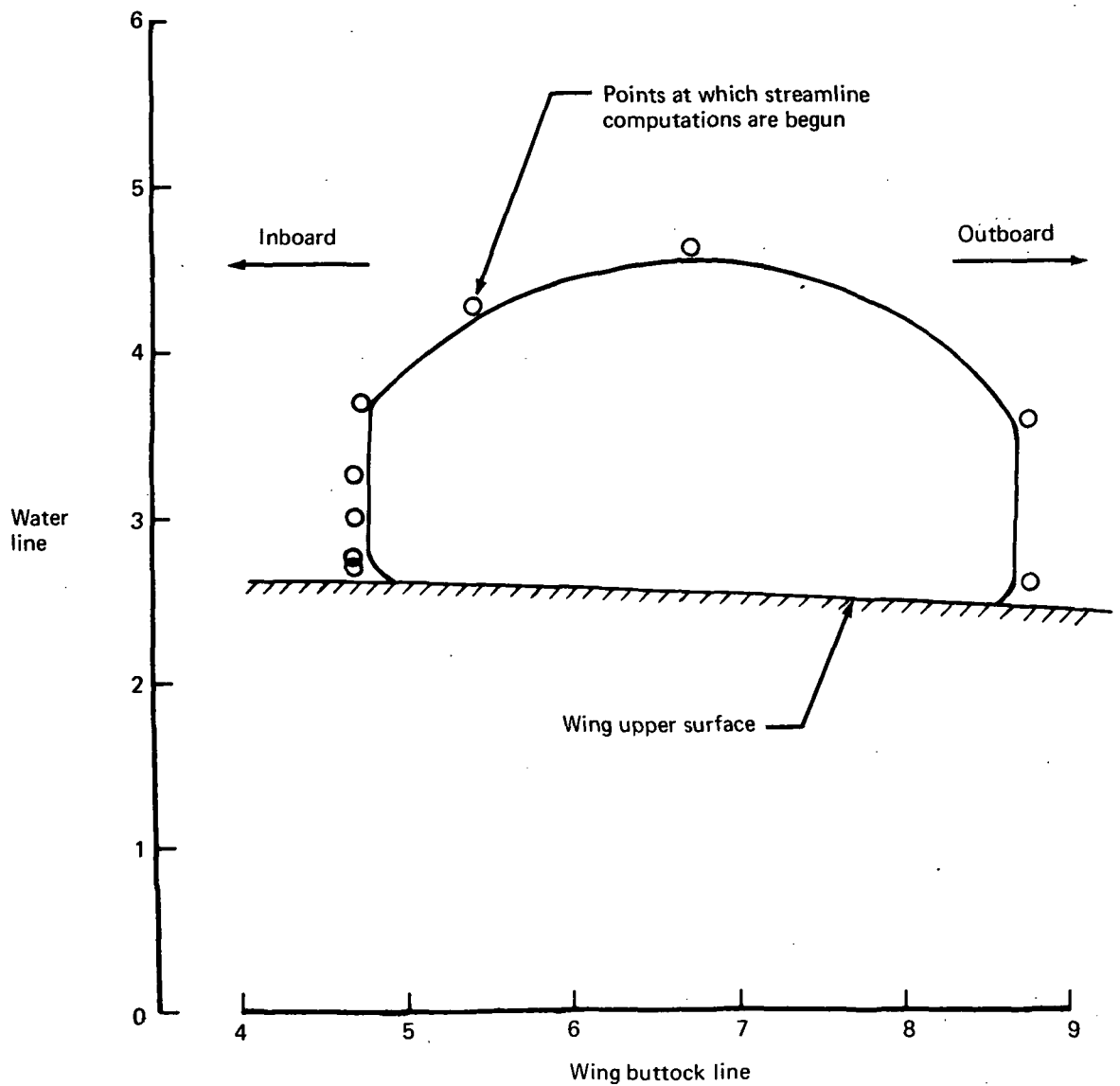


FIGURE 17.—STARTING POINTS AROUND NACELLE EXIT PLANE FOR CALCULATION OF NINE STREAMLINES IN POTENTIAL FLOW ANALYSIS, TWO-ENGINE D-NOZZLE CASE

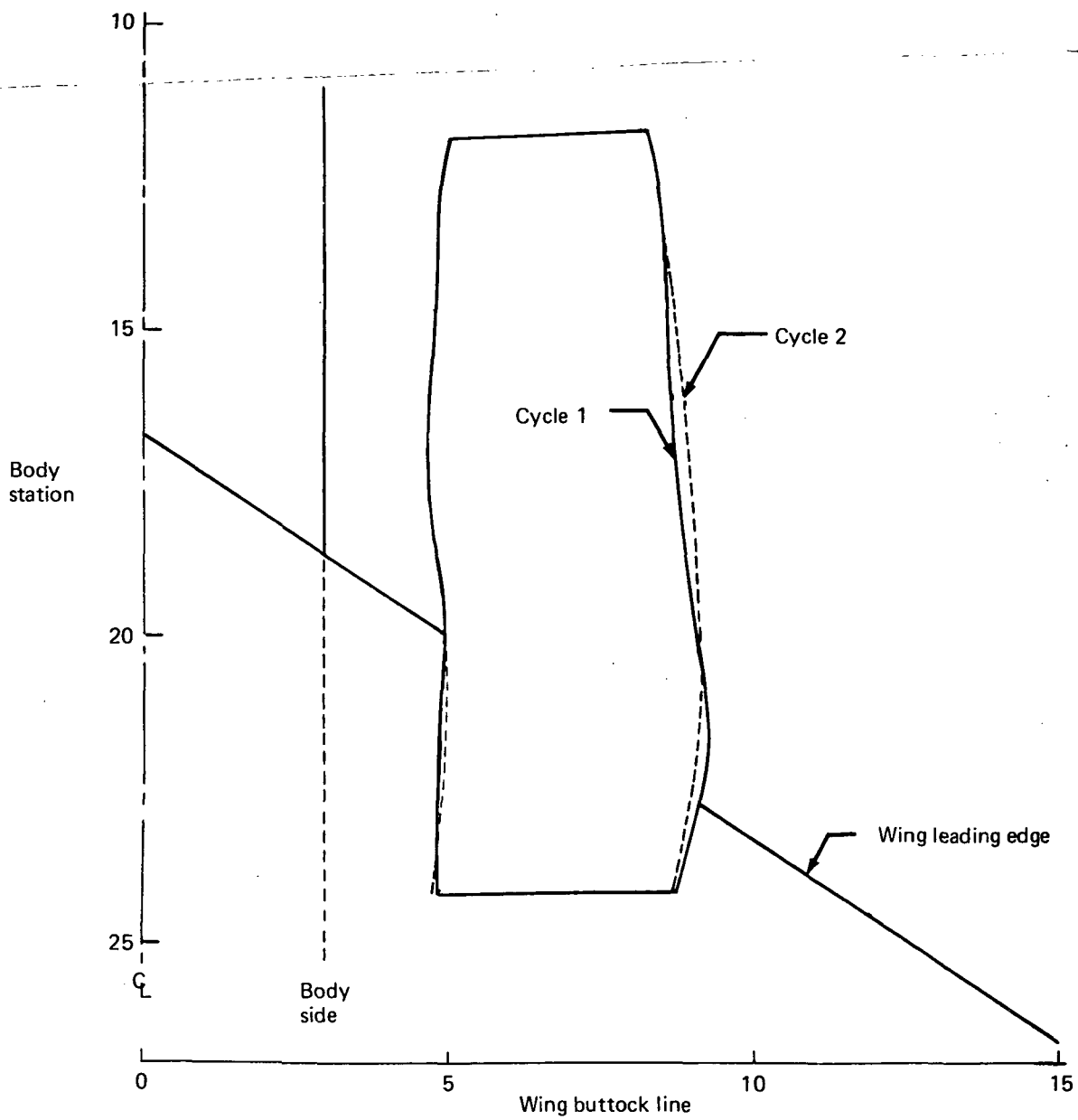


FIGURE 18.—D-NOZZLE NACELLE, TWO-ENGINE AIRPLANE

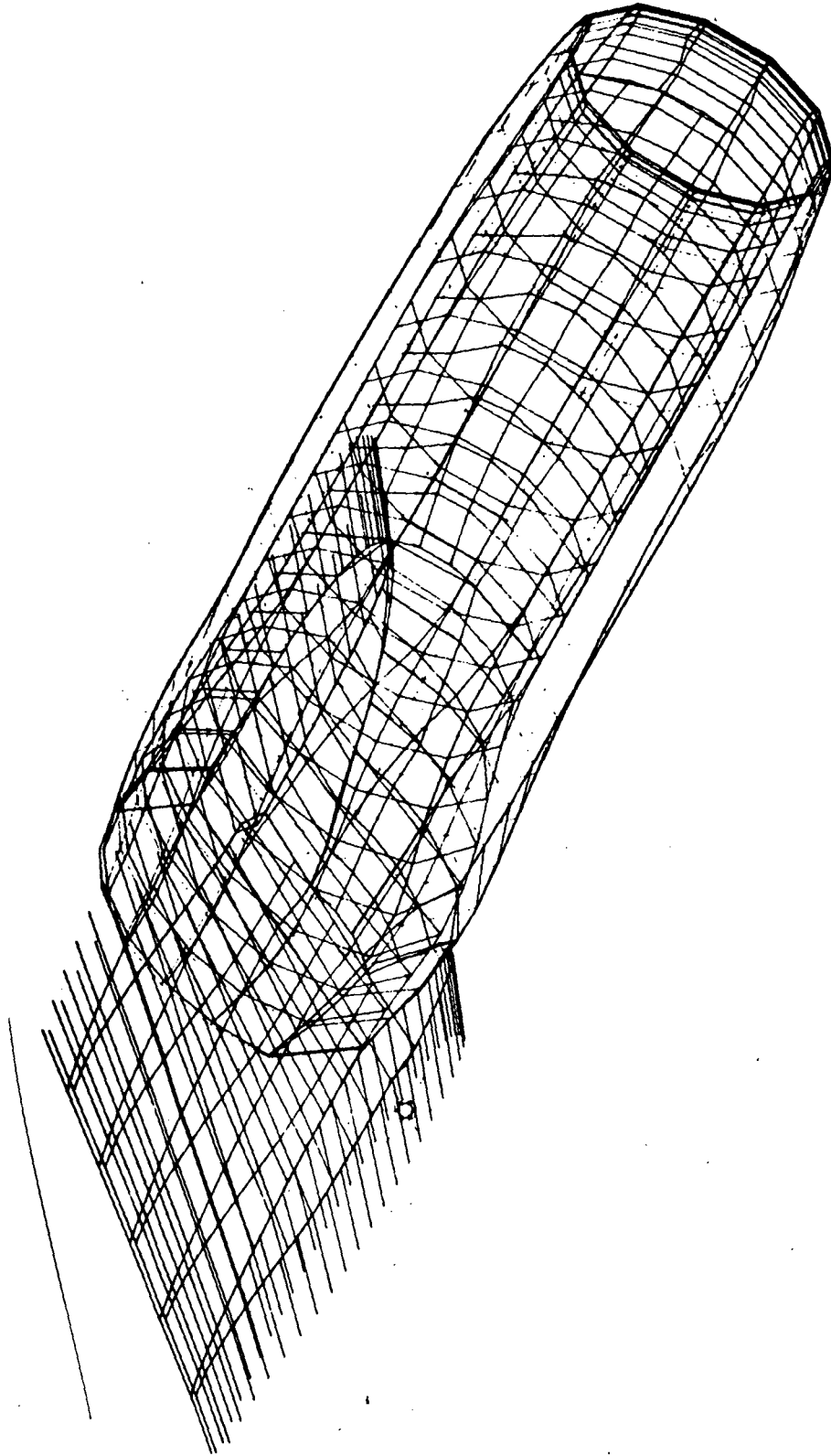
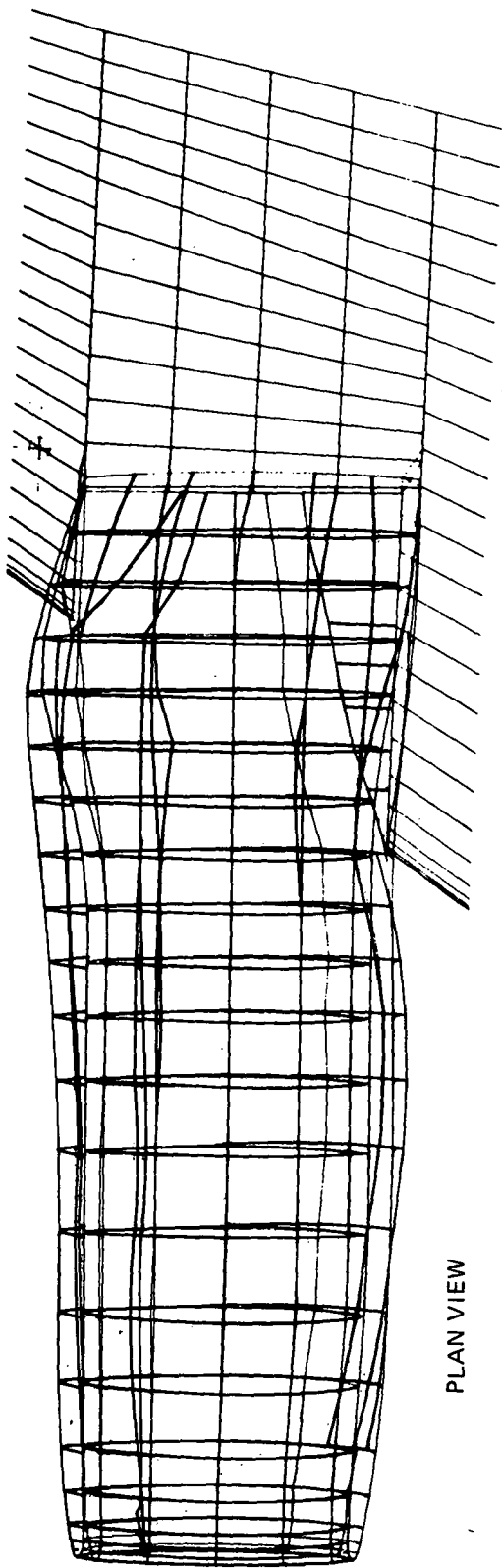
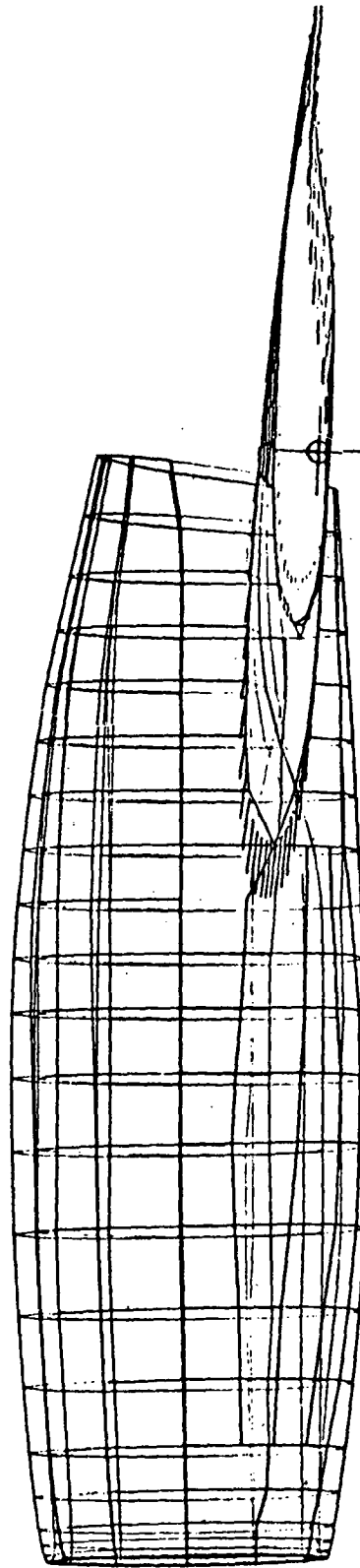


FIGURE 19.—NACELLE SURFACE PANELING, TWO-ENGINE D-NOZZLE CASE (ISOMETRIC VIEW)



PLAN VIEW



SIDE VIEW

FIGURE 20.—NACELLE SURFACE PANELING, TWO-ENGINE D-NOZZLE CASE (PLAN AND SIDE VIEWS)

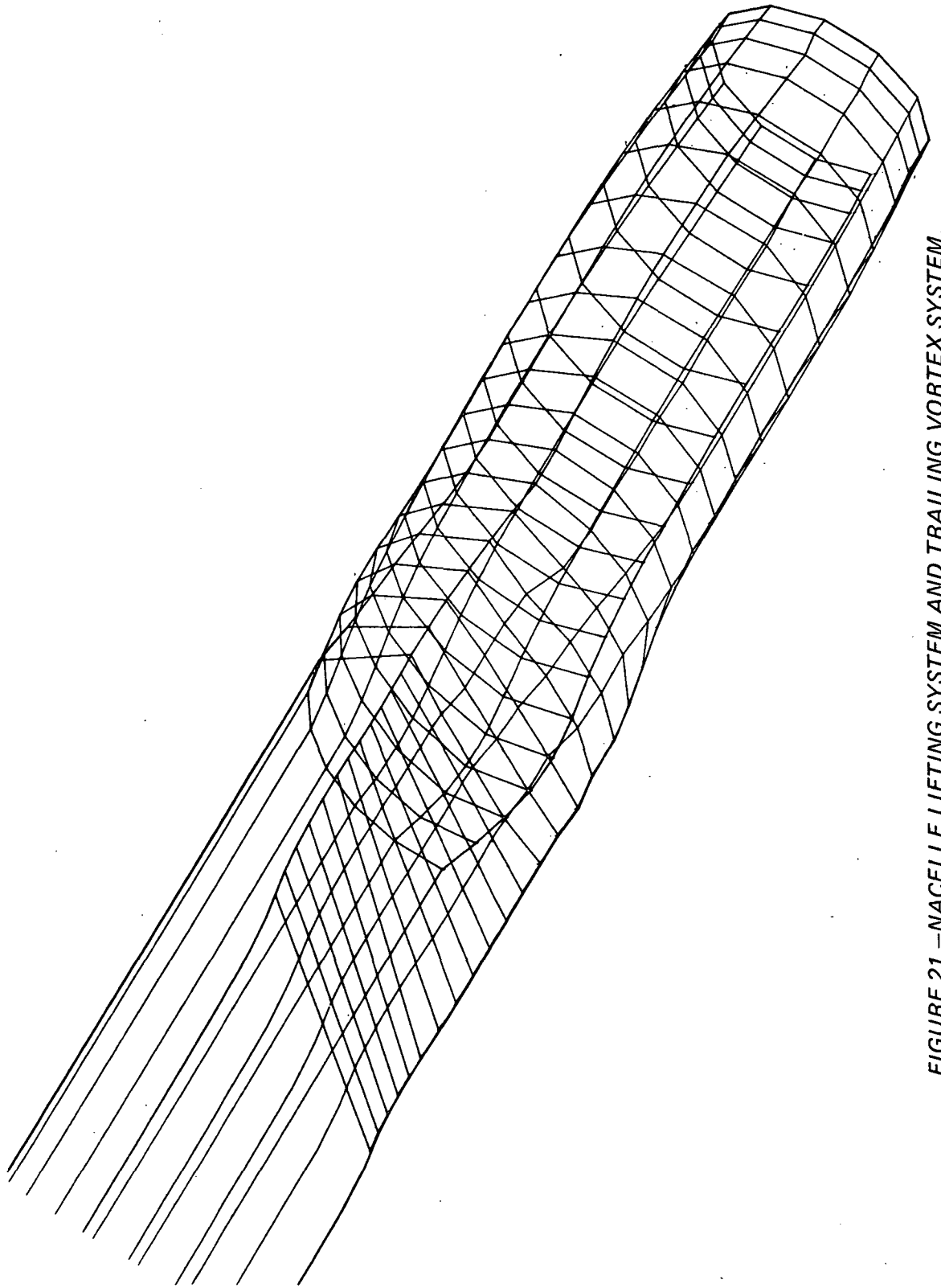


FIGURE 21.—NACELLE LIFTING SYSTEM AND TRAILING VORTEX SYSTEM,
TWO-ENGINE D-NOZZLE CASE

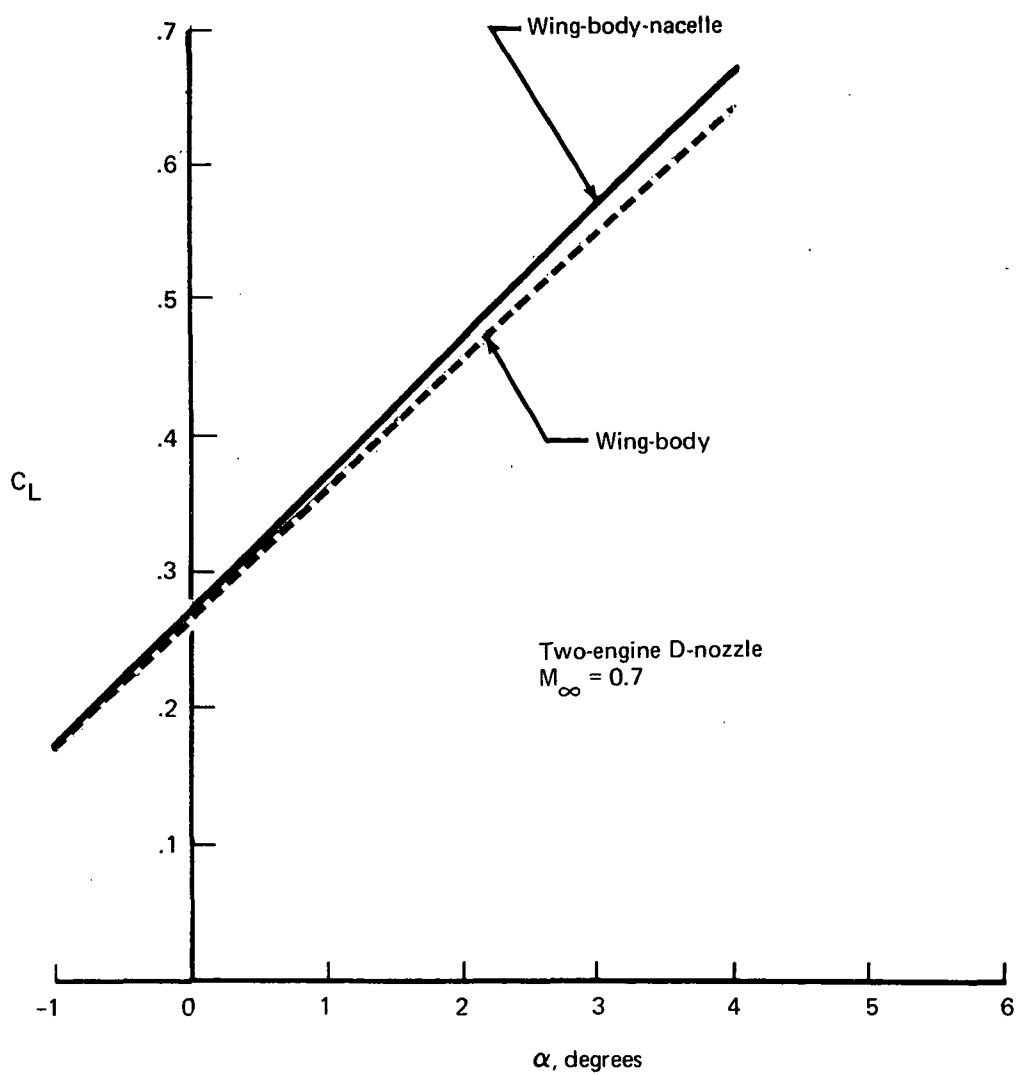


FIGURE 22.—EFFECT OF NACELLE ON LIFT CURVE

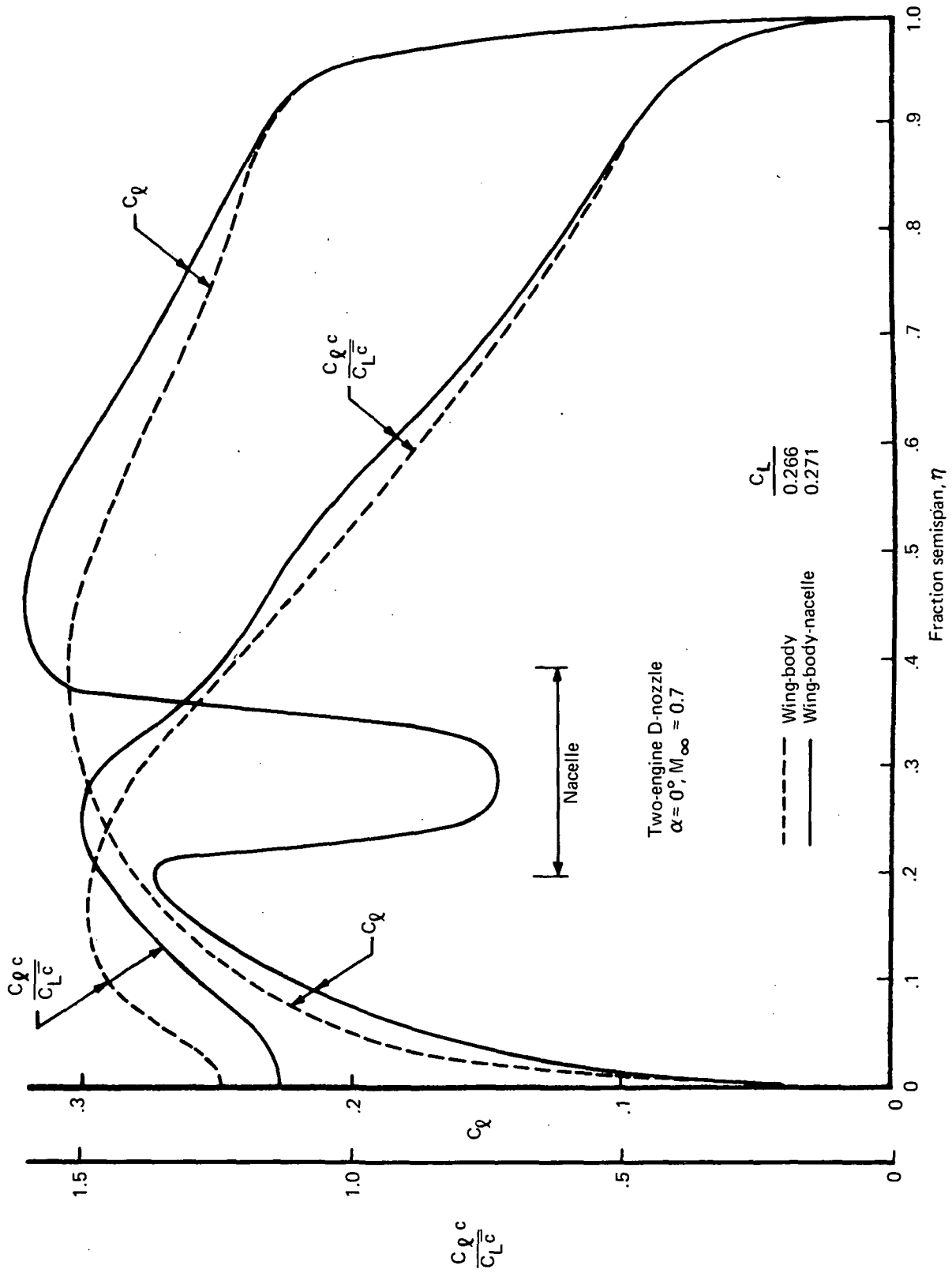


FIGURE 23.—EFFECT OF NACELLE ON WING LOAD DISTRIBUTION AND SECTIONAL LIFT DISTRIBUTION

$\alpha = 0^\circ$
 $M_\infty = 0.7$

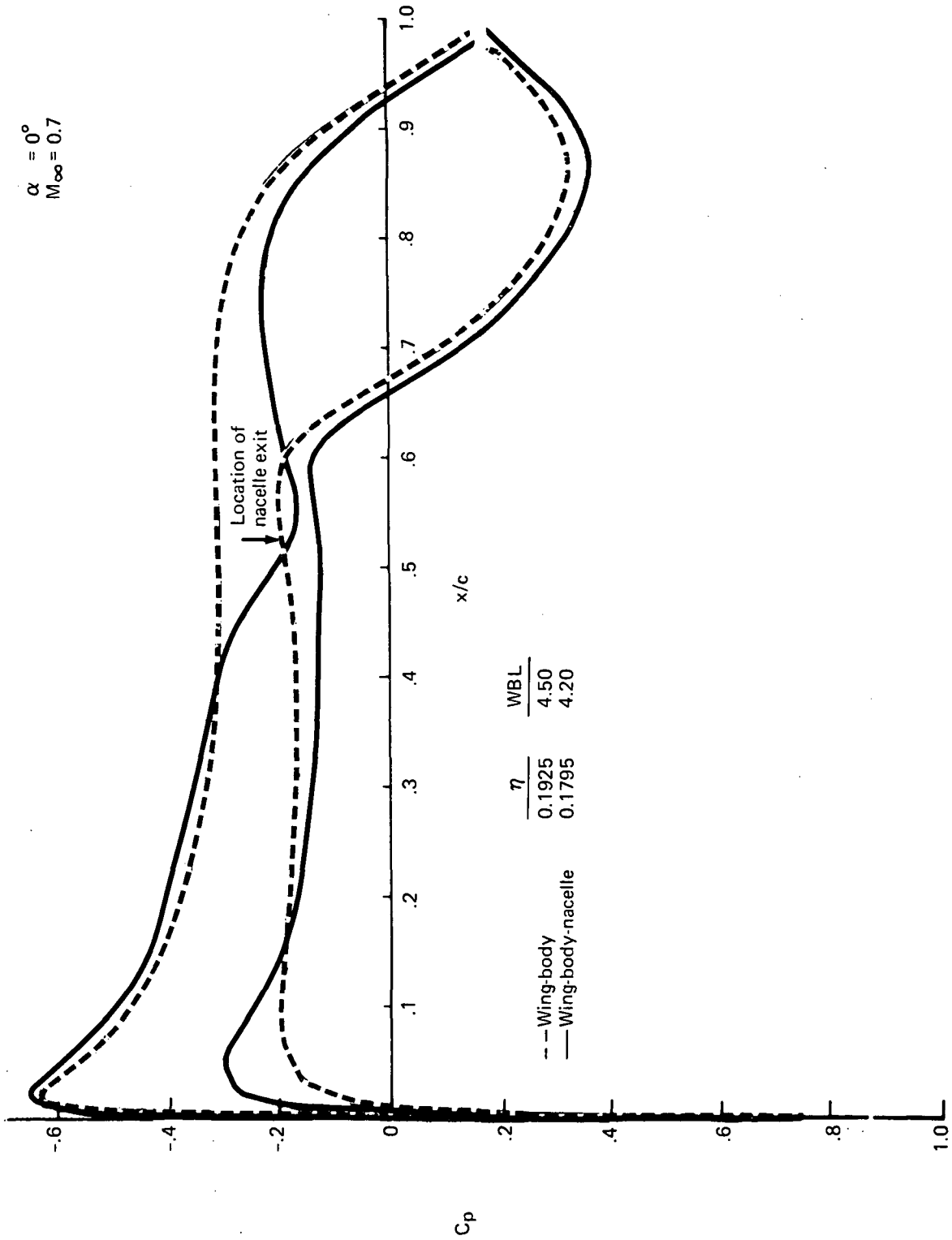


FIGURE 24.—EFFECT OF NACELLE ON WING PRESSURES INBOARD OF NACELLE, TWO-ENGINE D-NOZZLE CASE

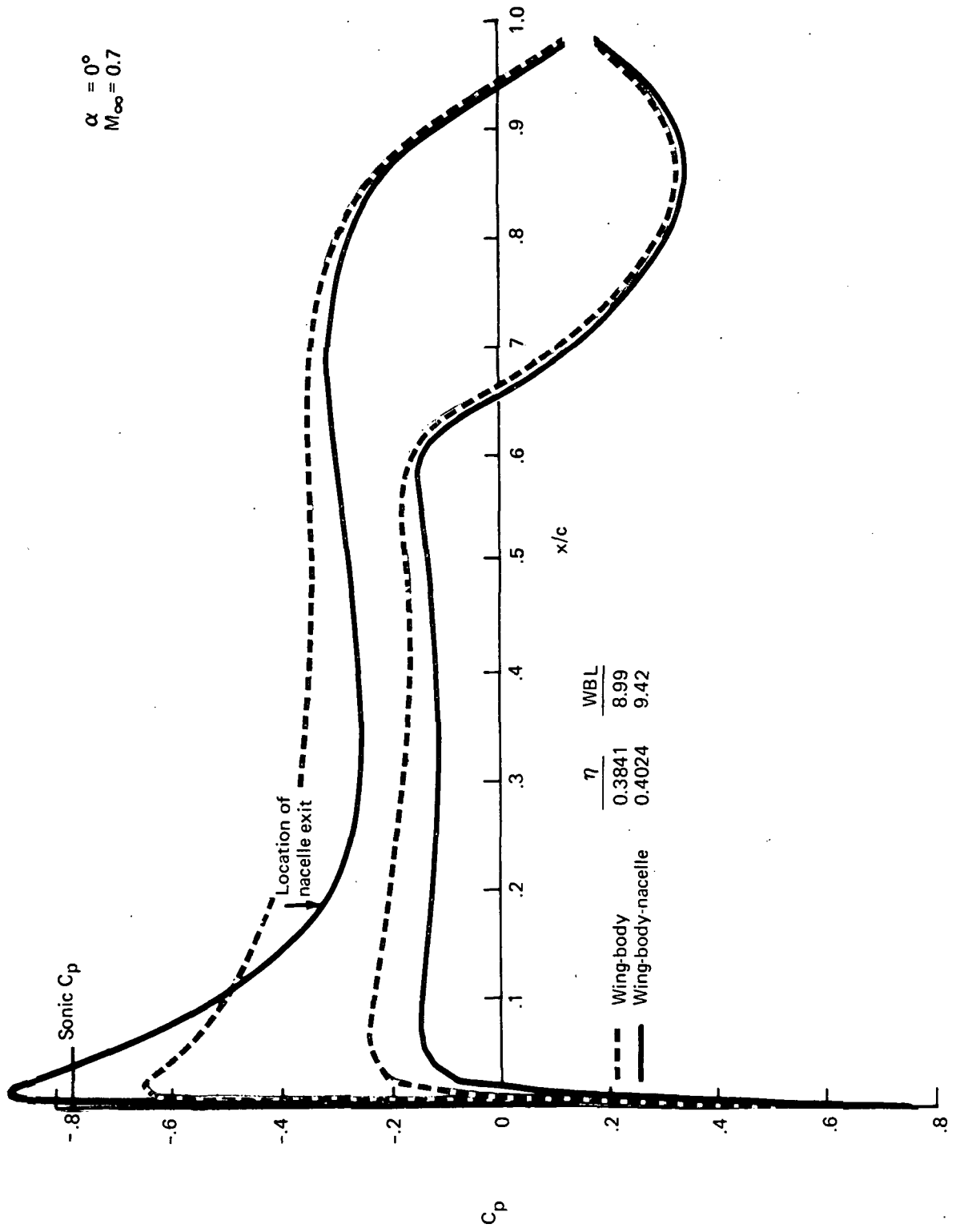


FIGURE 25.—EFFECT OF NACELLE ON WING PRESSURES OUTBOARD OF NACELLE, TWO-ENGINE D-NOZZLE CASE.

Two-engine D-nozzle
 $\alpha = 0^\circ$
 $M_\infty = 0.7$

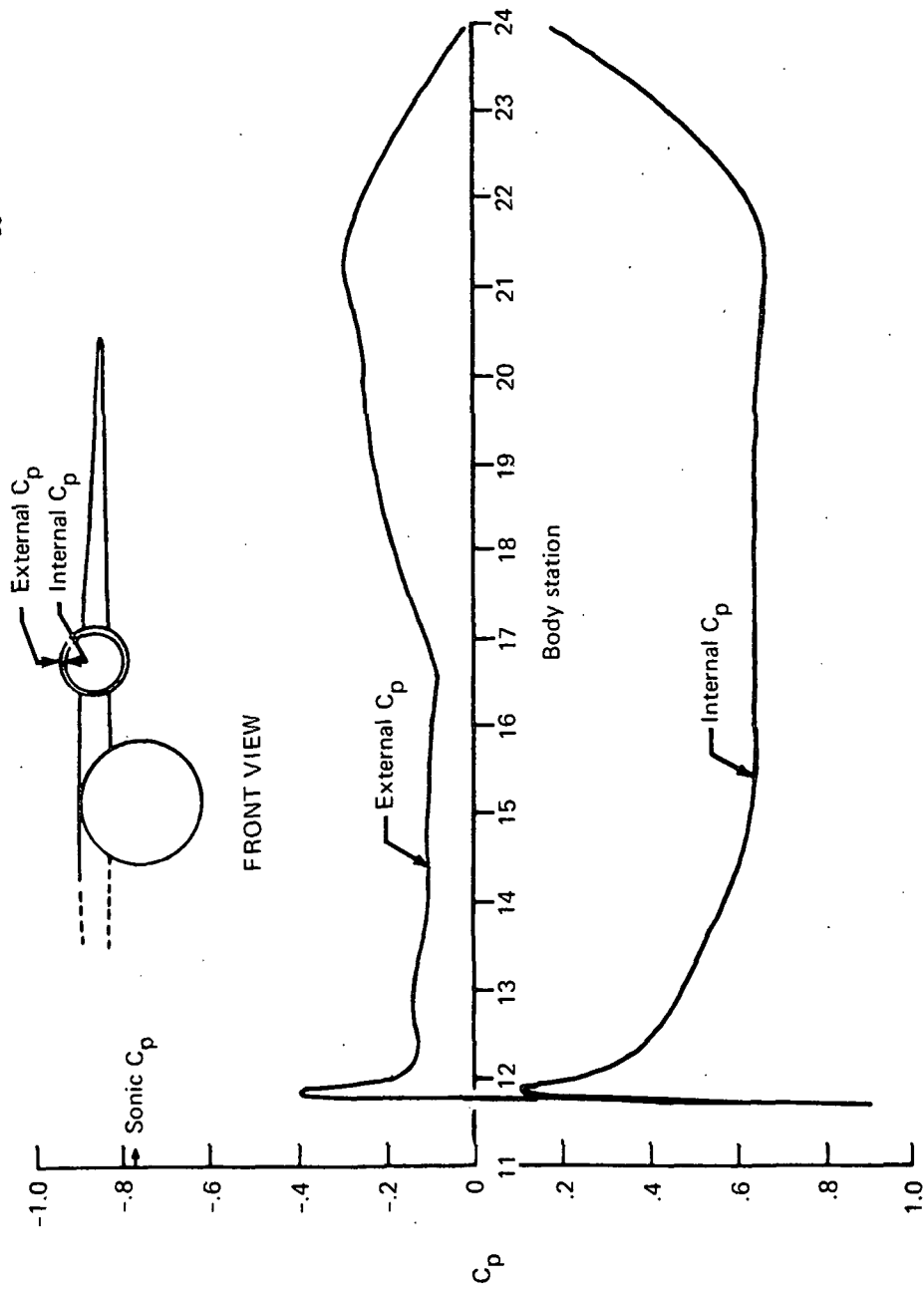


FIGURE 26.—PRESSURE DISTRIBUTION ALONG NACELLE CROWN LINE, INTERNAL AND EXTERNAL SURFACES

Two-engine D-nozzle
 $\alpha = 0^\circ$
 $M_\infty = 0.7$

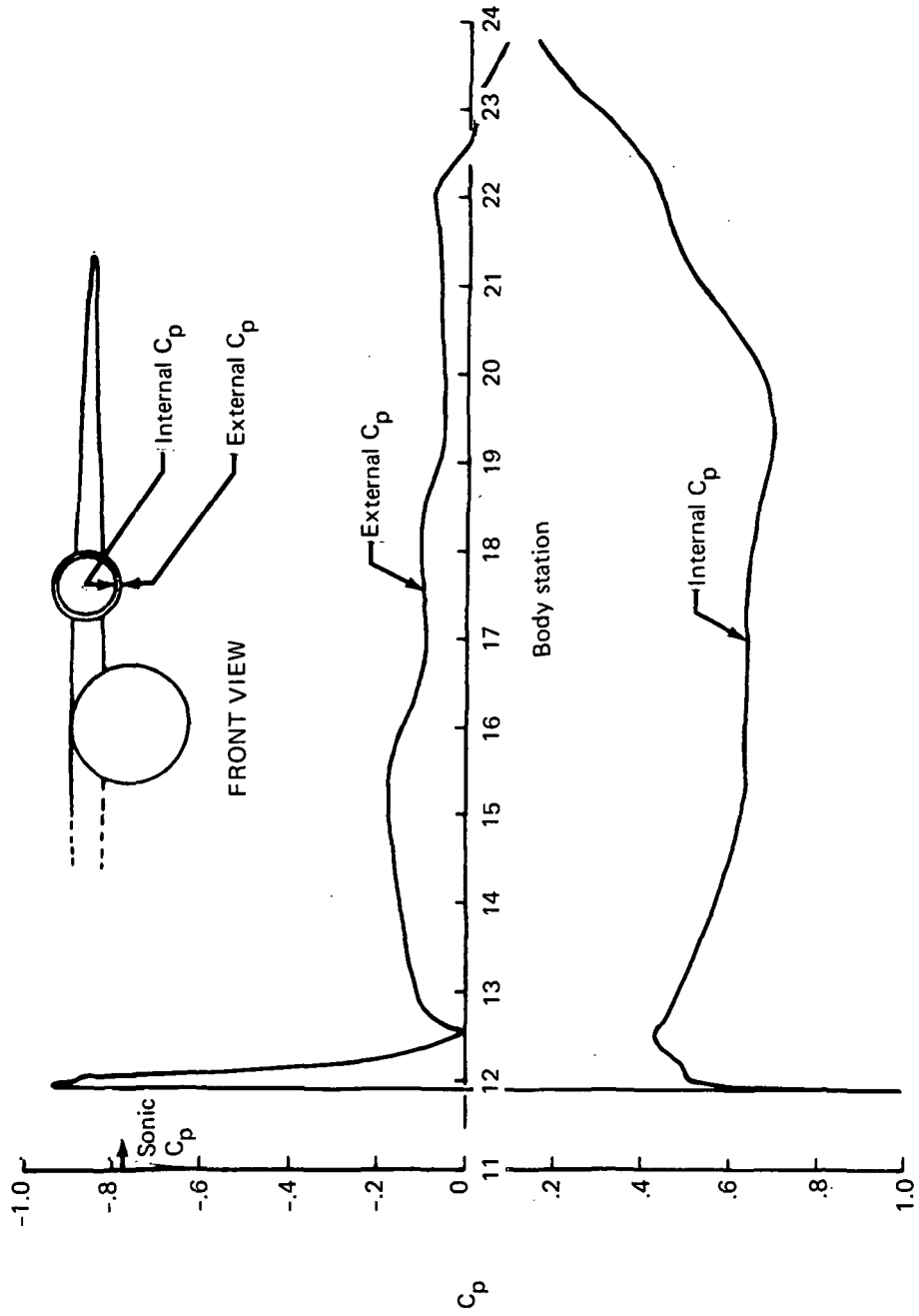


FIGURE 27.—PRESSURE DISTRIBUTION ALONG NACELLE KEEL LINE, INTERNAL AND EXTERNAL SURFACES

Two-engine D-nozzle
 $\alpha = 0^\circ$
 $M_\infty = 0.7$

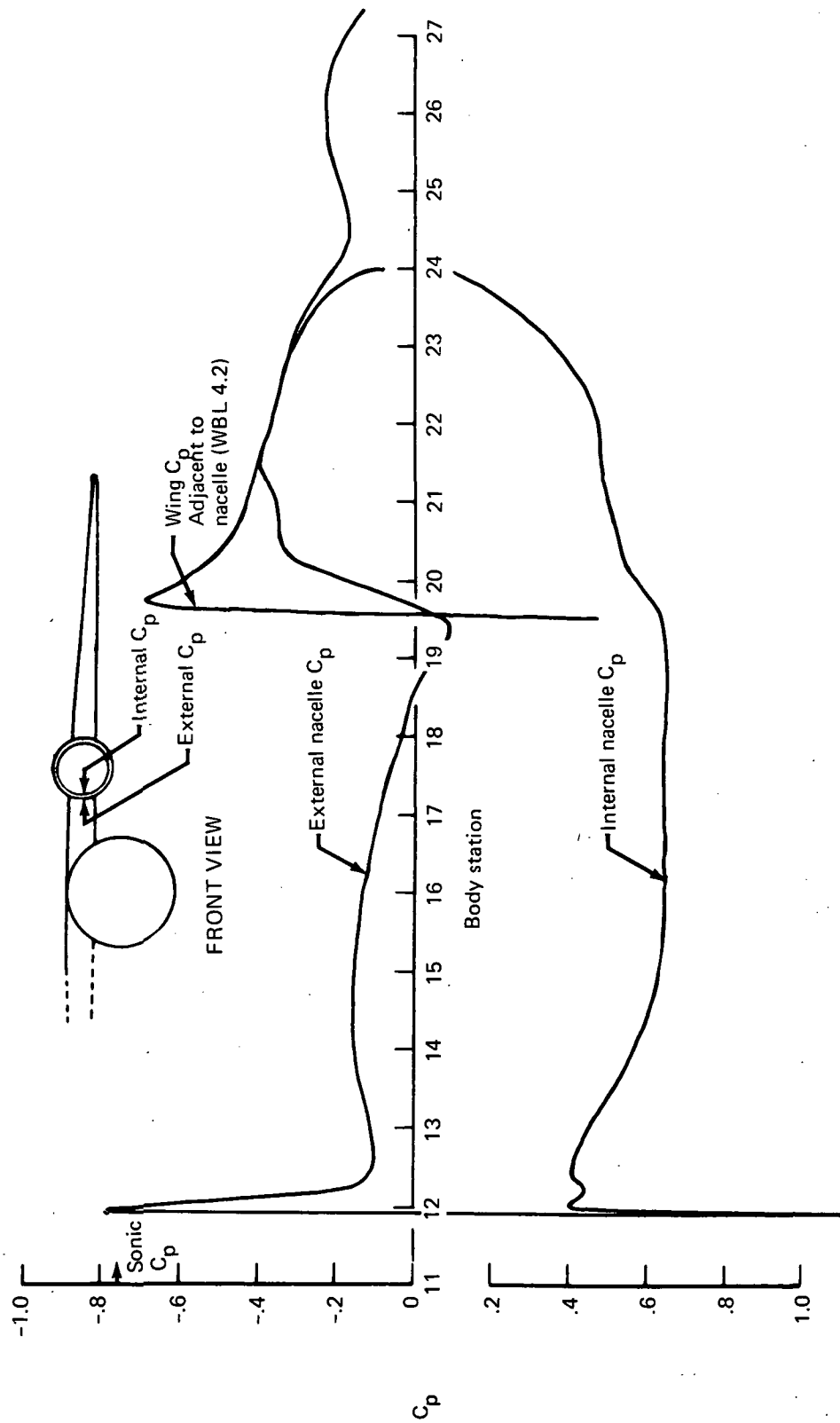


FIGURE 28.—PRESSURE DISTRIBUTION ALONG INBOARD SIDE OF NACELLE, INTERNAL AND EXTERNAL SURFACES

Two-engine D-nozzle
 $\alpha = 0^\circ$
 $M_\infty = 0.7$

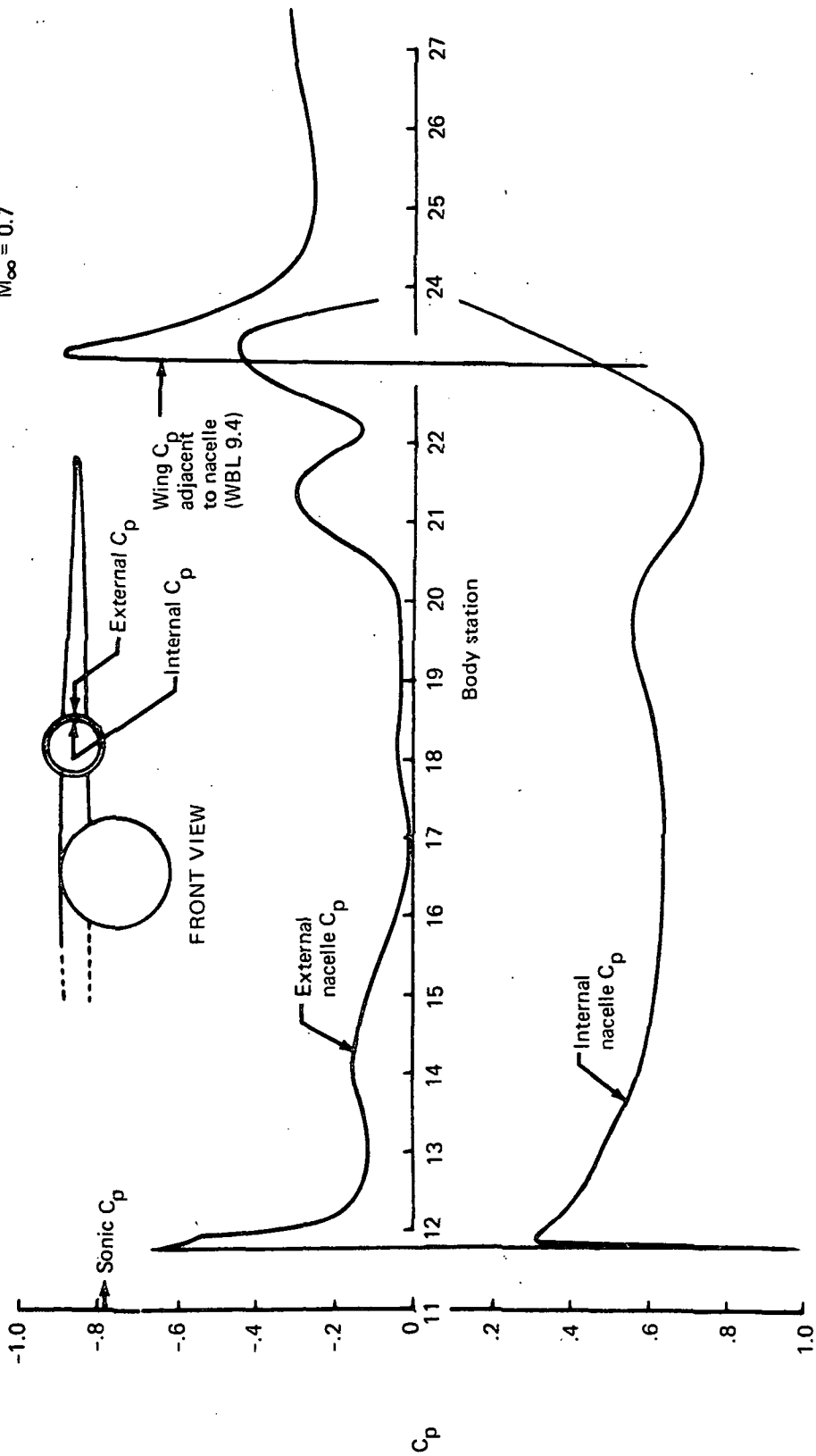


FIGURE 29.—PRESSURE DISTRIBUTION ALONG OUTBOARD SIDE OF NACELLE, INTERNAL AND EXTERNAL SURFACES

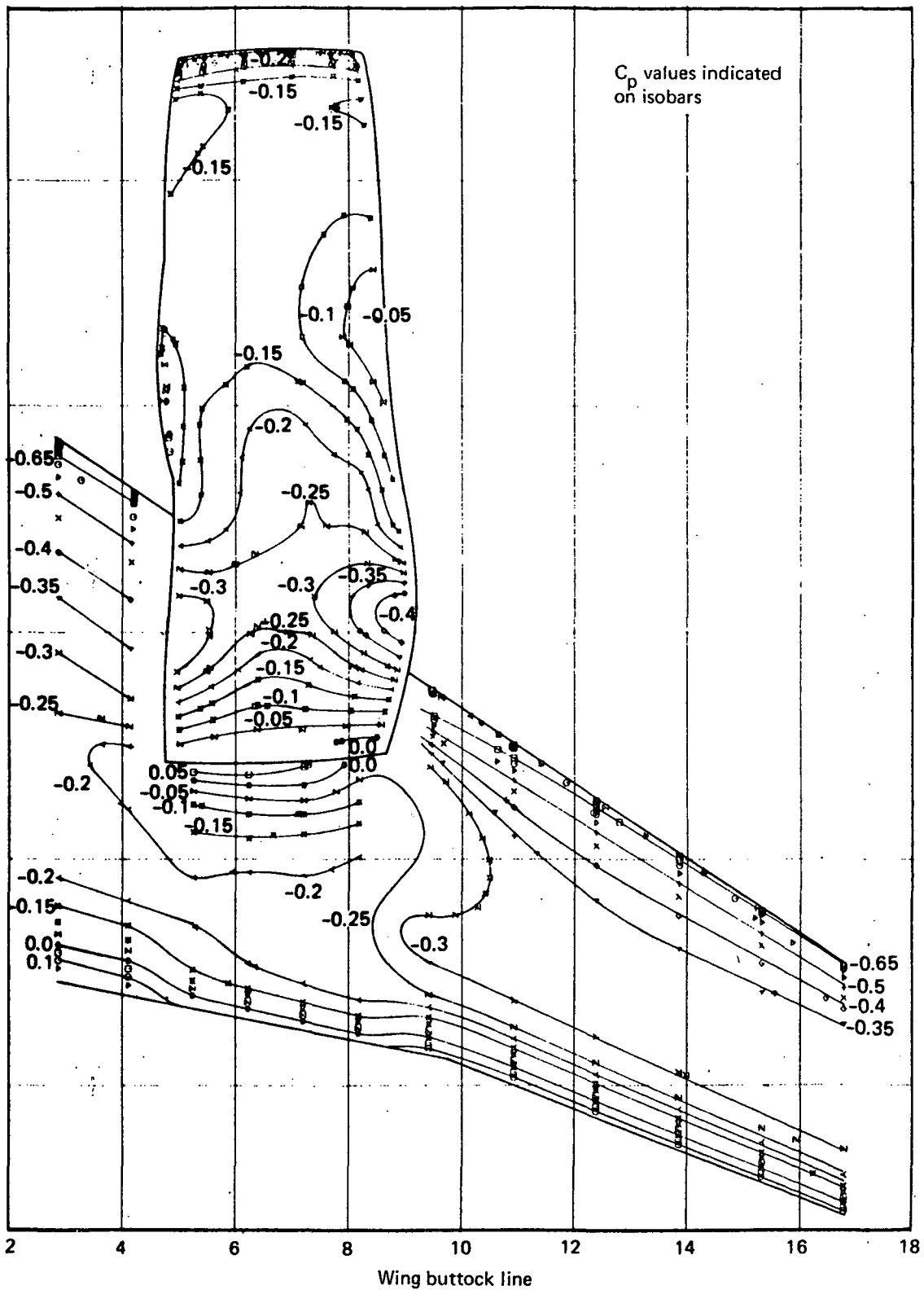
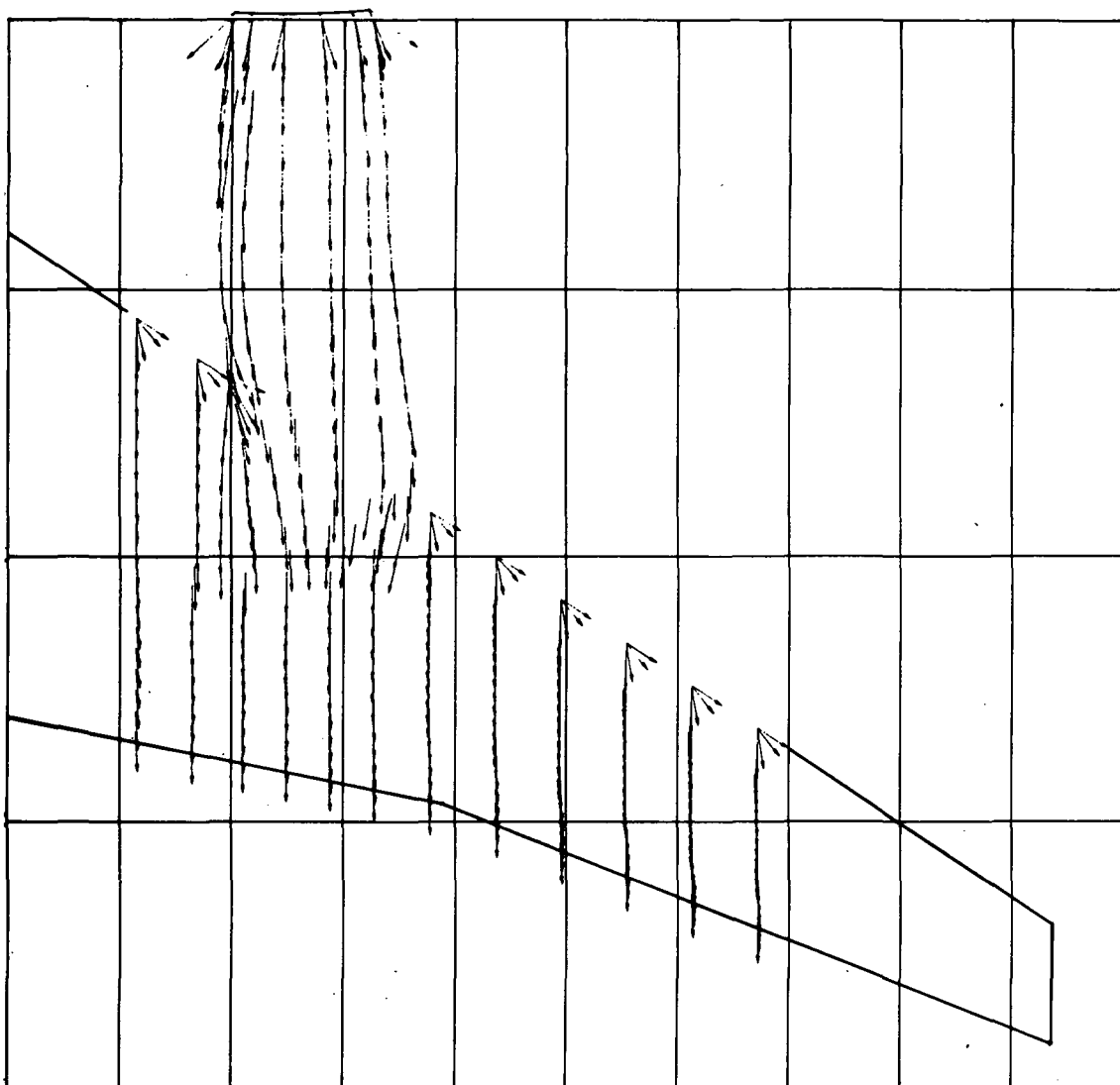


FIGURE 30.—UPPER-SURFACE ISOBARS, TWO-ENGINE D-NOZZLE CASE,
 $\alpha = 0^\circ, M_\infty = 0.7$



*FIGURE 31.—VELOCITY VECTORS AT PANEL MIDPOINTS ON WING AND NACELLE
(LOWER SURFACE)*

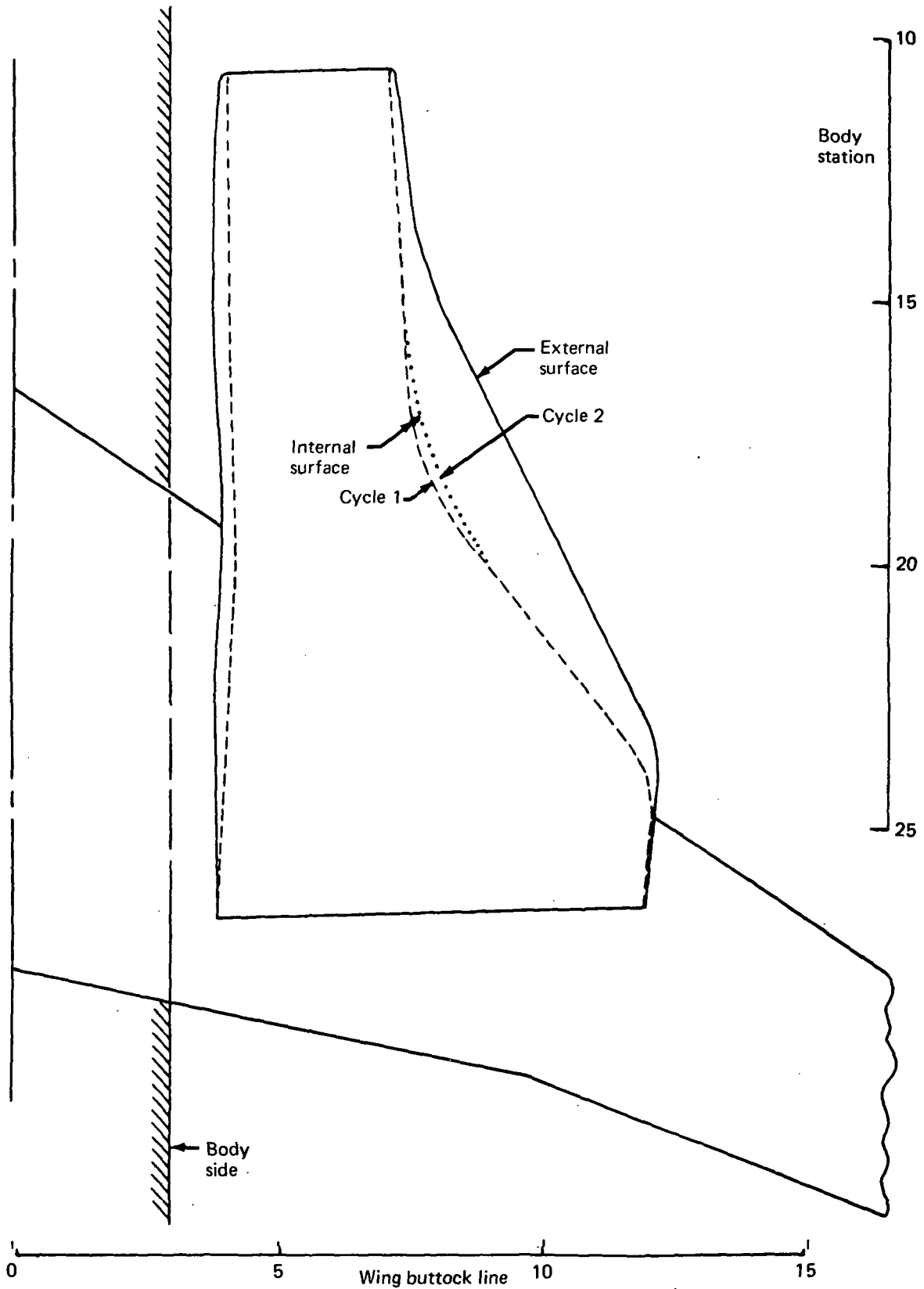
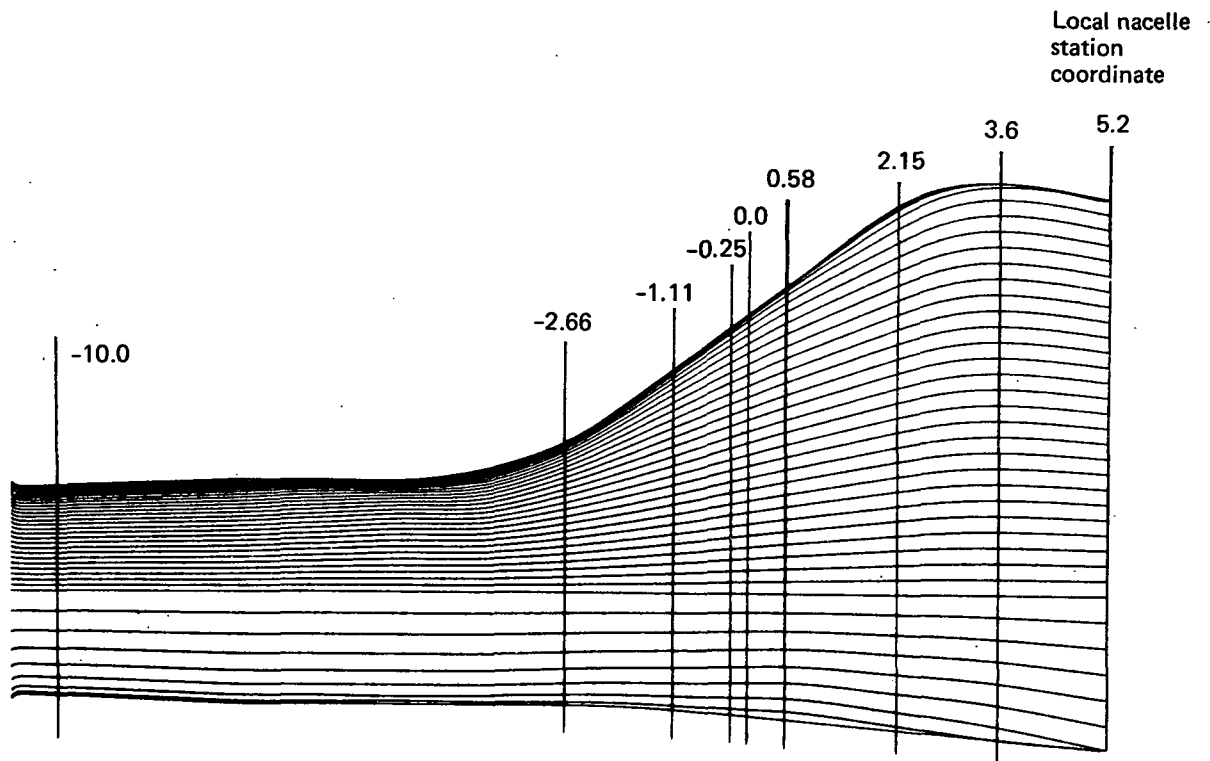
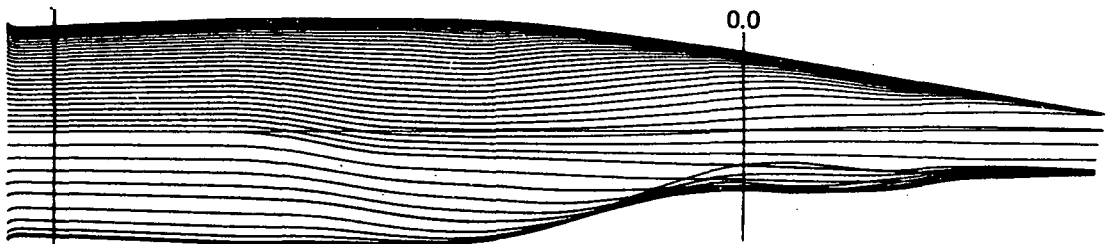


FIGURE 32.—SPREAD NOZZLE NACELLE, TWO-ENGINE AIRPLANE



PLAN VIEW



SIDE VIEW

FIGURE 33.—LOFT LINES OF NACELLE INTERNAL SURFACE, TWO-ENGINE SPREAD NOZZLE CASE

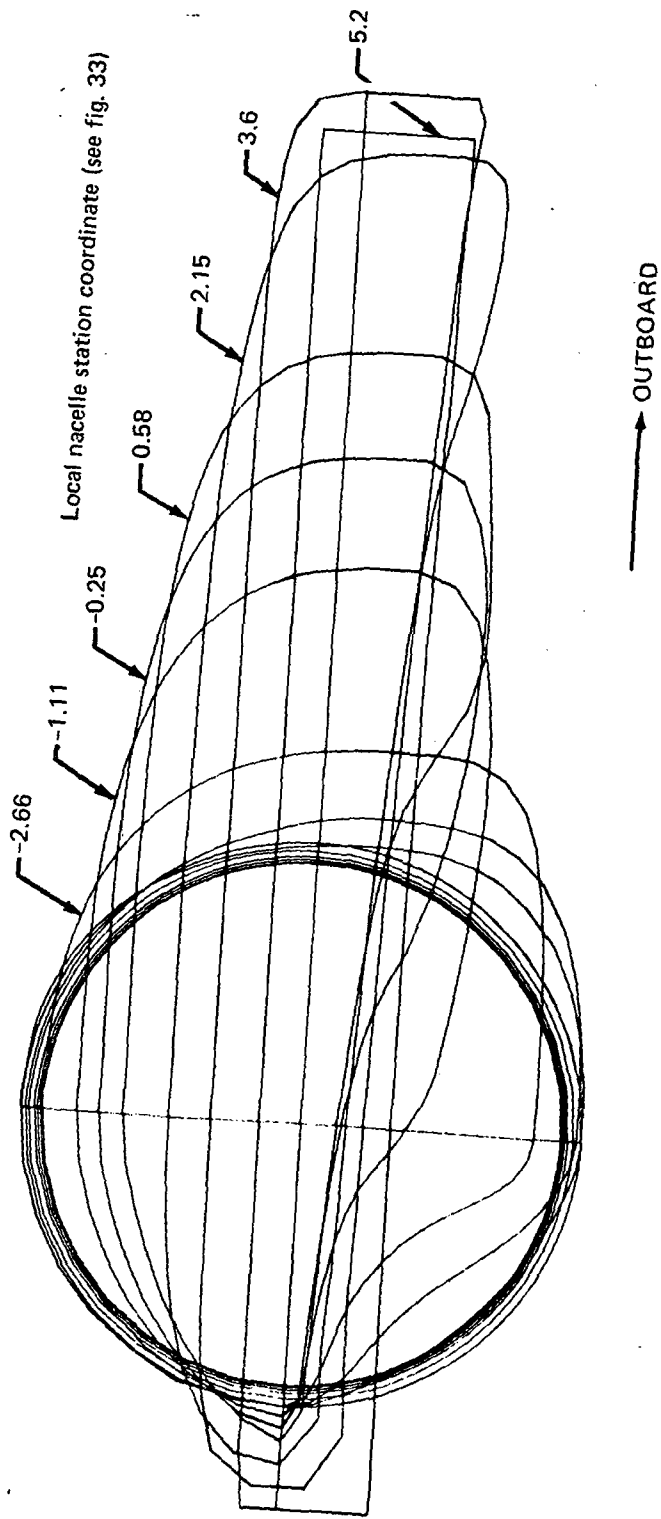


FIGURE 34. — DEFINING CROSS SECTIONS FOR NACELLE INTERNAL SURFACE, TWO-ENGINE SPREAD NOZZLE CASE

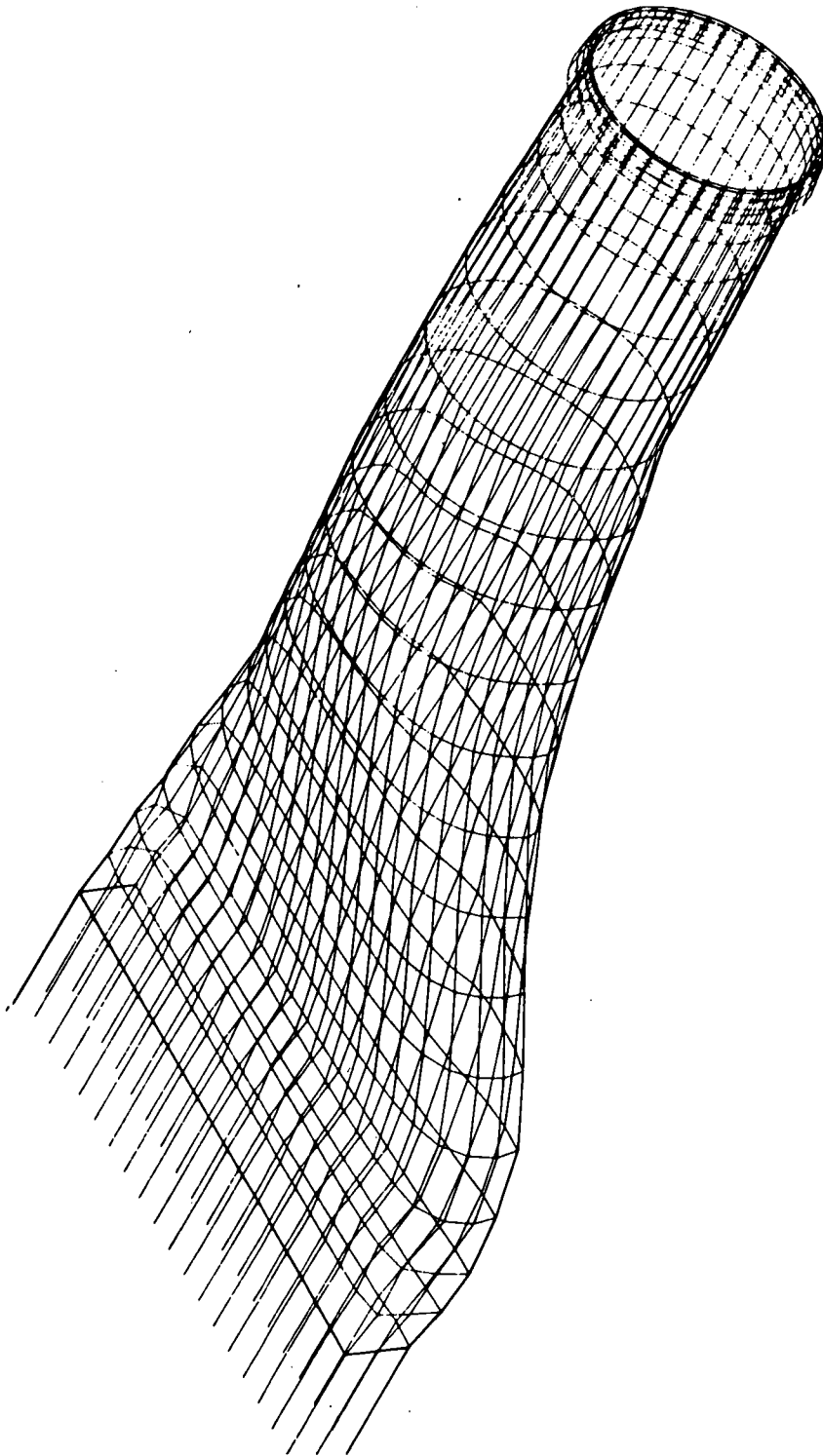


FIGURE 35.—PANEL REPRESENTATION OF INTERNAL SURFACE, TWO-ENGINE SPREAD NOZZLE CASE (ISOMETRIC VIEW)

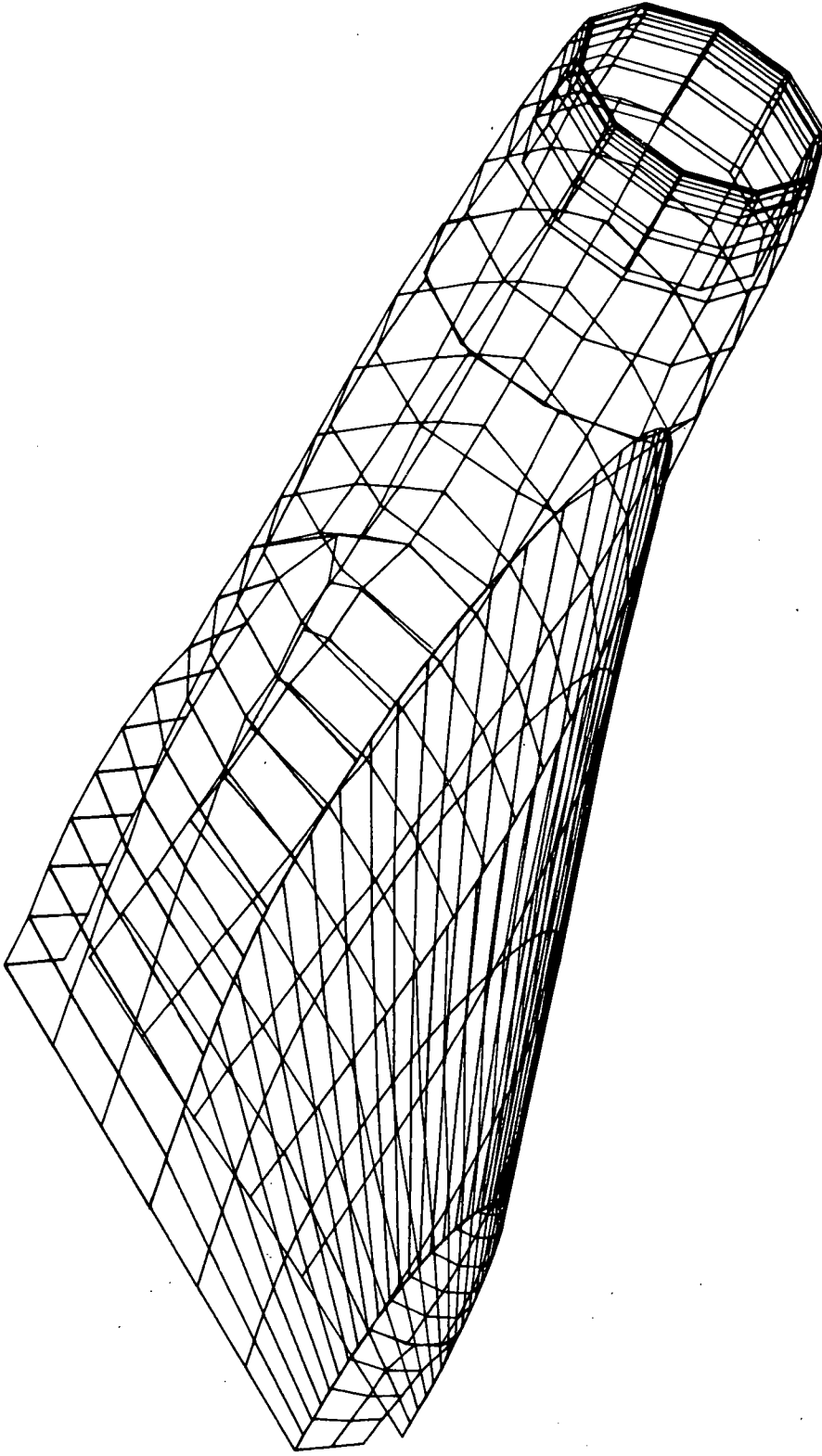


FIGURE 36.—PANEL REPRESENTATION OF EXTERNAL SURFACE, TWO-ENGINE SPREAD NOZZLE
CASE (ISOMETRIC VIEW)

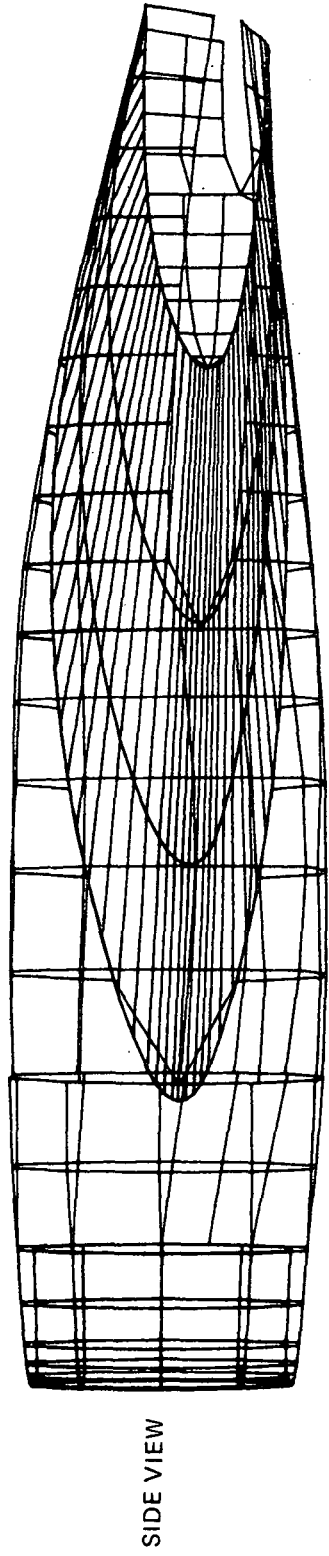
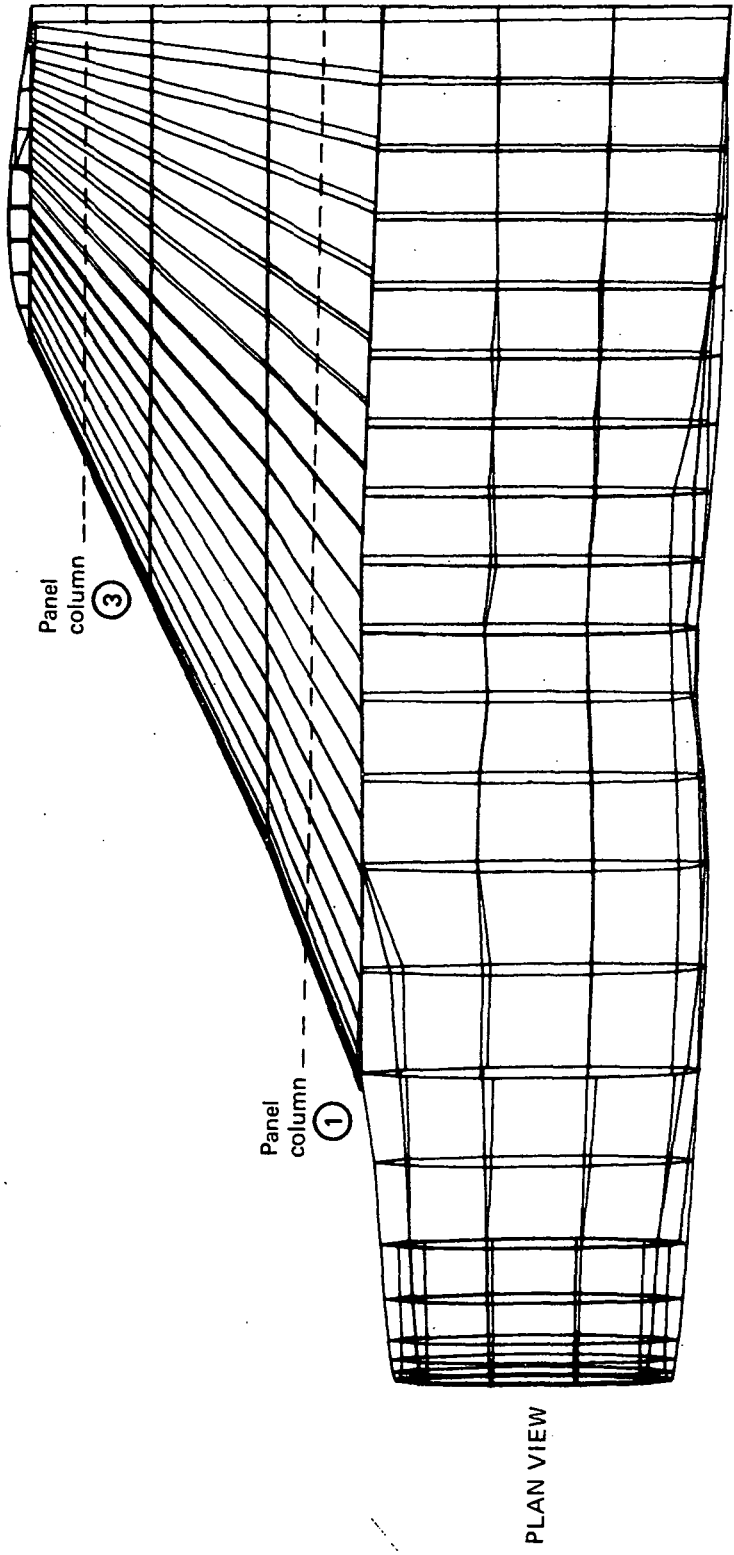


FIGURE 37.—PANEL REPRESENTATION OF EXTERNAL SURFACE, TWO-ENGINE SPREAD NOZZLE
CASE (PLAN AND SIDE VIEWS)

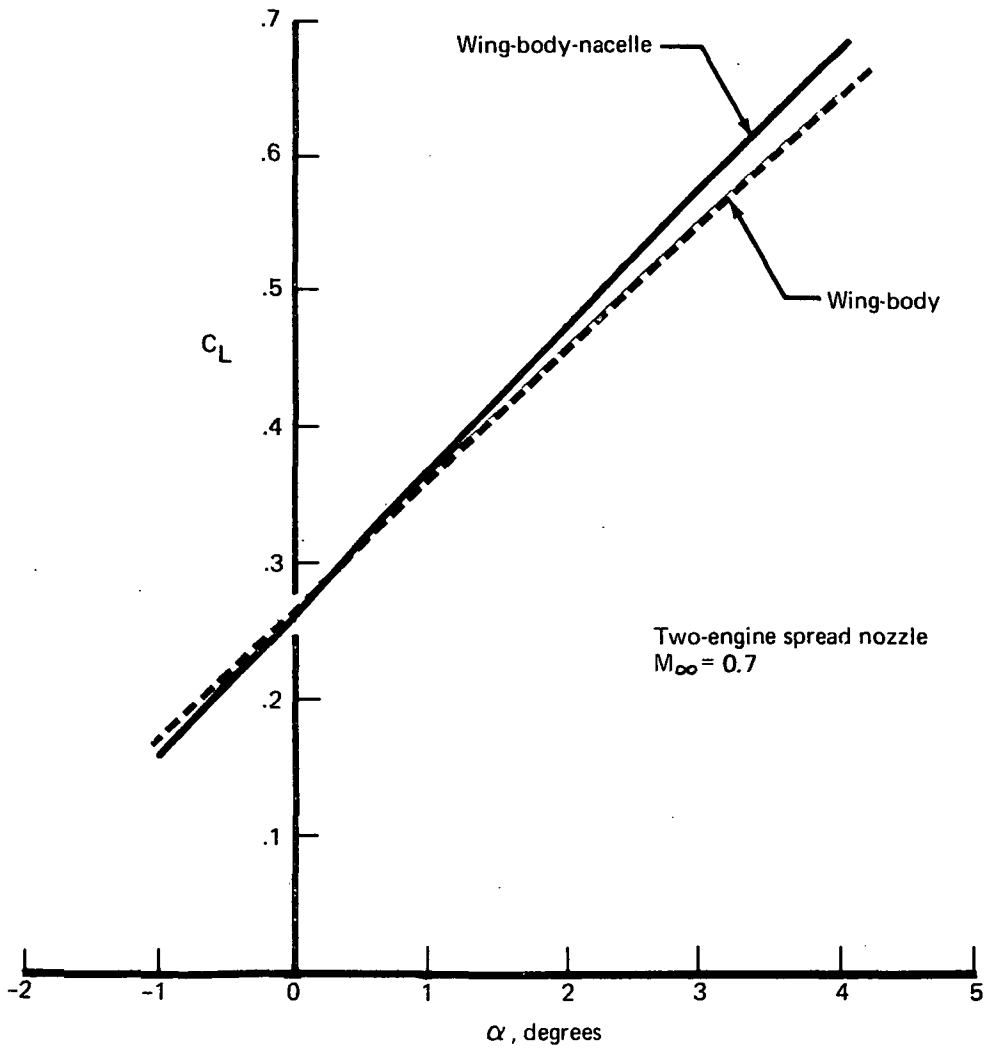
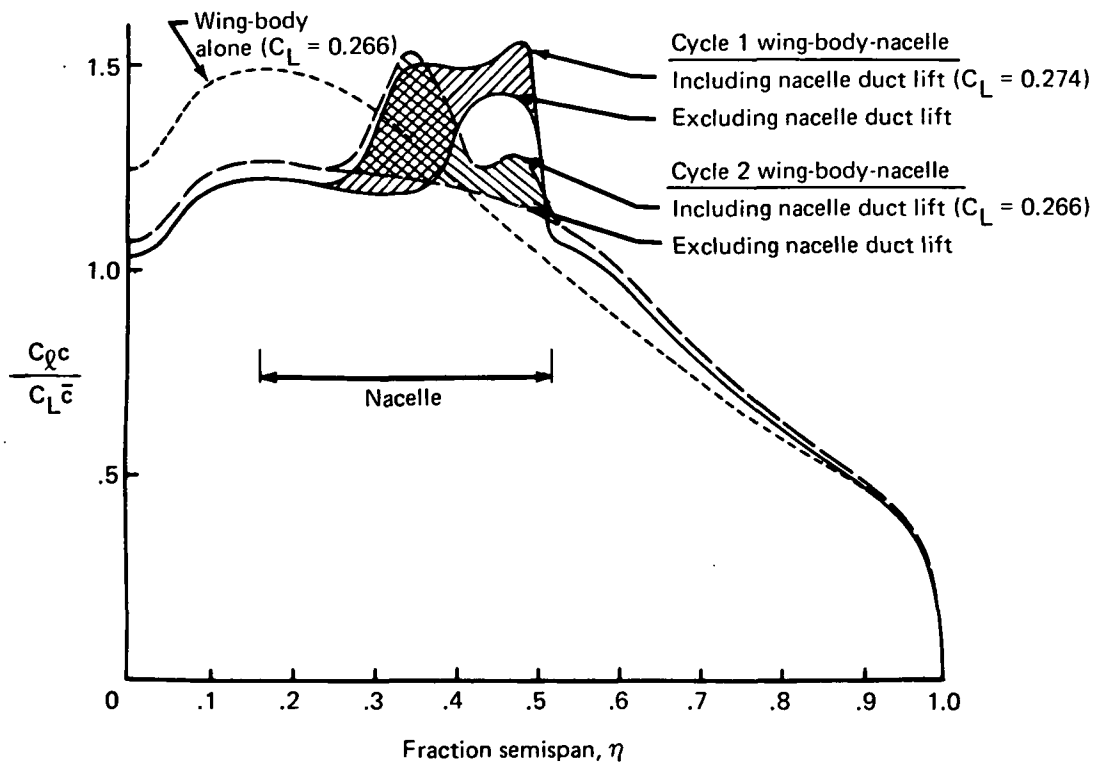


FIGURE 38.—EFFECT OF NACELLE ON LIFT CURVE



Two-engine spread nozzle
 $\alpha = 0^\circ, M_\infty = 0.7$

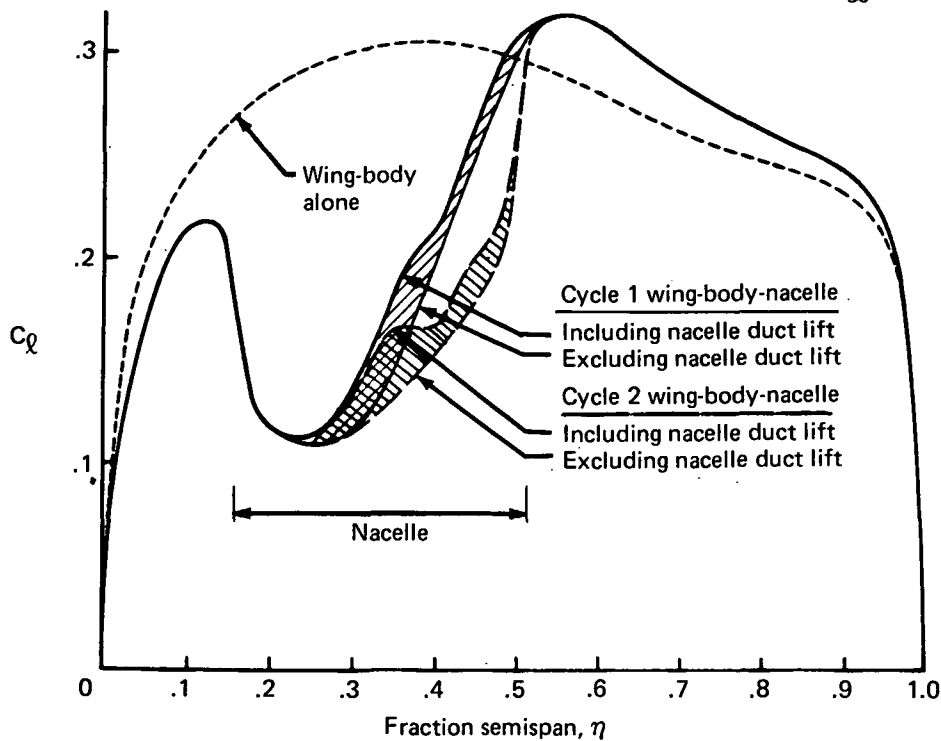


FIGURE 39.—EFFECT OF NACELLE ON WING LOAD DISTRIBUTION AND SECTIONAL LIFT DISTRIBUTION

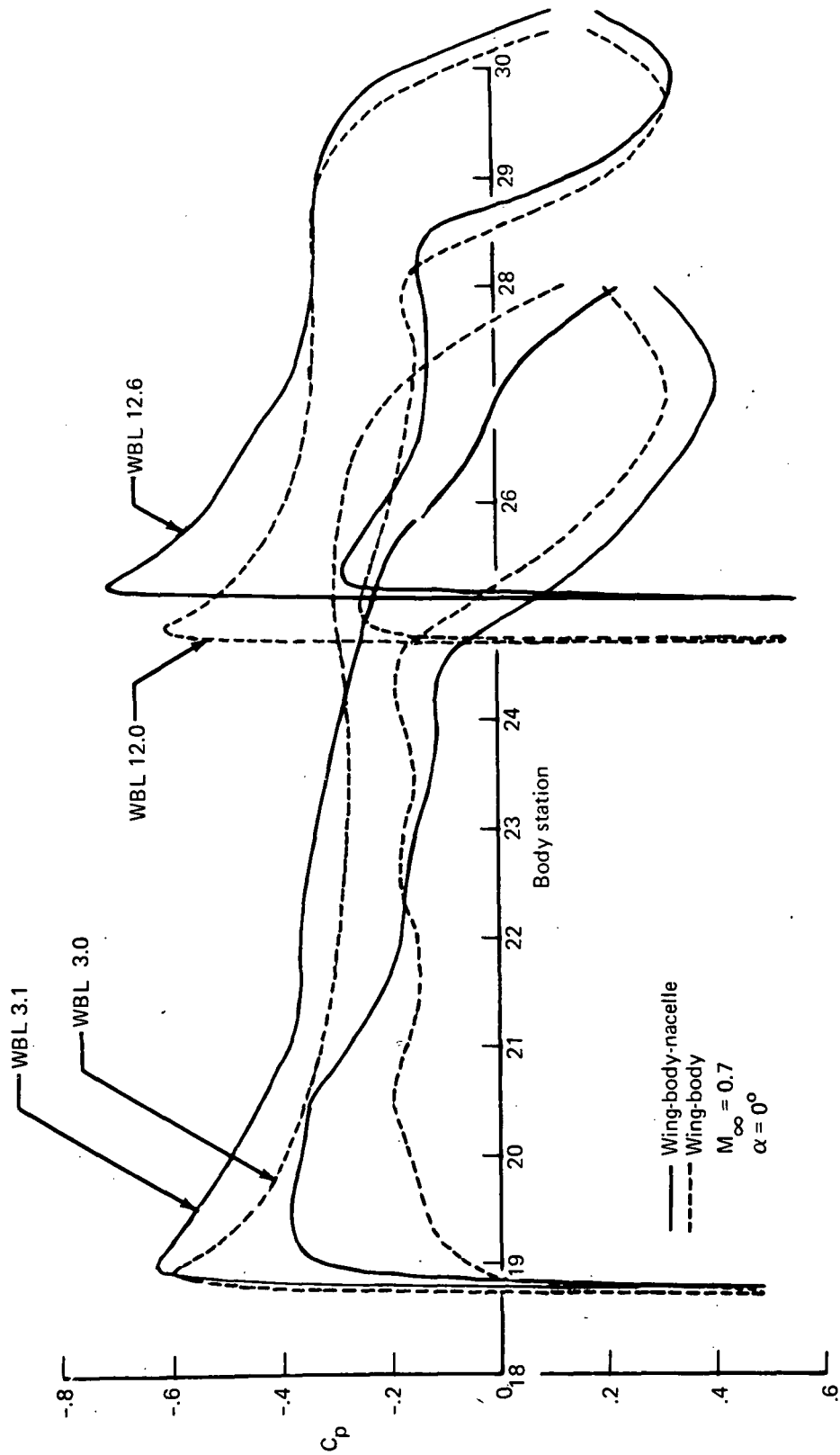


FIGURE 40.—EFFECT OF NACELLE ON ADJACENT-WING PRESSURES, TWO-ENGINE SPREAD NOZZLE CASE

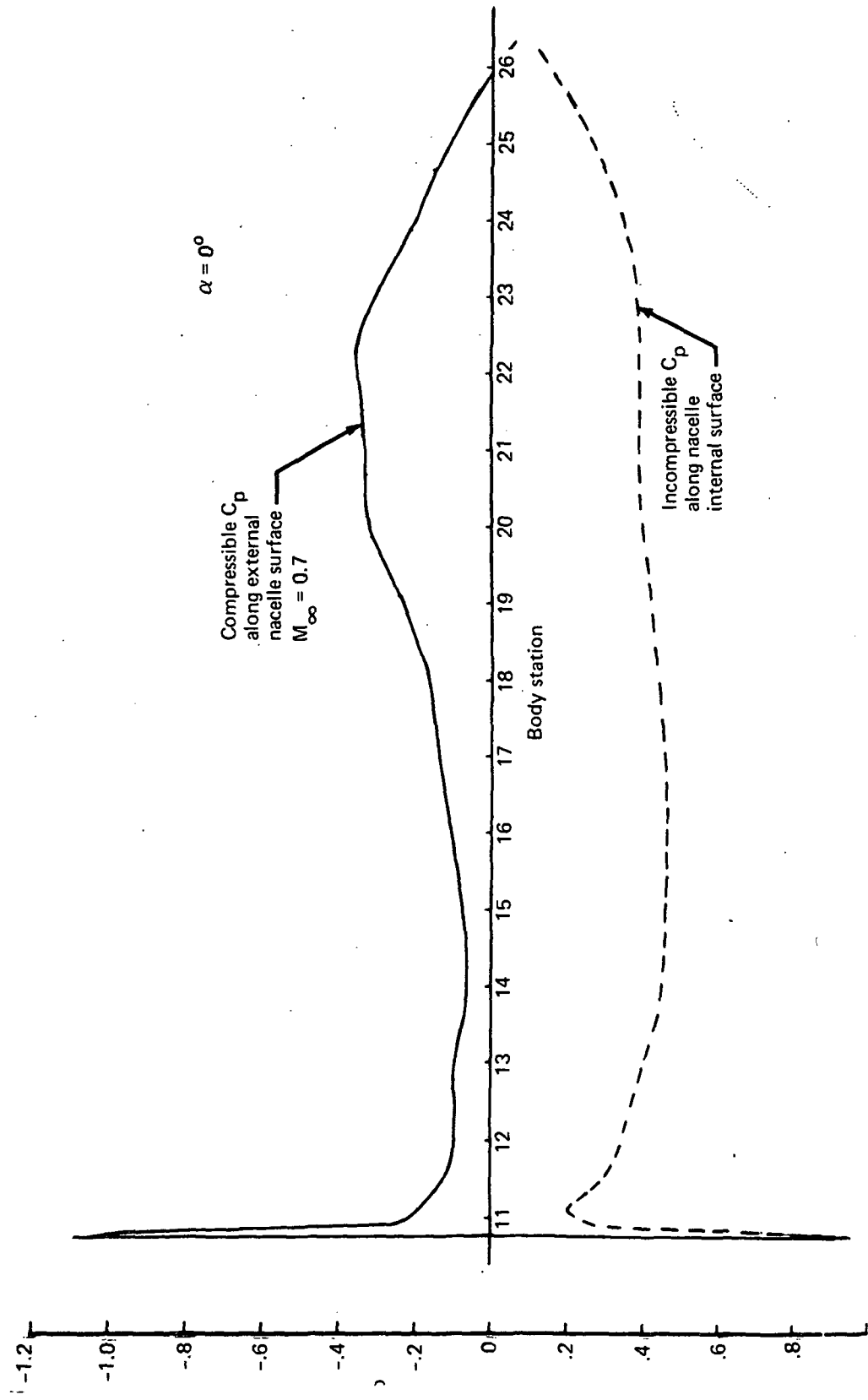


FIGURE 41.—PRESSURE DISTRIBUTION ALONG NACELLE CROWN LINE,
TWO-ENGINE SPREAD NOZZLE CASE

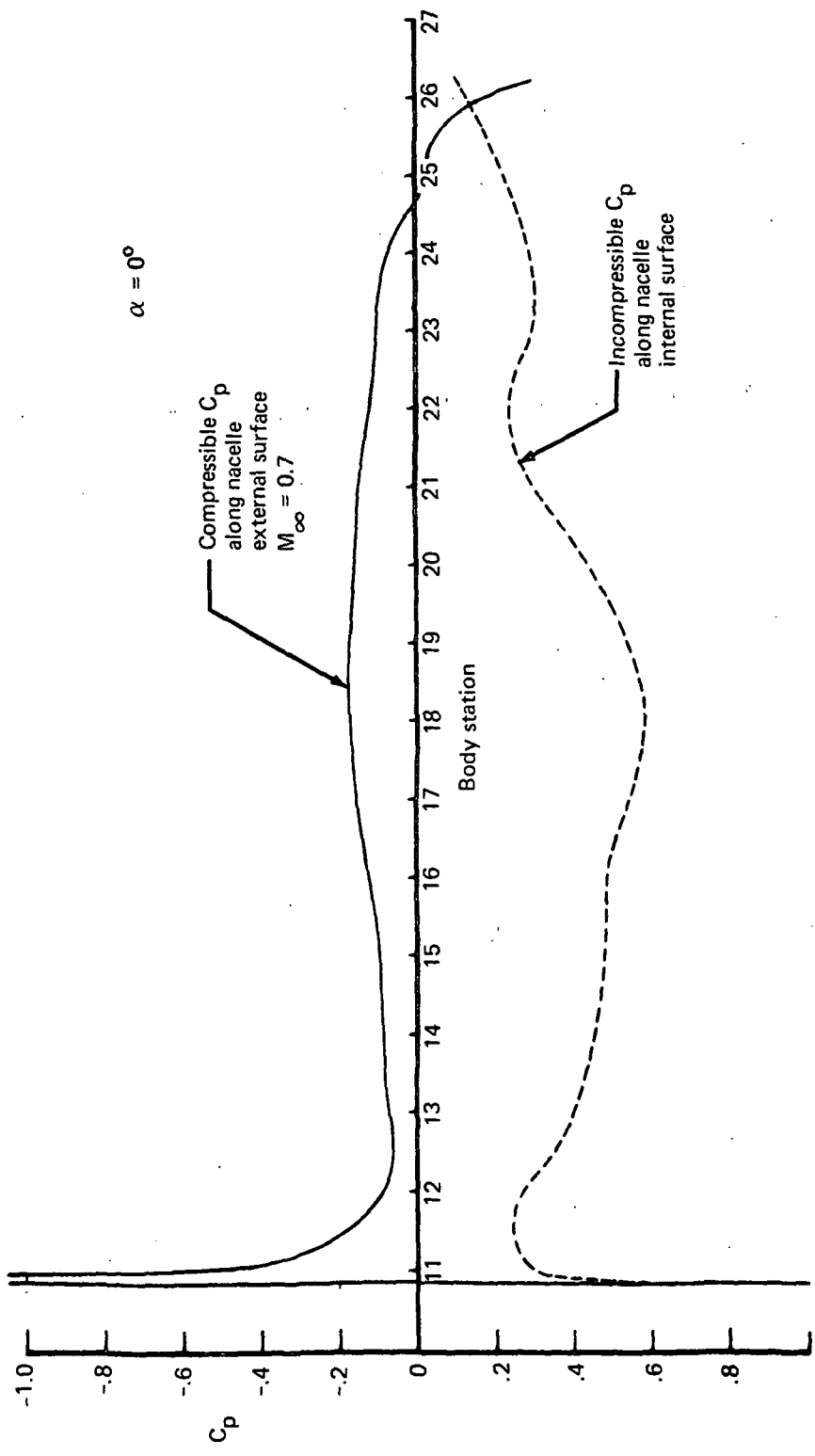


FIGURE 42.—PRESSURE DISTRIBUTION ALONG NACELLE KEEL LINE,
TWO-ENGINE, SPREAD NOZZLE CASE

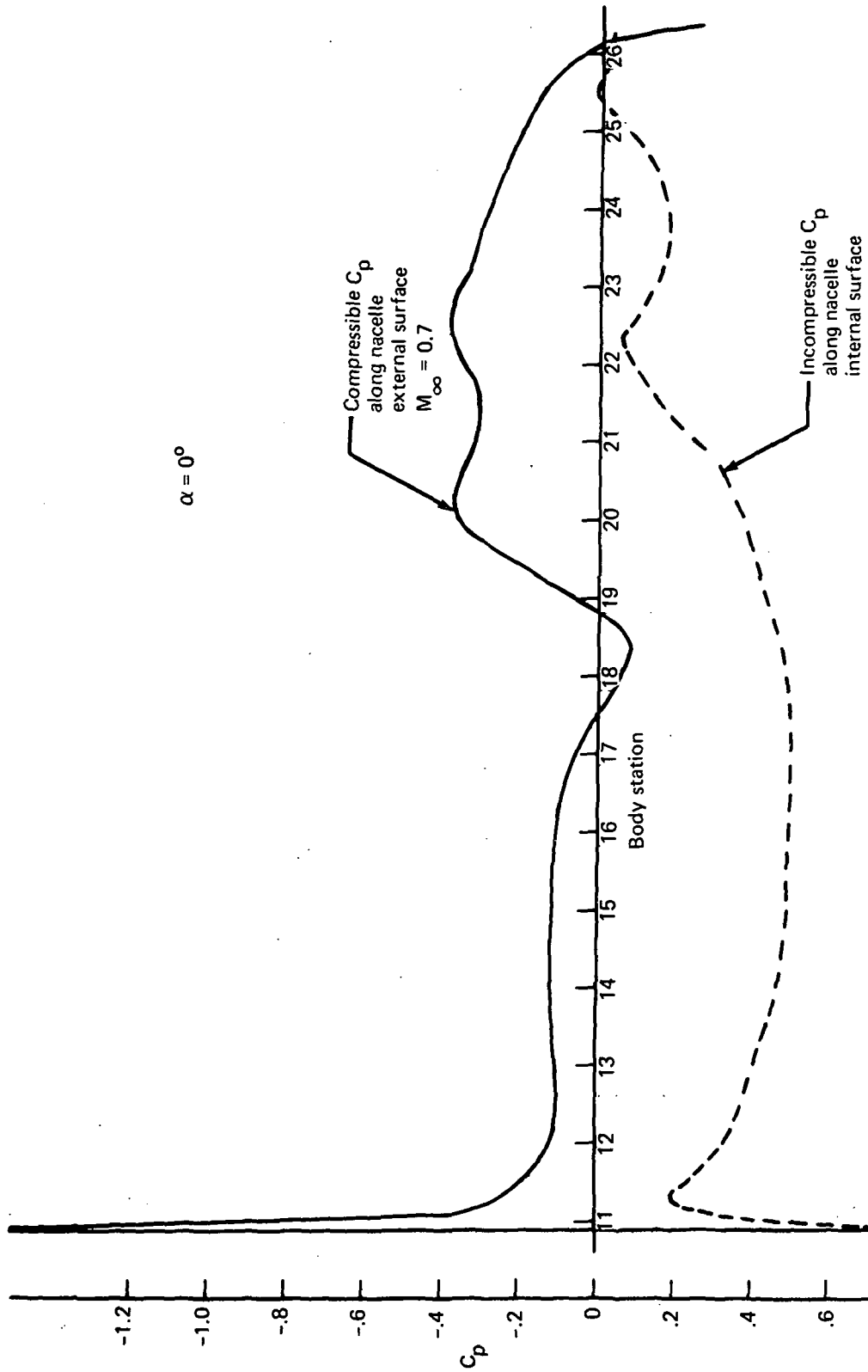


FIGURE 43.—PRESSURE DISTRIBUTION ALONG INBOARD SIDE OF NACELLE,
TWO-ENGINE SPREAD NOZZLE CASE

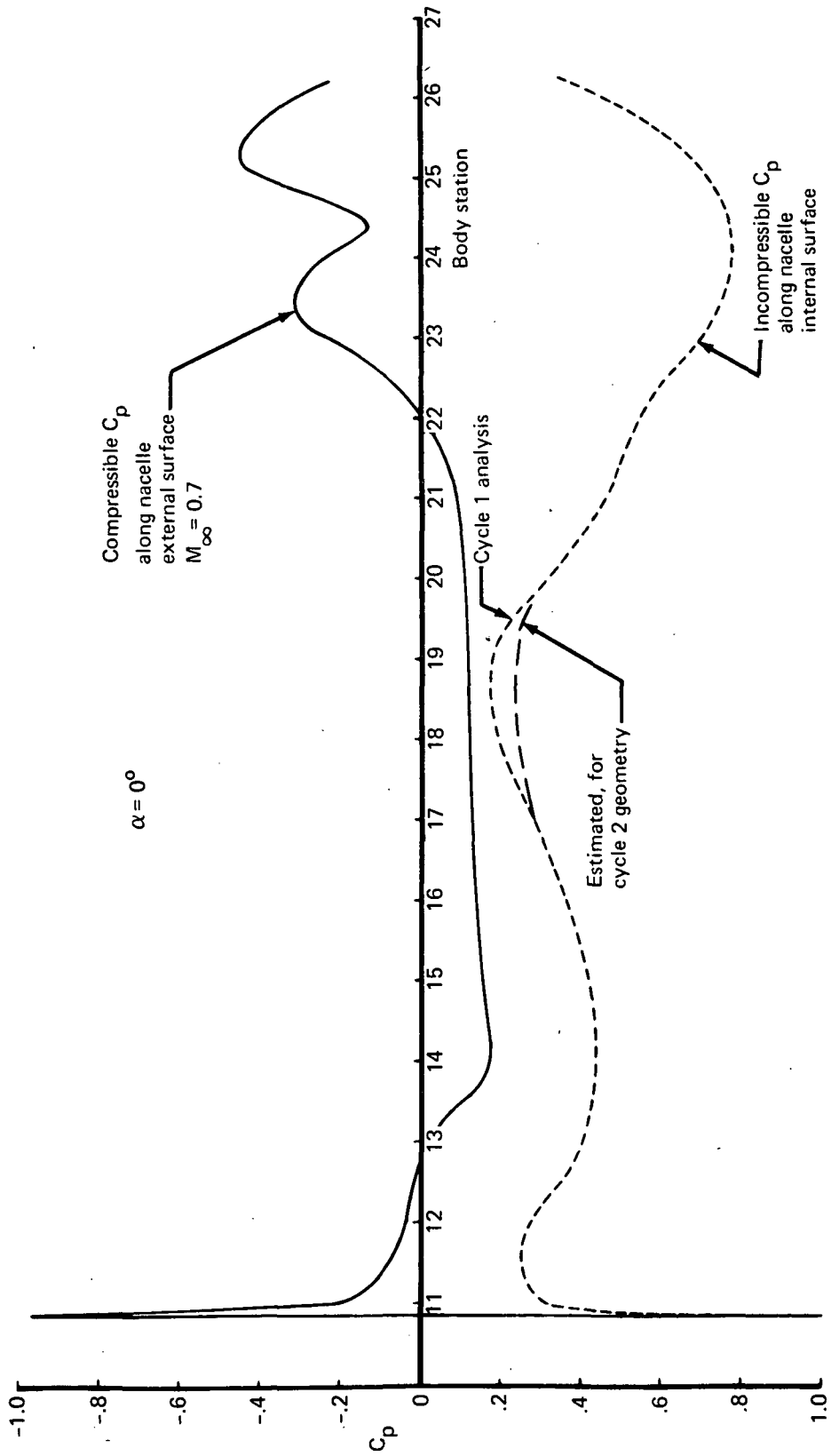


FIGURE 44.—PRESSURE DISTRIBUTION ALONG OUTBOARD SIDE OF NACELLE,
TWO-ENGINE SPREAD NOZZLE CASE

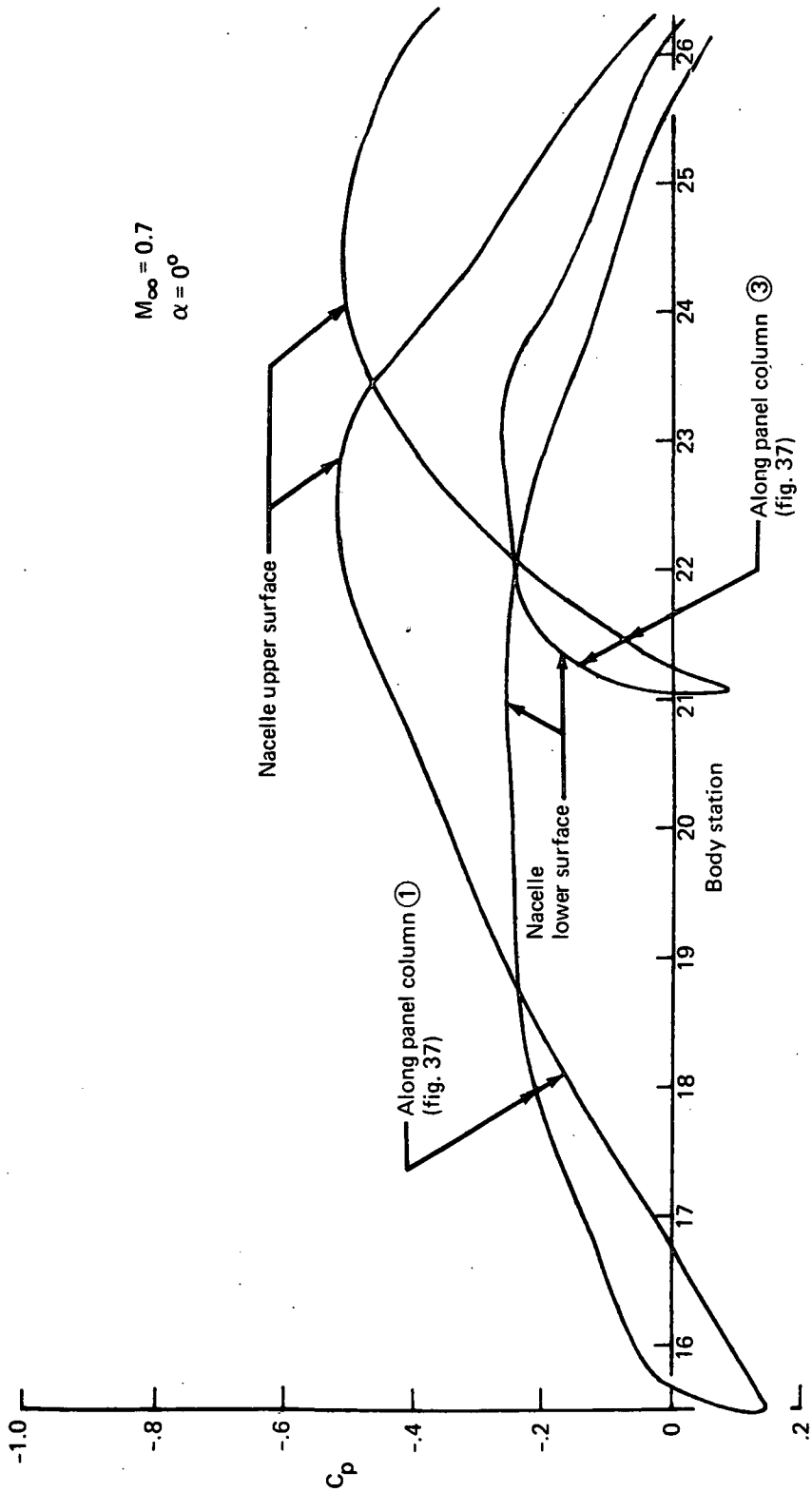


FIGURE 45.—PRESSURE DISTRIBUTIONS ON OUTBOARD PART OF CYCLE 1 NACELLE, TWO-ENGINE SPREAD NOZZLE CASE (EXTERNAL SURFACE)

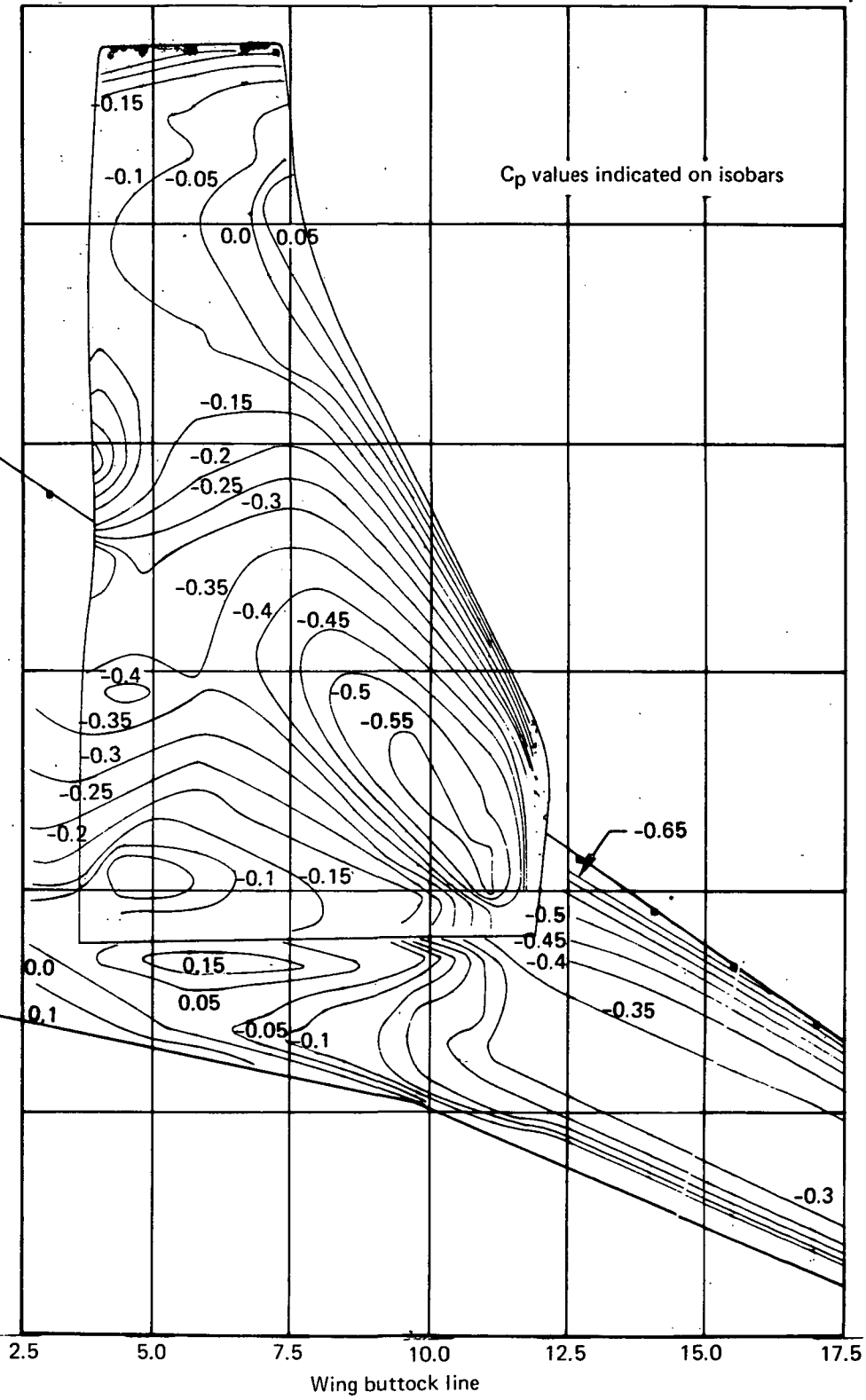


FIGURE 46.—UPPER-SURFACE ISOBARS, TWO-ENGINE SPREAD NOZZLE CASE, $M_\infty = 0.7$, $\alpha = 0^\circ$

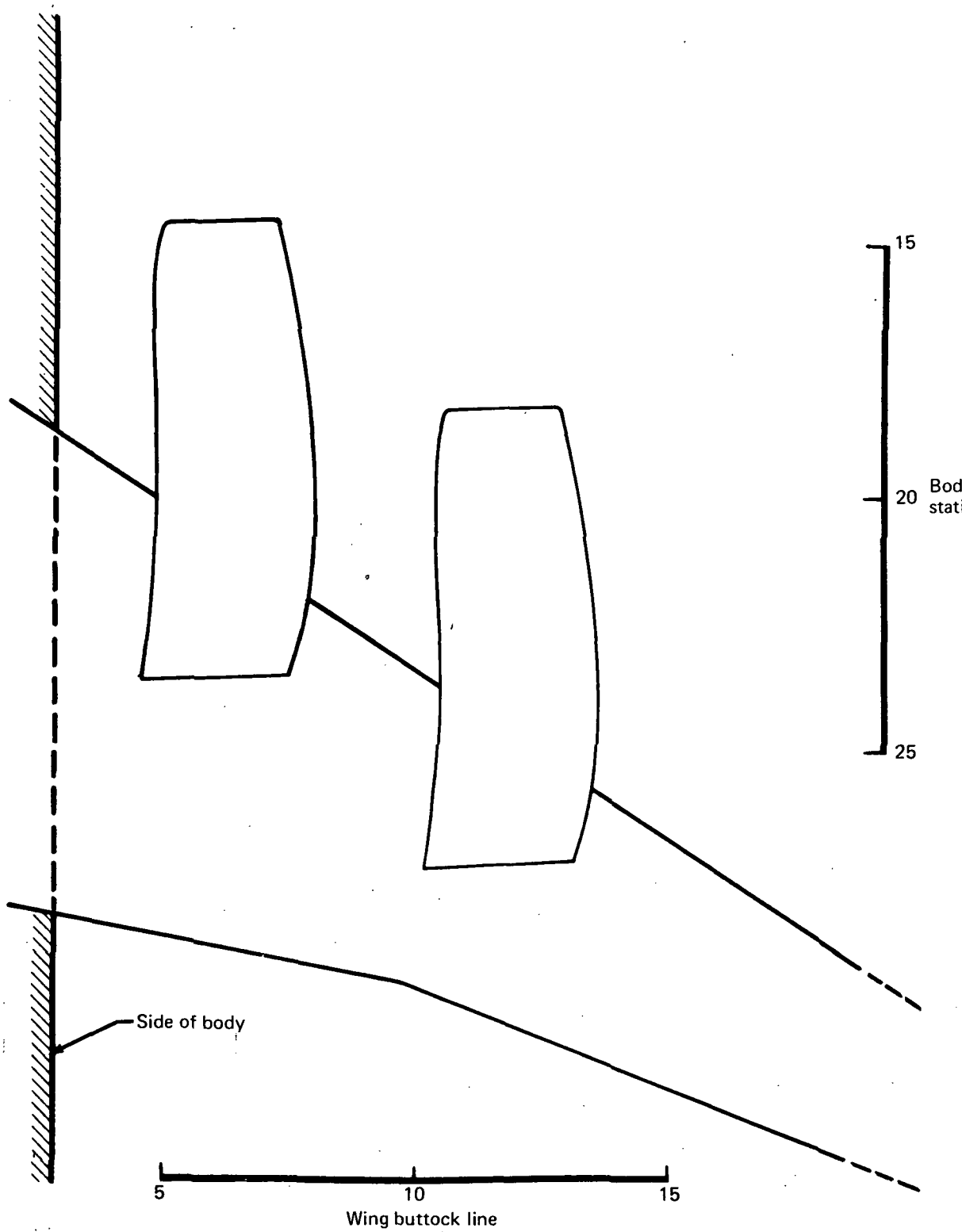


FIGURE 47.—D-NOZZLE NACELLES, FOUR-ENGINE AIRPLANE

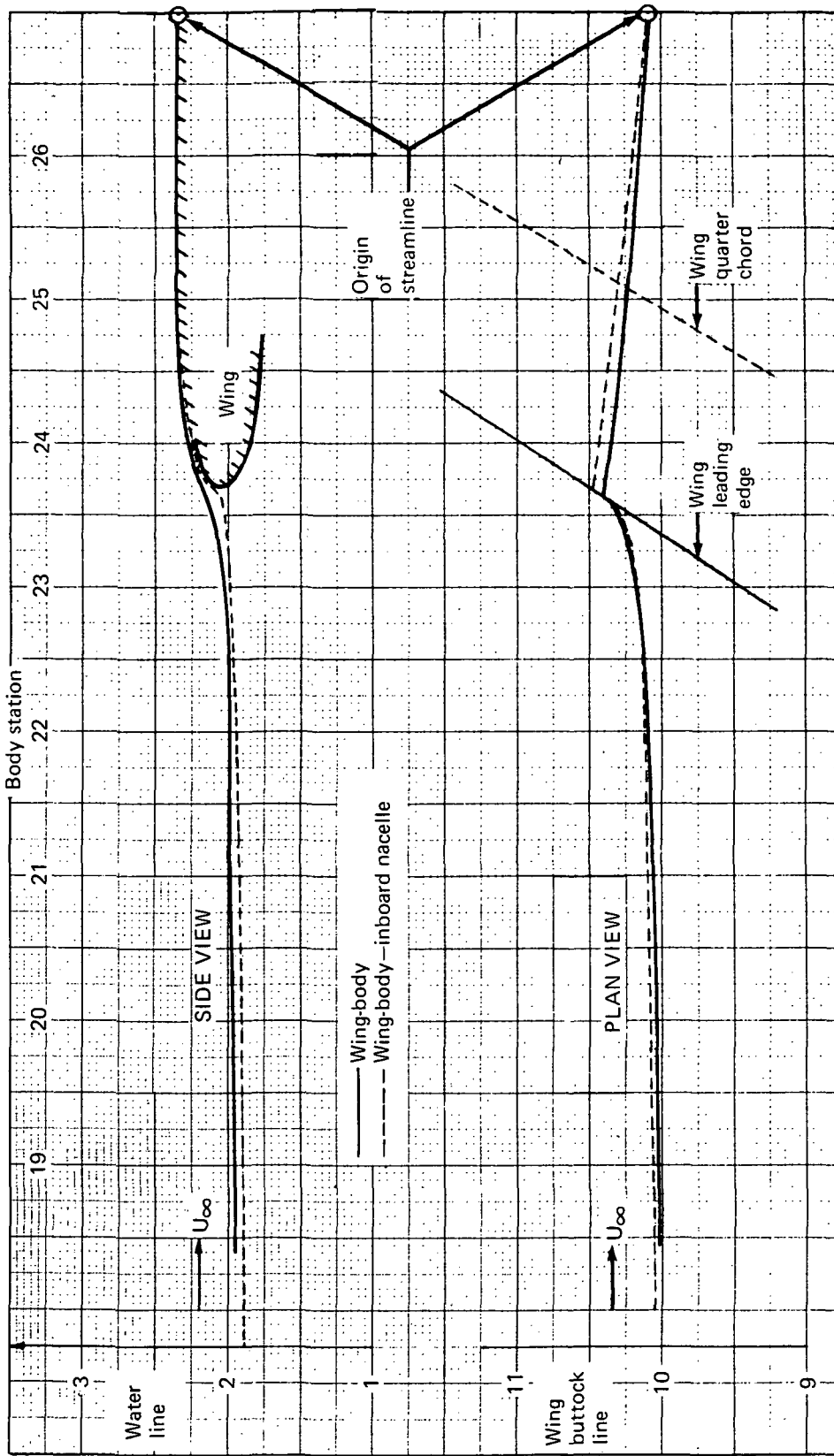


FIGURE 48.—EFFECT OF INBOARD NACELLE ON STREAMLINE PASSING OVER WING WHERE OUTBOARD NACELLE WILL BE LOCATED, FOUR-ENGINE D-NOZZLE CASE

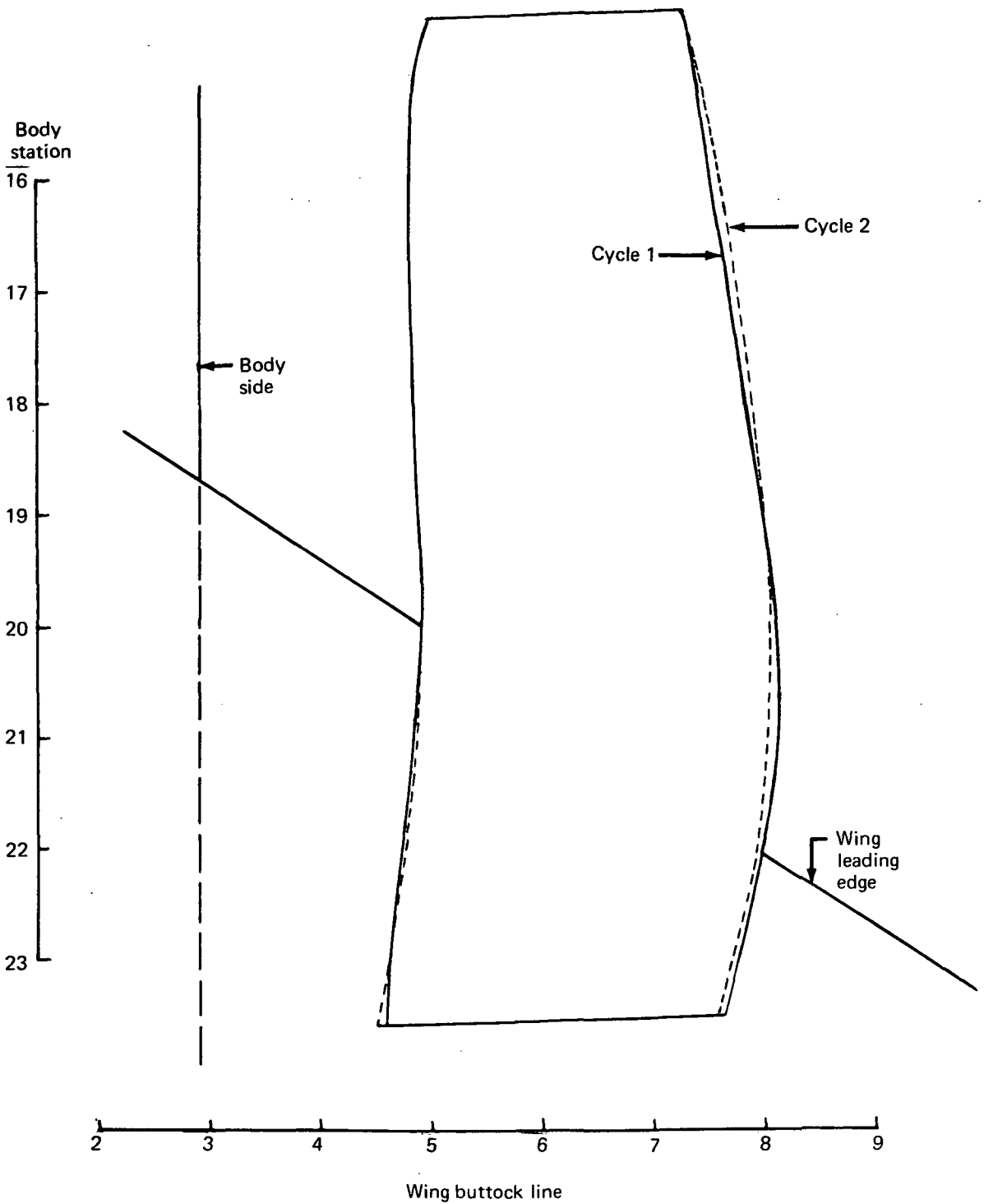


FIGURE 49.—CYCLE 2 GEOMETRY MODIFICATIONS ON INBOARD NACELLE,
FOUR-ENGINE D-NOZZLE CASE

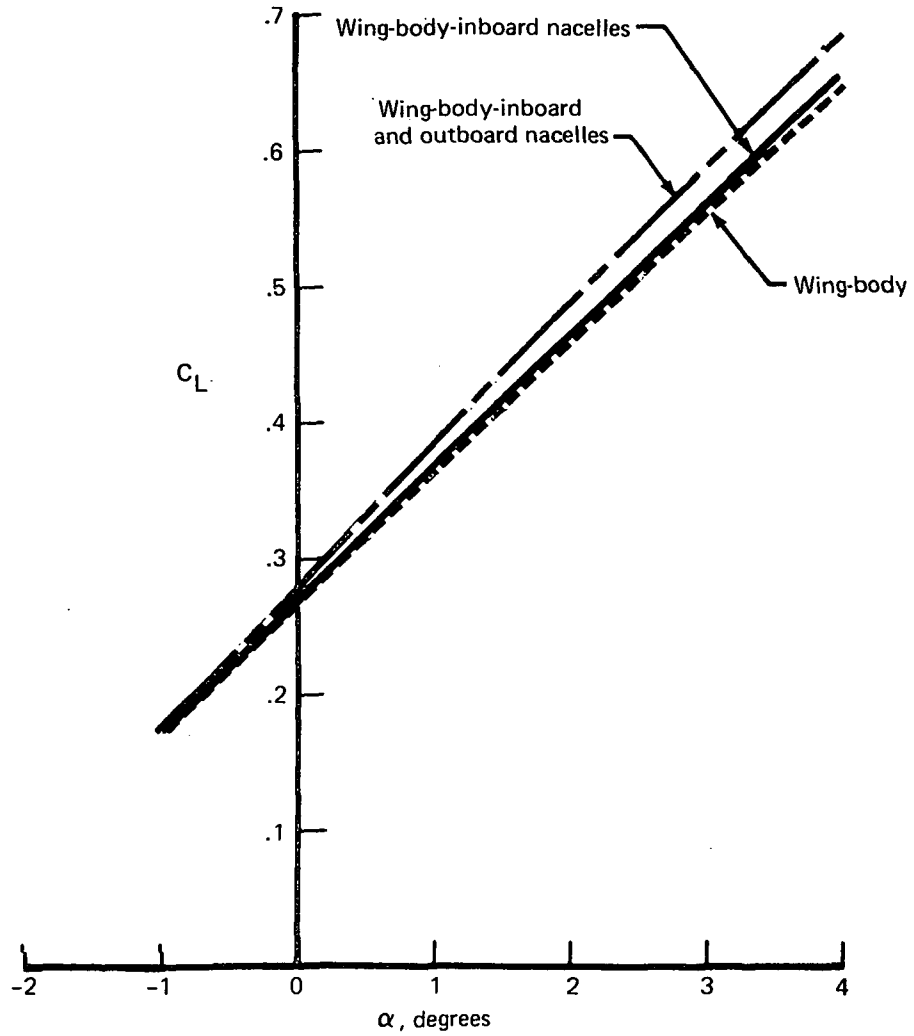


FIGURE 50.—EFFECT OF NACELLES ON CONFIGURATION LIFT CURVE, FOUR-ENGINE D-NOZZLE CASE

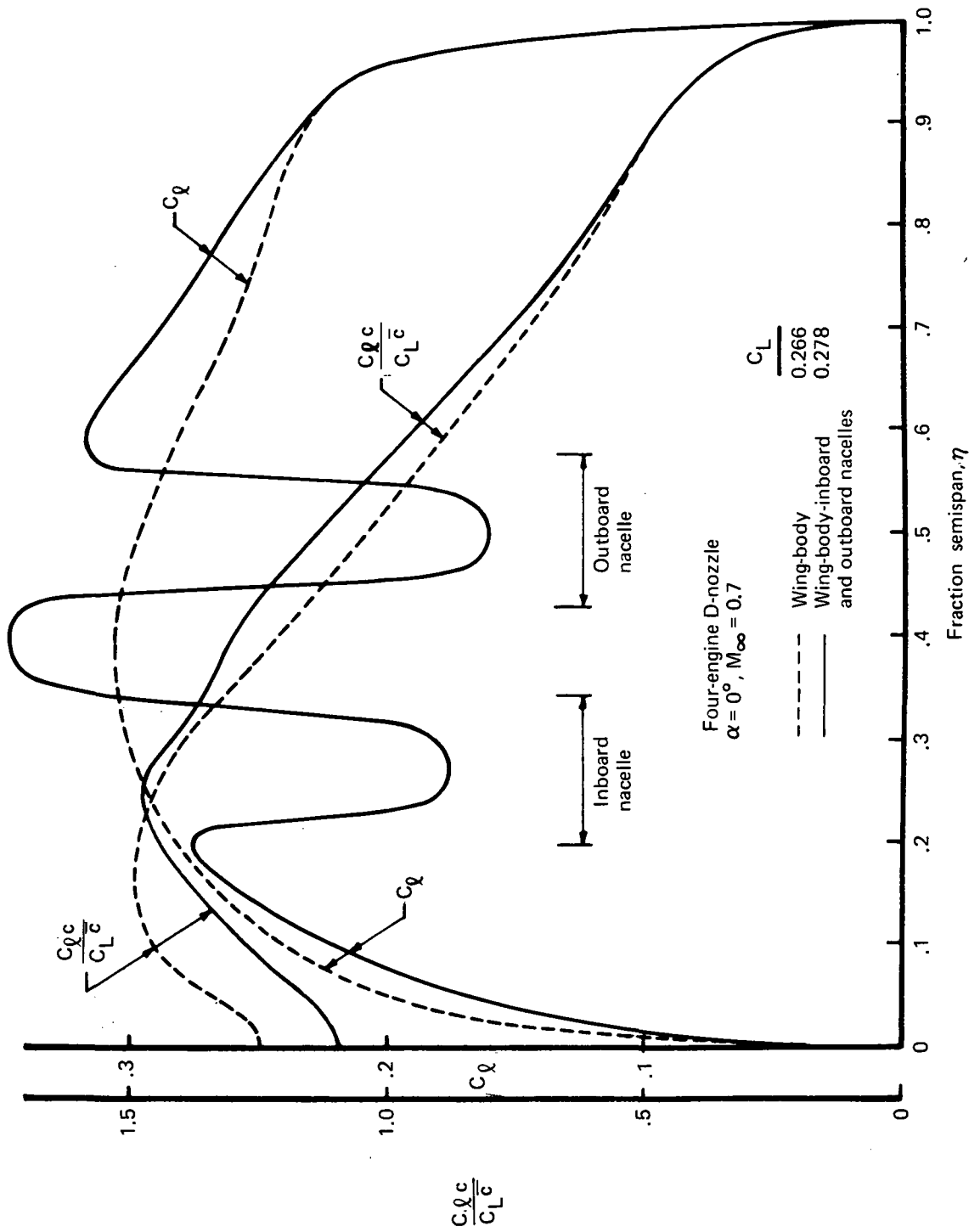


FIGURE 51.—EFFECT OF NACELLES ON WING LOAD DISTRIBUTION AND SECTIONAL LIFT DISTRIBUTION

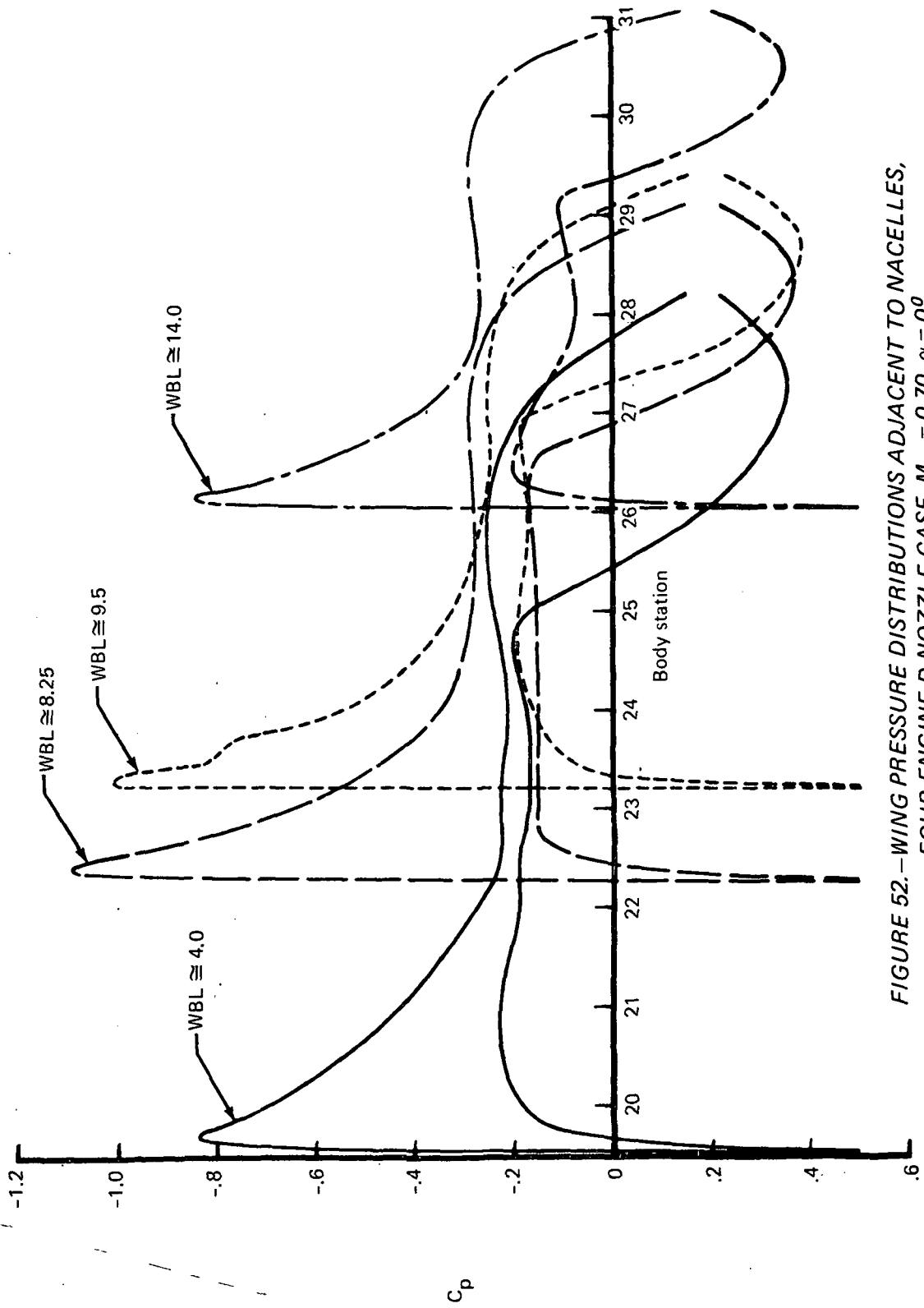


FIGURE 52.—WING PRESSURE DISTRIBUTIONS ADJACENT TO NACELLES,
 FOUR-ENGINE D-NOZZLE CASE, $M_\infty = 0.70$, $\alpha = 0^\circ$

$\alpha = 0^\circ$
 $M_\infty = 0.7$

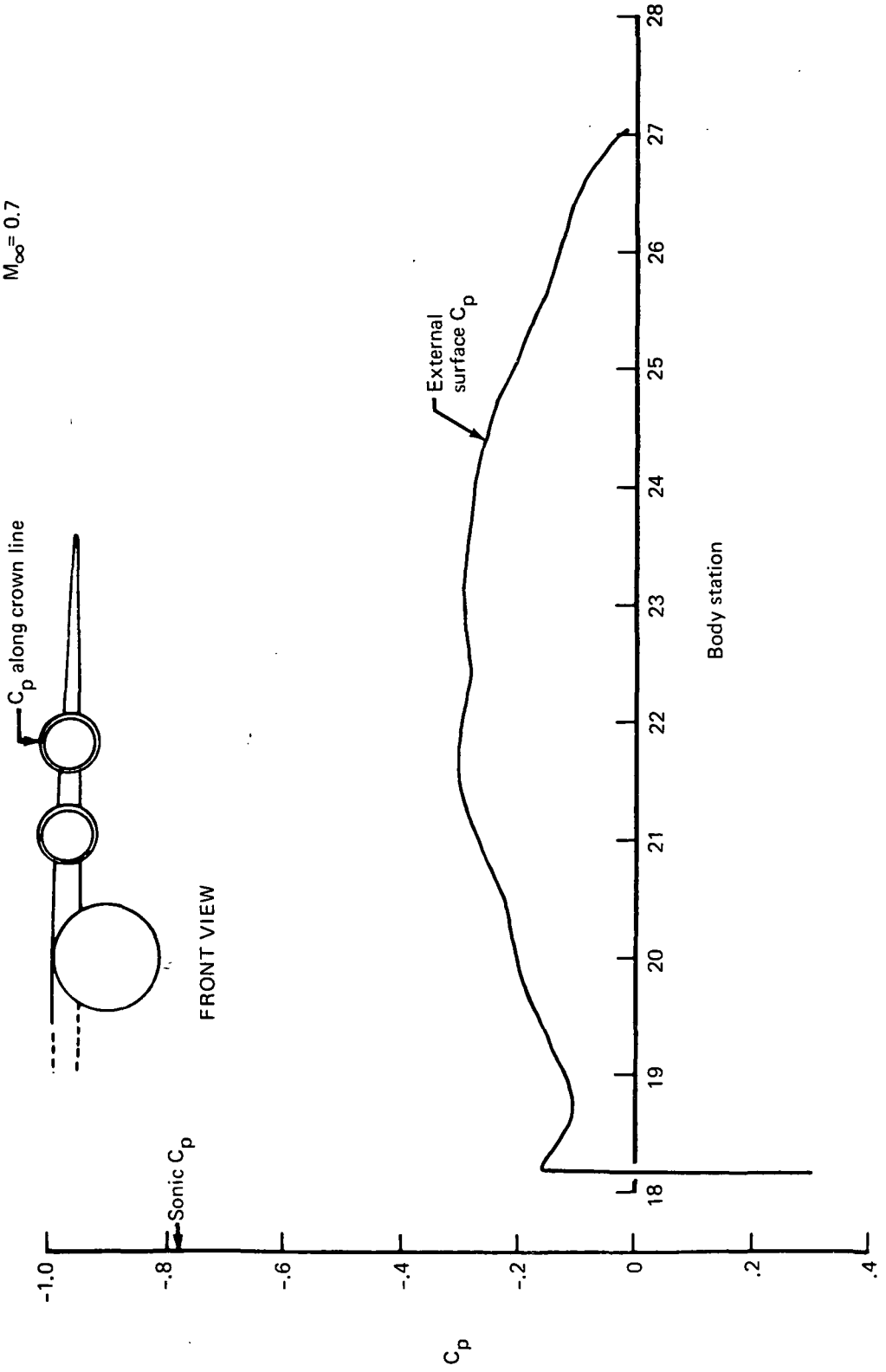


FIGURE 53.—PRESSURE DISTRIBUTION ALONG NACELLE CROWN LINE—OUTBOARD NACELLE, FOUR-ENGINE D-NOZZLE CASE

$\alpha = 0^\circ$
 $M_\infty = 0.7$

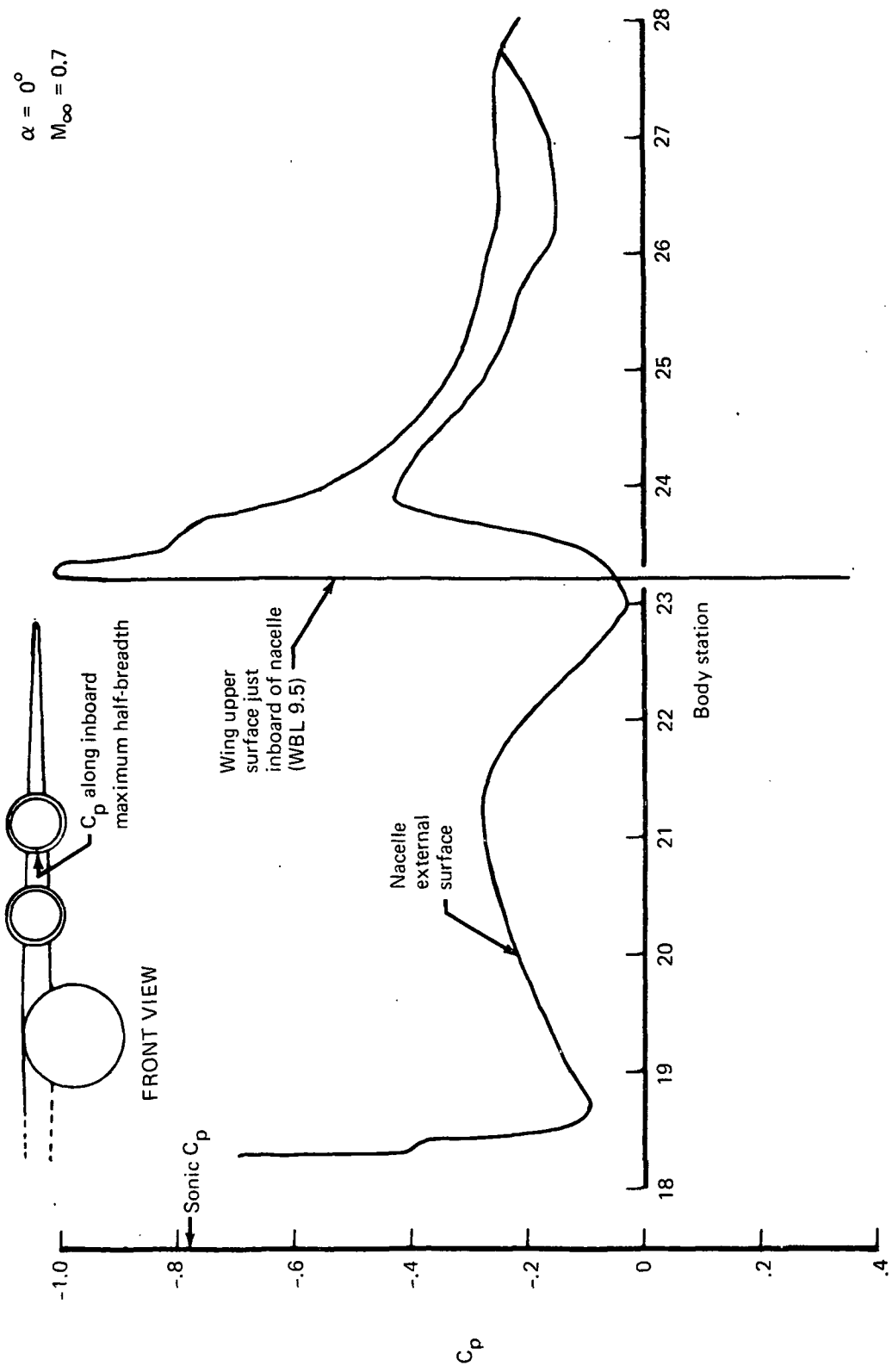


FIGURE 54.—PRESSURE DISTRIBUTION ALONG INBOARD SIDE OF NACELLE—OUTBOARD NACELLE, FOUR-ENGINE, D-NOZZLE CASE

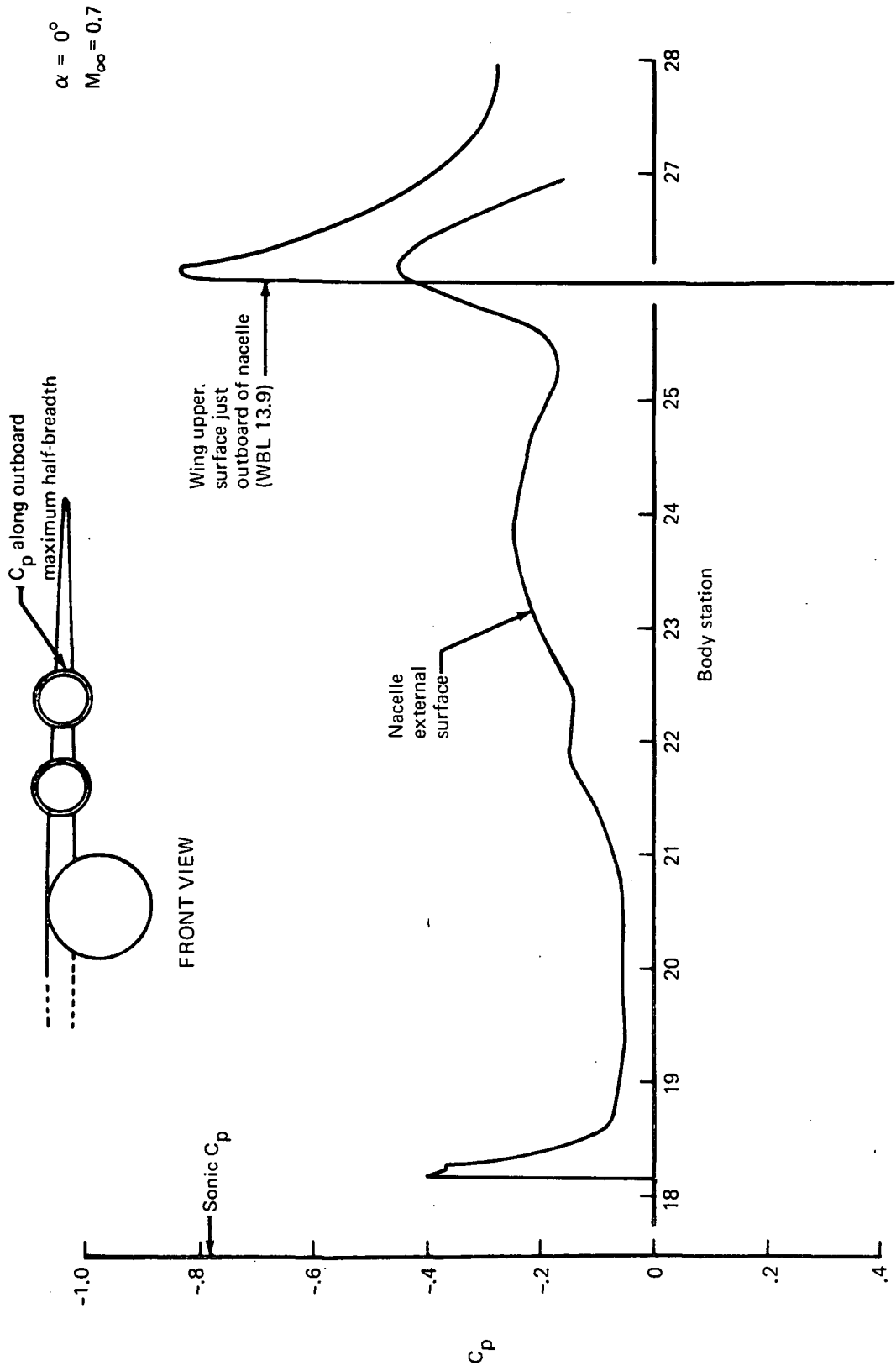
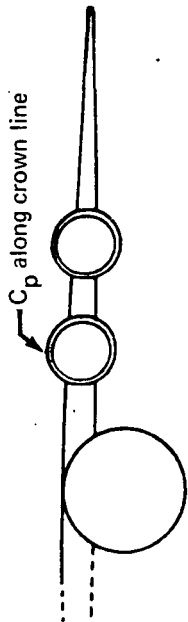


FIGURE 55.—PRESSURE DISTRIBUTION ALONG OUTBOARD SIDE OF NACELLE—OUTBOARD NACELLE, FOUR-ENGINE D-NOZZLE CASE



FRONT VIEW

Four-engine, D-nozzle
 $\alpha = 0^\circ$, $M_\infty = 0.7$

— Sonic C_p level

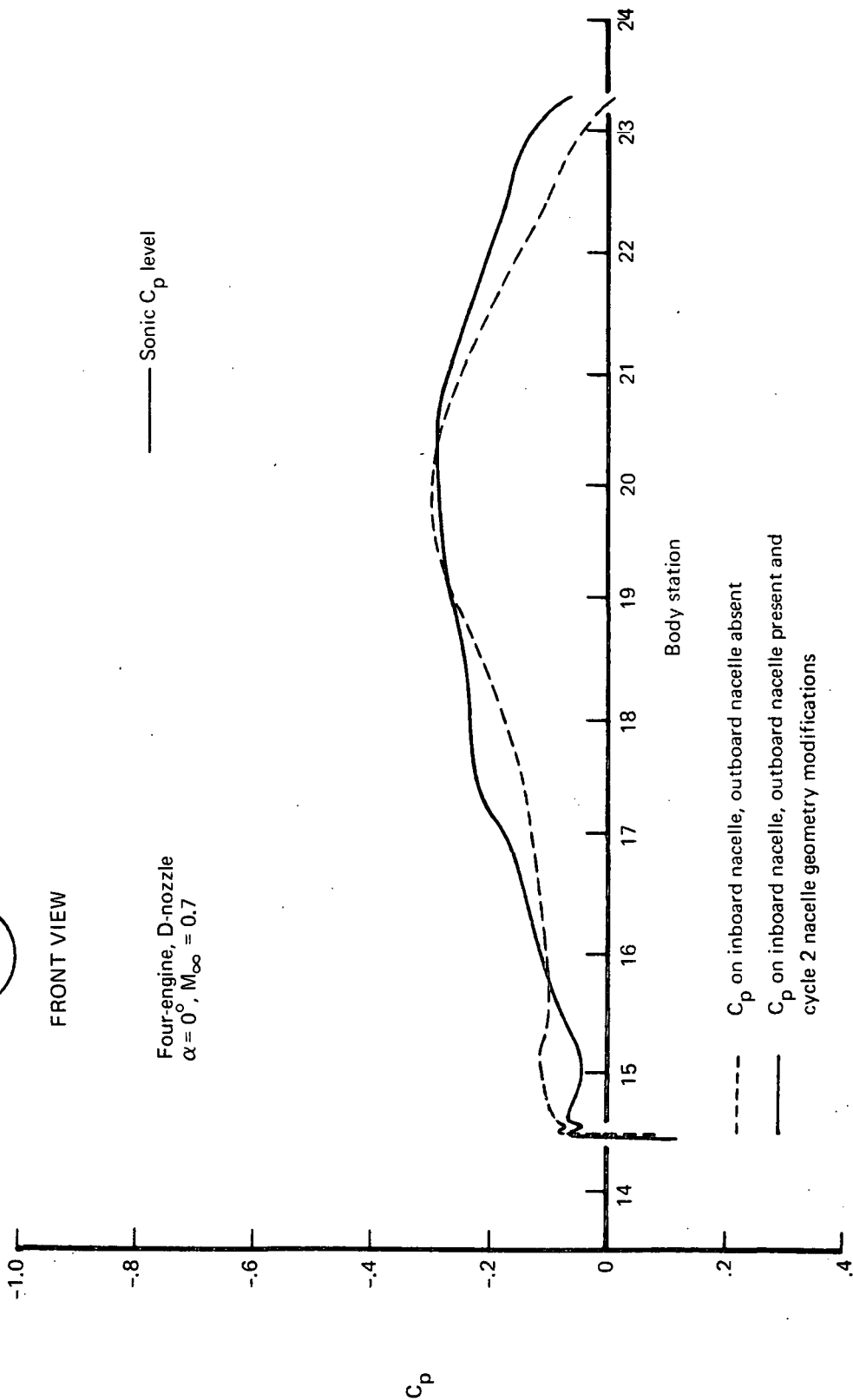


FIGURE 56.—PRESSURE DISTRIBUTION ALONG NACELLE CROWN LINE—
 INBOARD NACELLE, EXTERNAL SURFACE

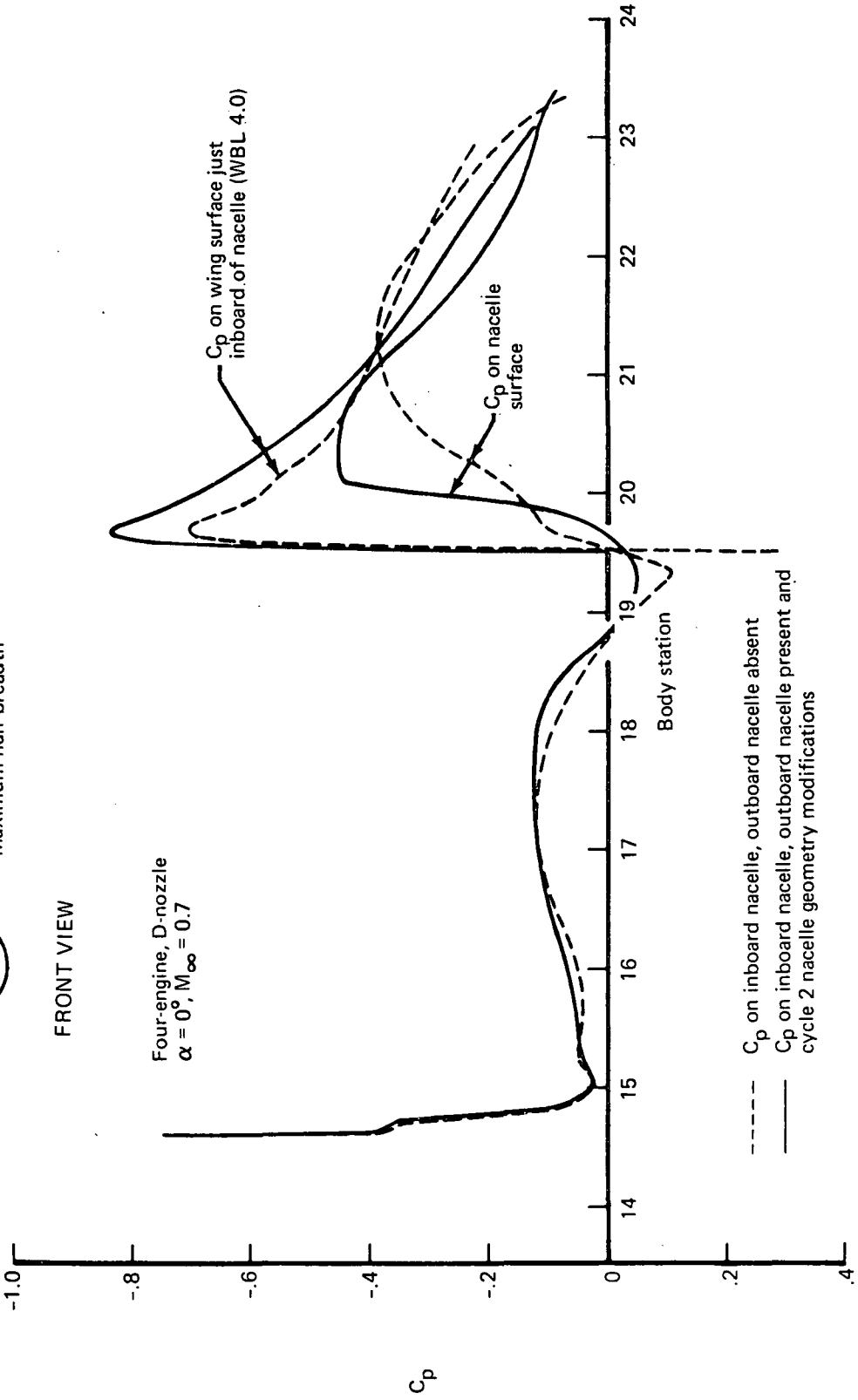
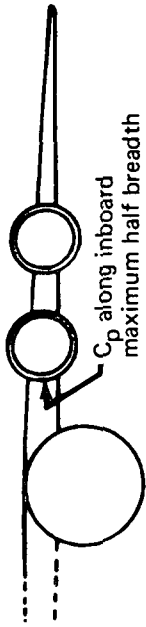


FIGURE 57.—PRESSURE DISTRIBUTION ALONG INBOARD SIDE OF NACELLE—INBOARD NACELLE, EXTERNAL SURFACE

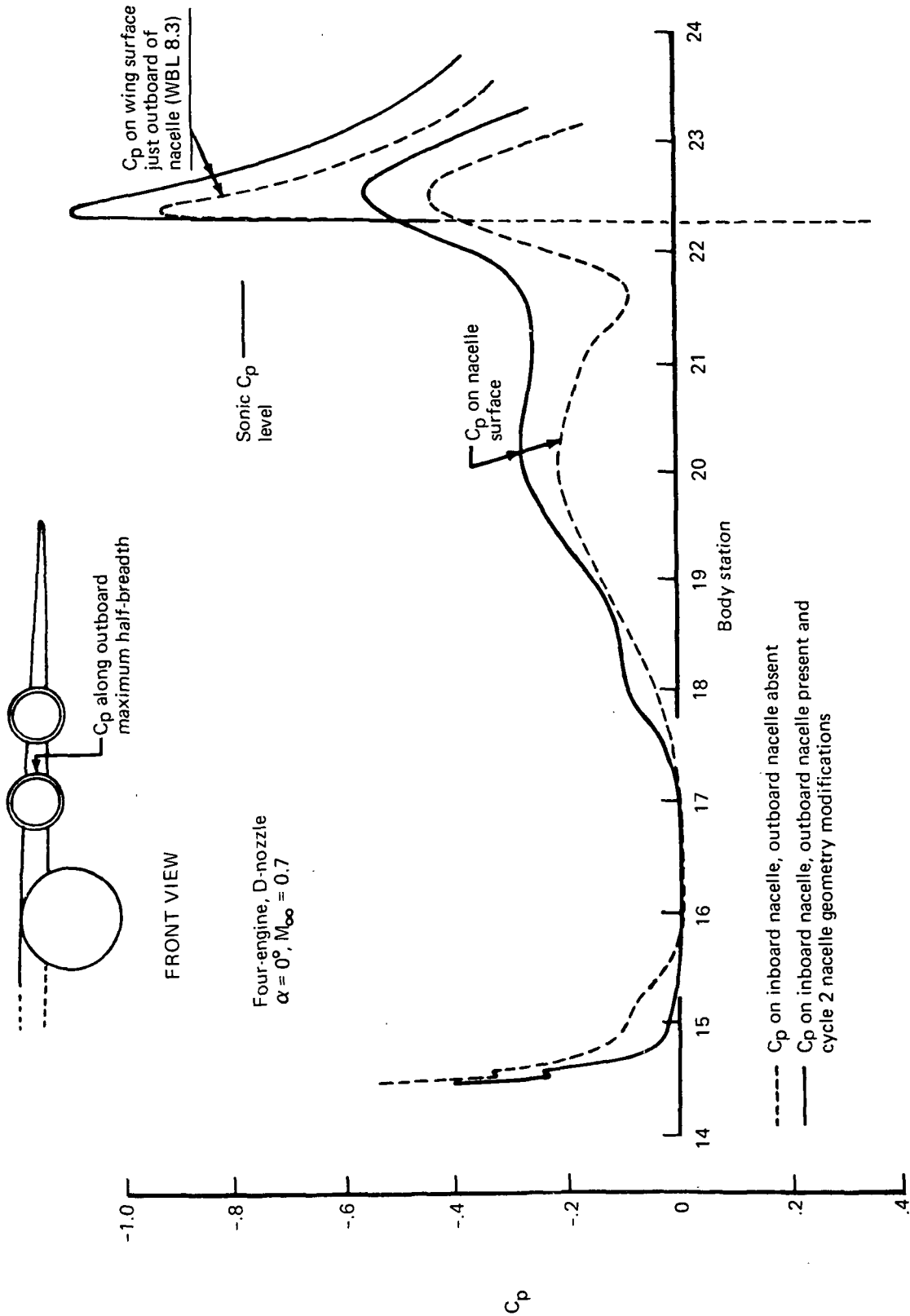


FIGURE 58.—PRESSURE DISTRIBUTION ALONG OUTBOARD SIDE OF NACELLE—INBOARD NACELLE, EXTERNAL SURFACE

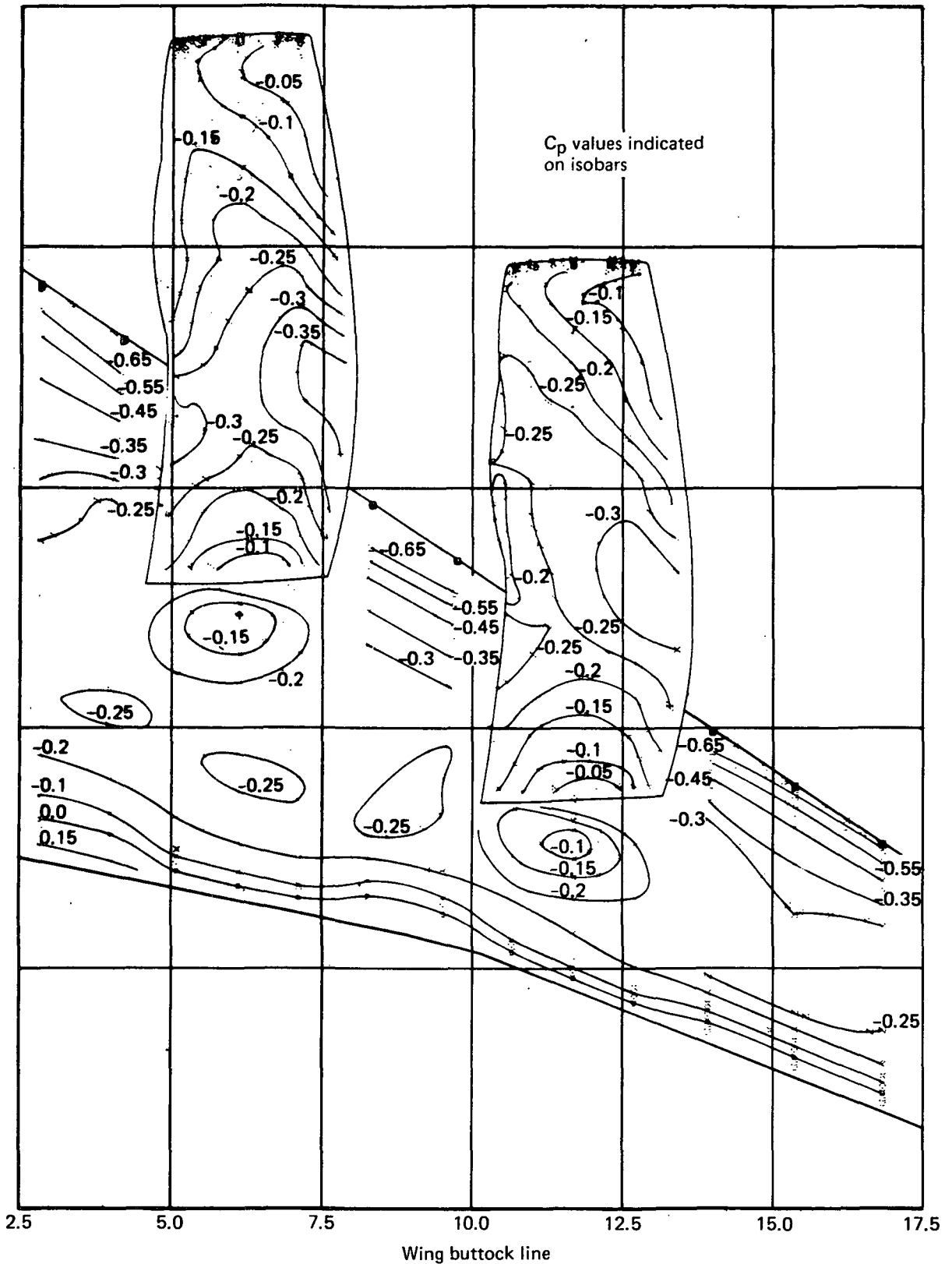


FIGURE 59.—UPPER-SURFACE ISOBARS, FOUR-ENGINE D-NOZZLE CASE, $M_\infty = 0.7$, $\alpha = 0^\circ$

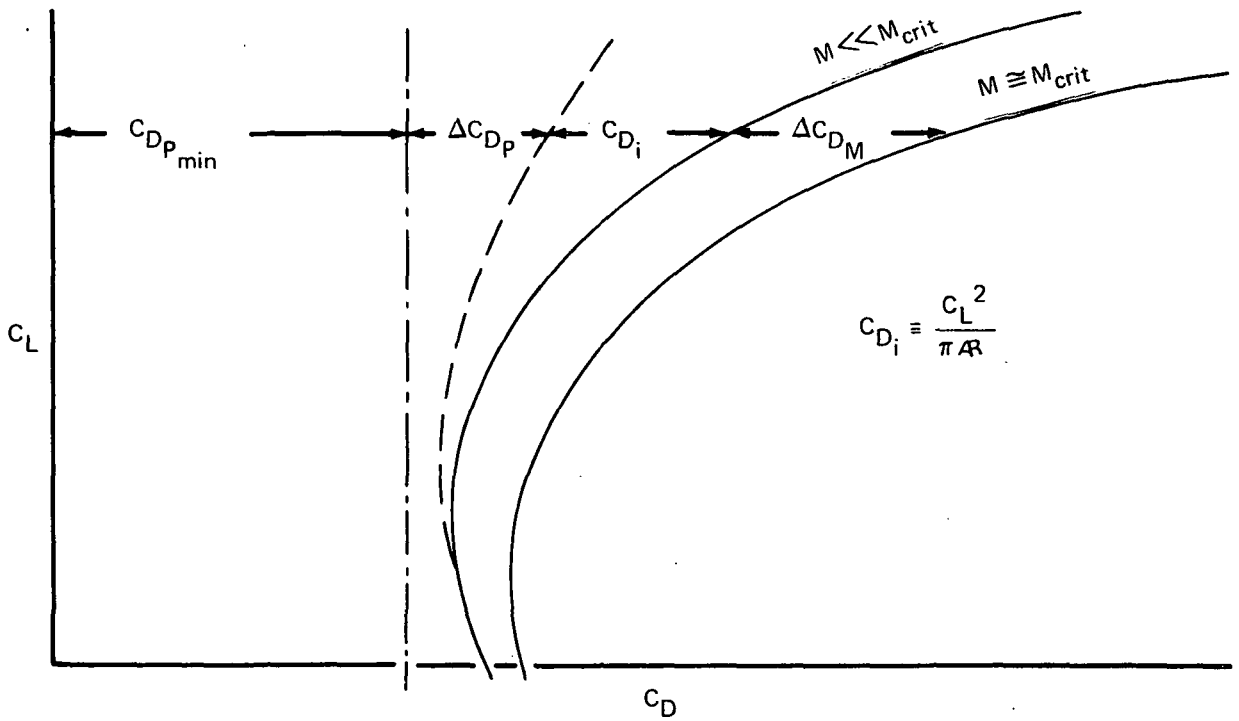


FIGURE 60.—DEFINITION OF DRAG TERMINOLOGY

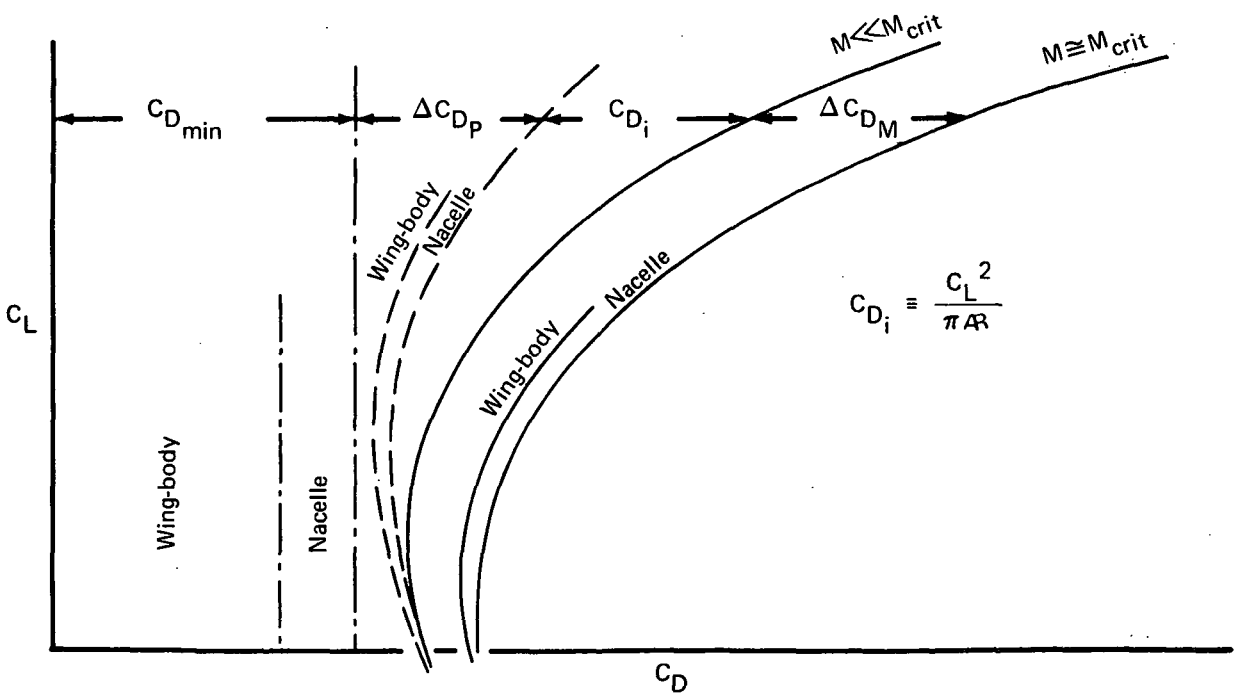


FIGURE 61.—ADDITION OF NACELLE DRAG TO WING-BODY DRAG

$$C_D = C_{D_{wing-body}} + \Delta C_{D_{nacelle}}$$

$$R_e = 11.5 \times 10^6 / m \quad (3.5 \times 10^6 \text{ ft})$$

Tripped at 10% chord
Flow-through nacelles

Nacelle configuration

- Two-engine D-nozzle
- — — Four engine D-nozzle
- - - Two-engine spread nozzle
- - - - Four-engine spread nozzle

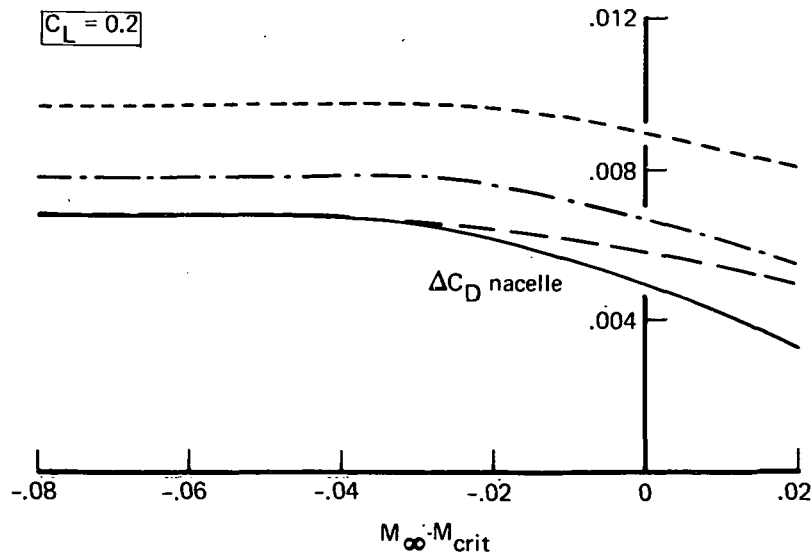
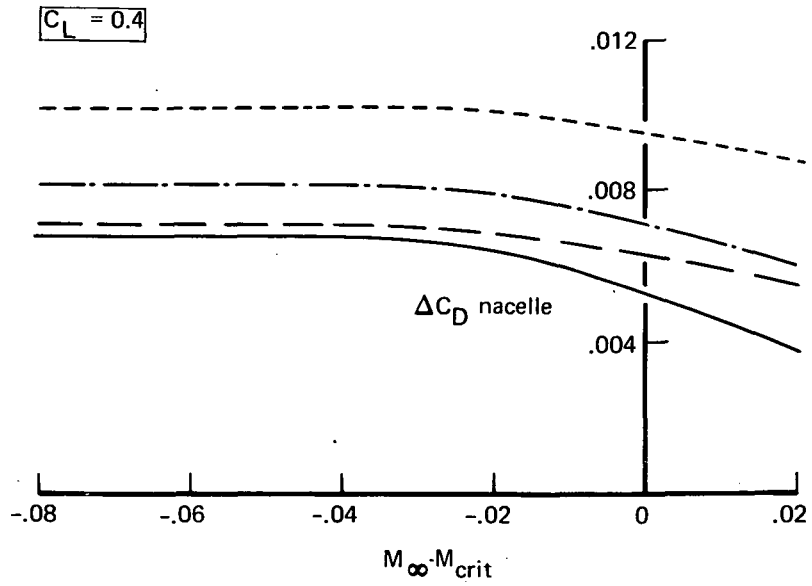


FIGURE 62.—ESTIMATED NACELLE DRAG INCREMENTS

Mixed flow turbofan engines

Design point SLS takeoff thrust 29°C (84°F)

- Turbine inlet temperature 1560°K (2800°R)
- Overall pressure ratio 25

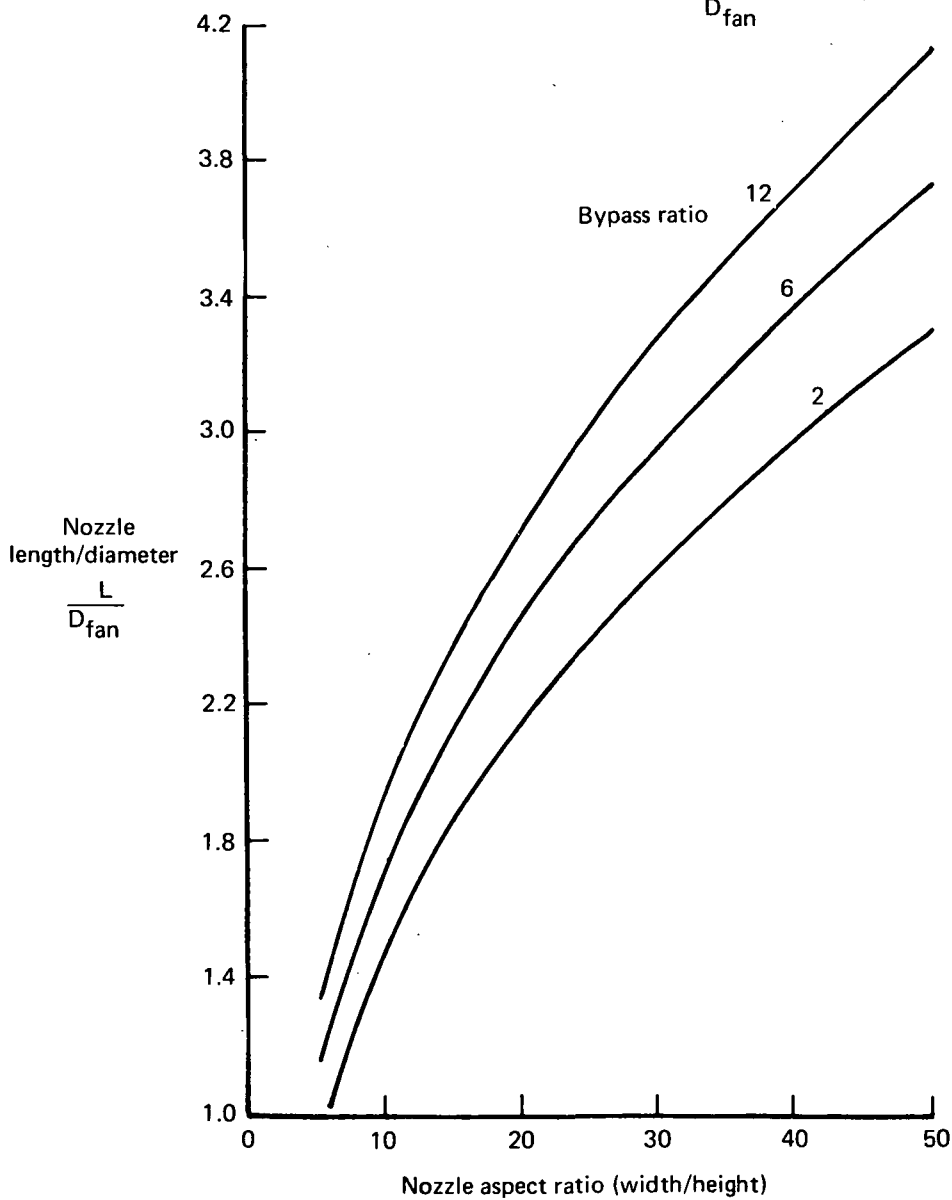
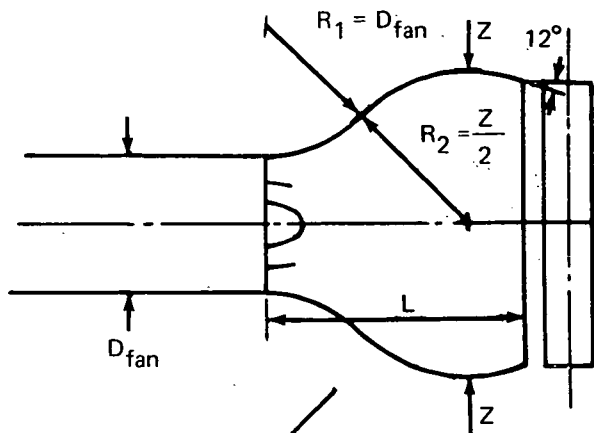


FIGURE 63.—GENERAL LENGTH REQUIREMENTS FOR SPREAD NOZZLES

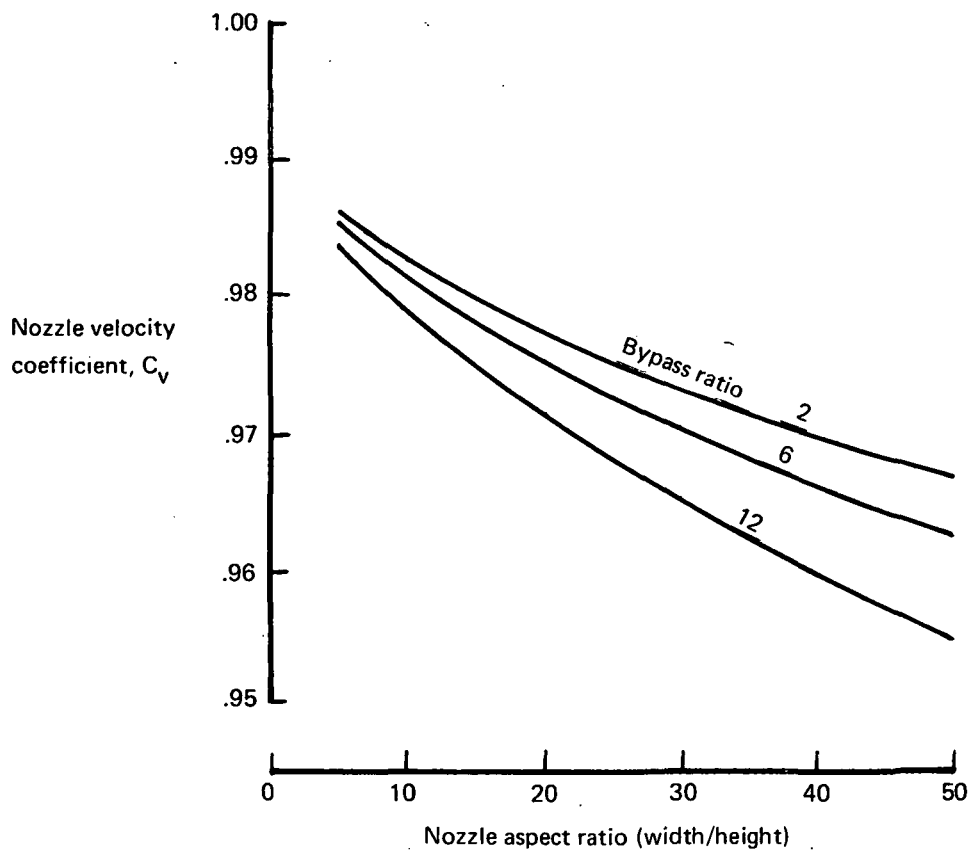


FIGURE 64.—EFFICIENCY OF SPREAD NOZZLES AT CRITICAL PRESSURE RATIO

$$\gamma = 1.40$$

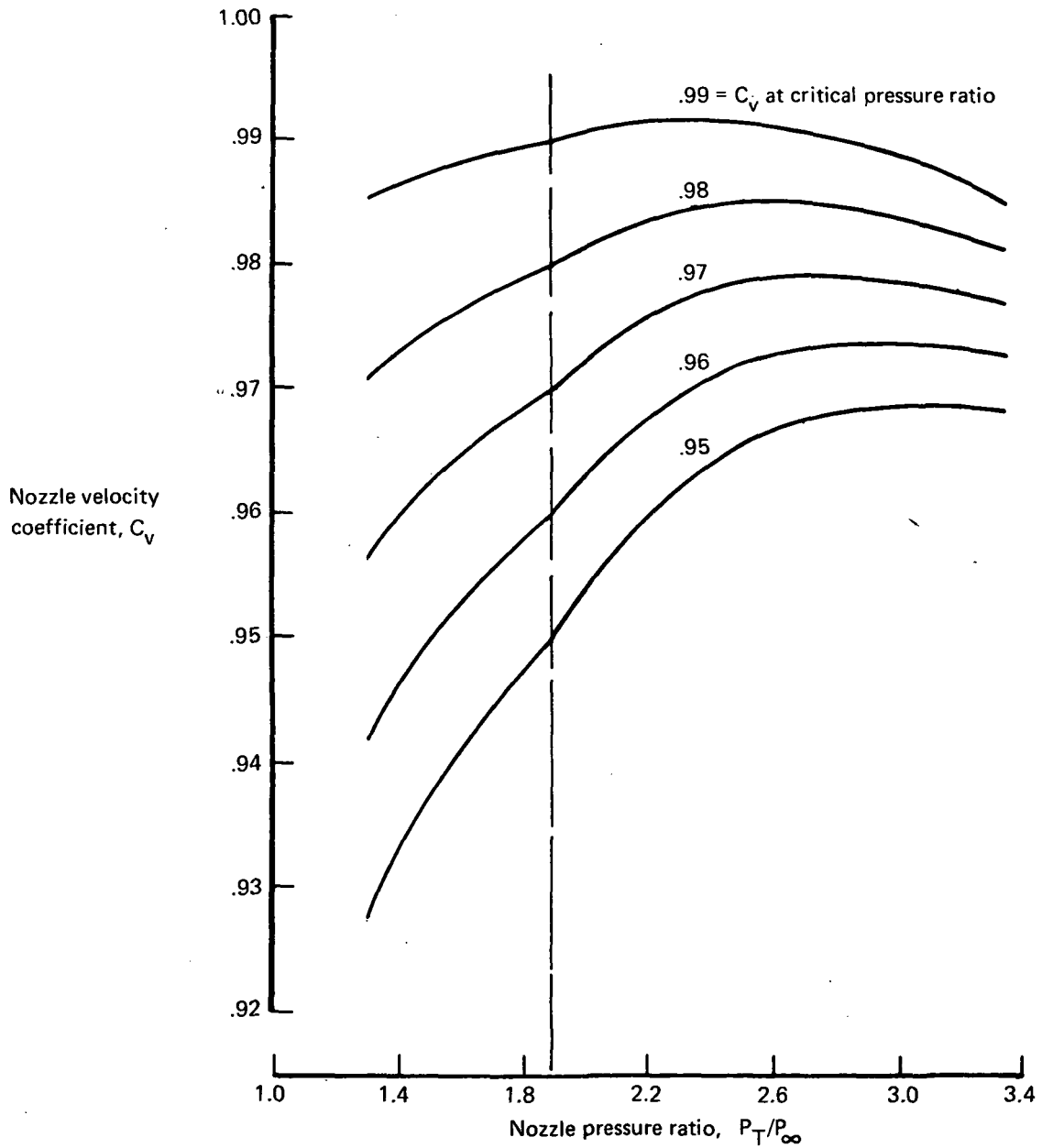


FIGURE 65.—EFFECT OF PRESSURE RATIO ON NOZZLE EFFICIENCY

Mixed flow turbofan engines
 Design point SLS takeoff thrust at 29°C (84°F)
 Turbine inlet temperature 1560°K (2800°R)
 Overall pressure ratio = 25

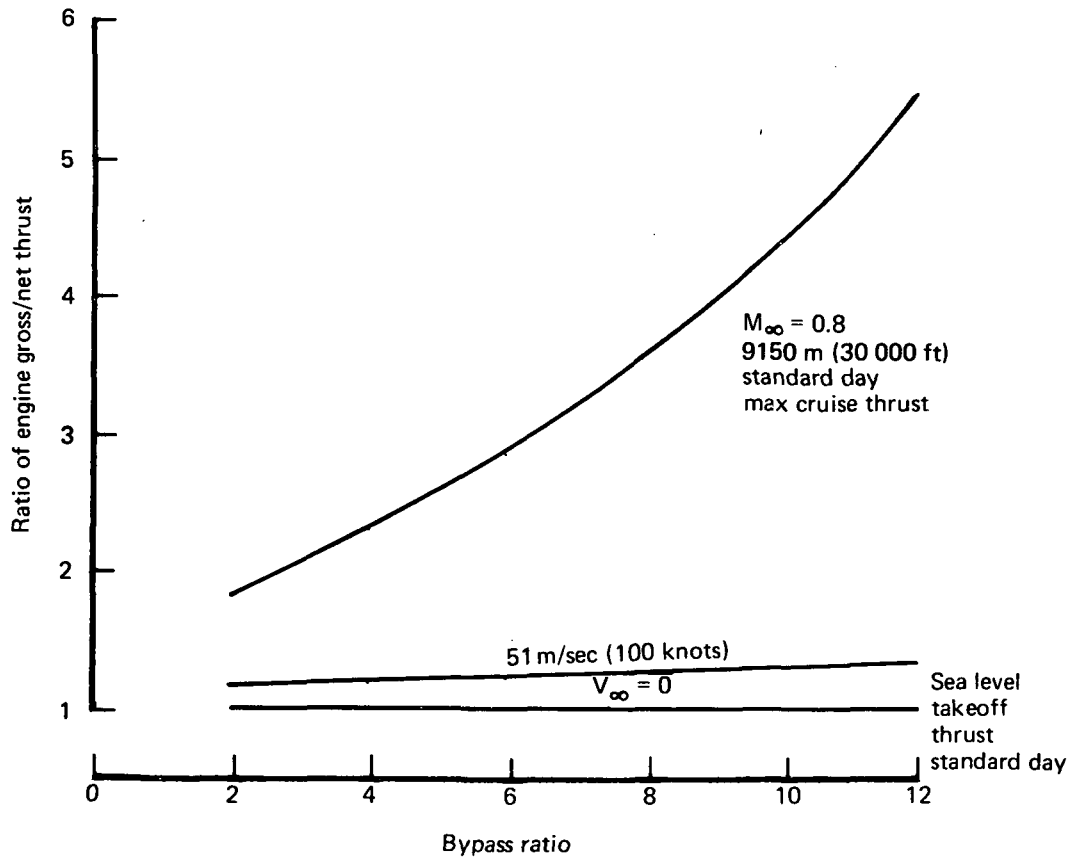


FIGURE 66.—RATIO OF ENGINE GROSS/NET THRUST

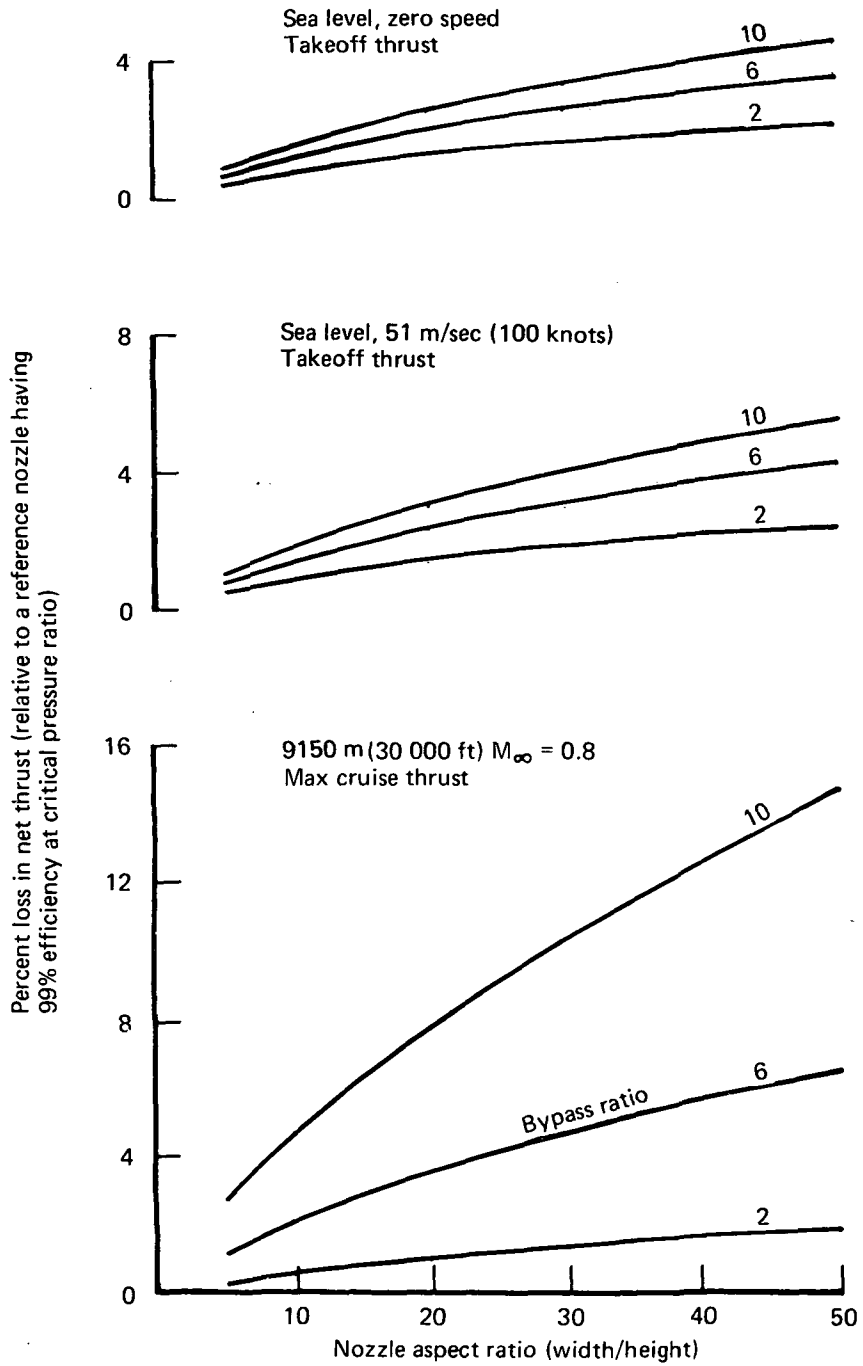


FIGURE 67.—THRUST LOSS OF SPREAD NOZZLES

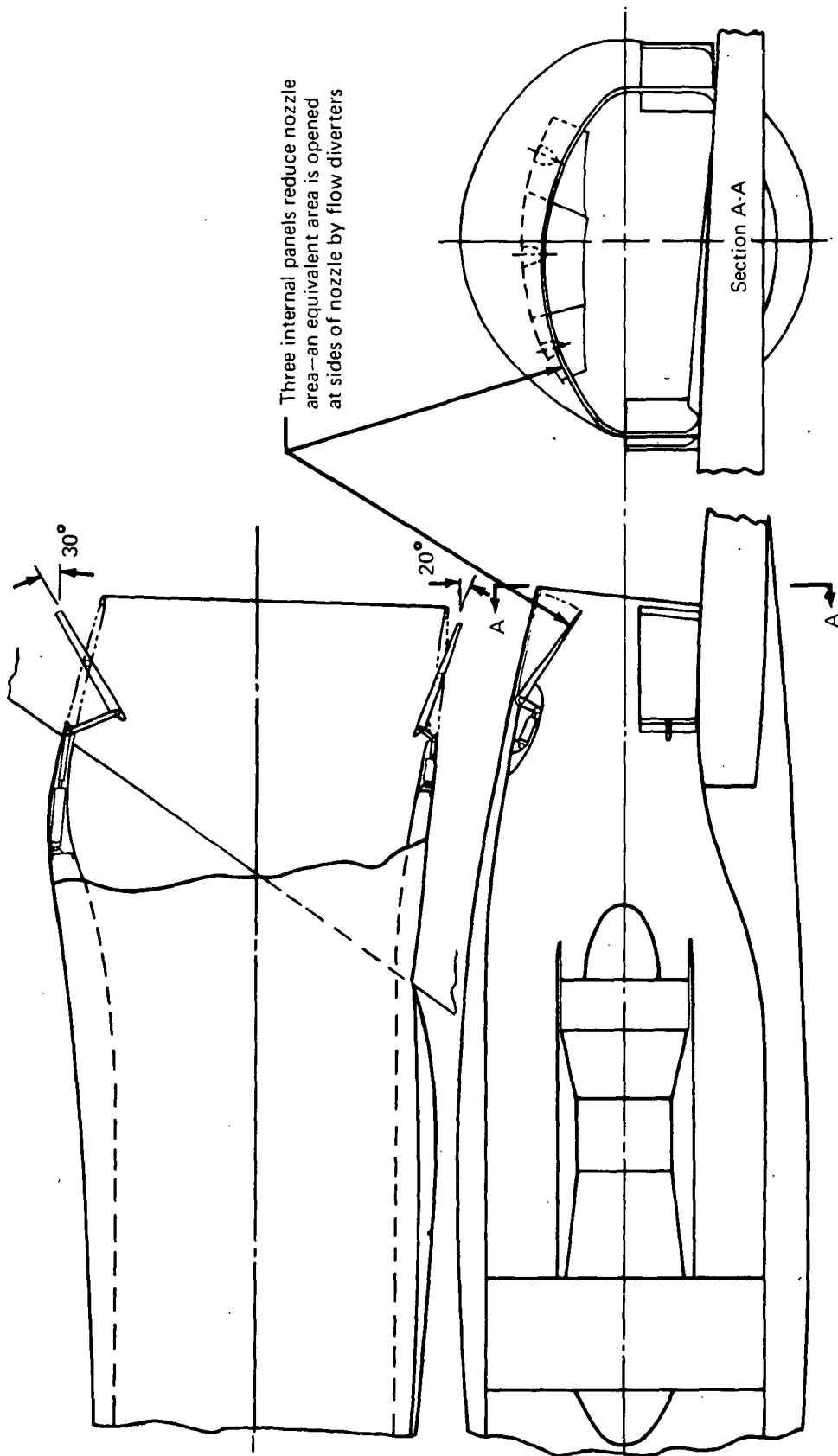


FIGURE 68.—VARIABLE GEOMETRY, TWO-ENGINE D-NOZZLE CASE

The fences that are required to stabilize the rectangular nozzle will be extended into movable fins that will divert the exhaust flow outward as desired.

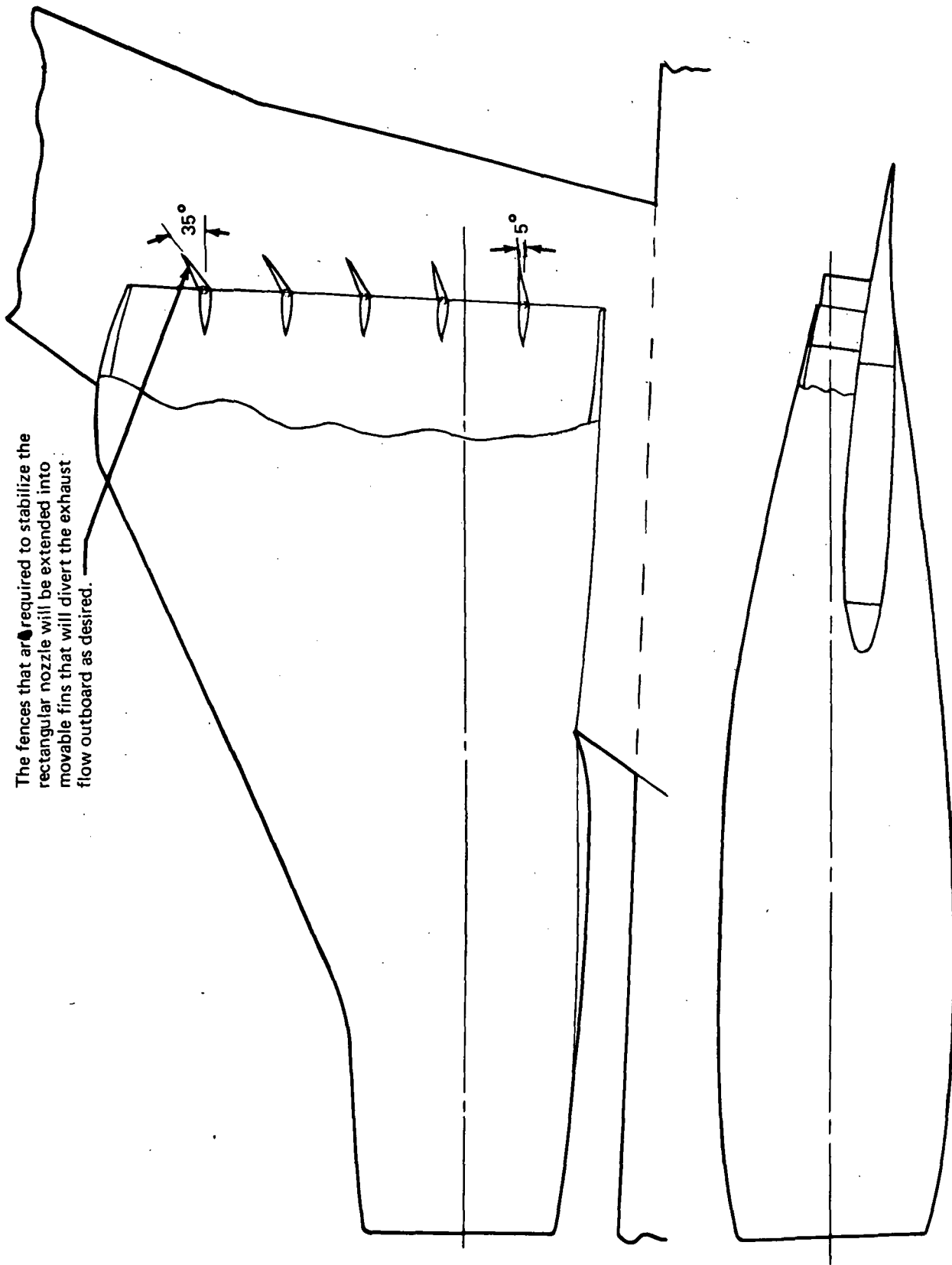


FIGURE 69. — VARIABLE GEOMETRY, TWO-ENGINE SPREAD NOZZLE CASE

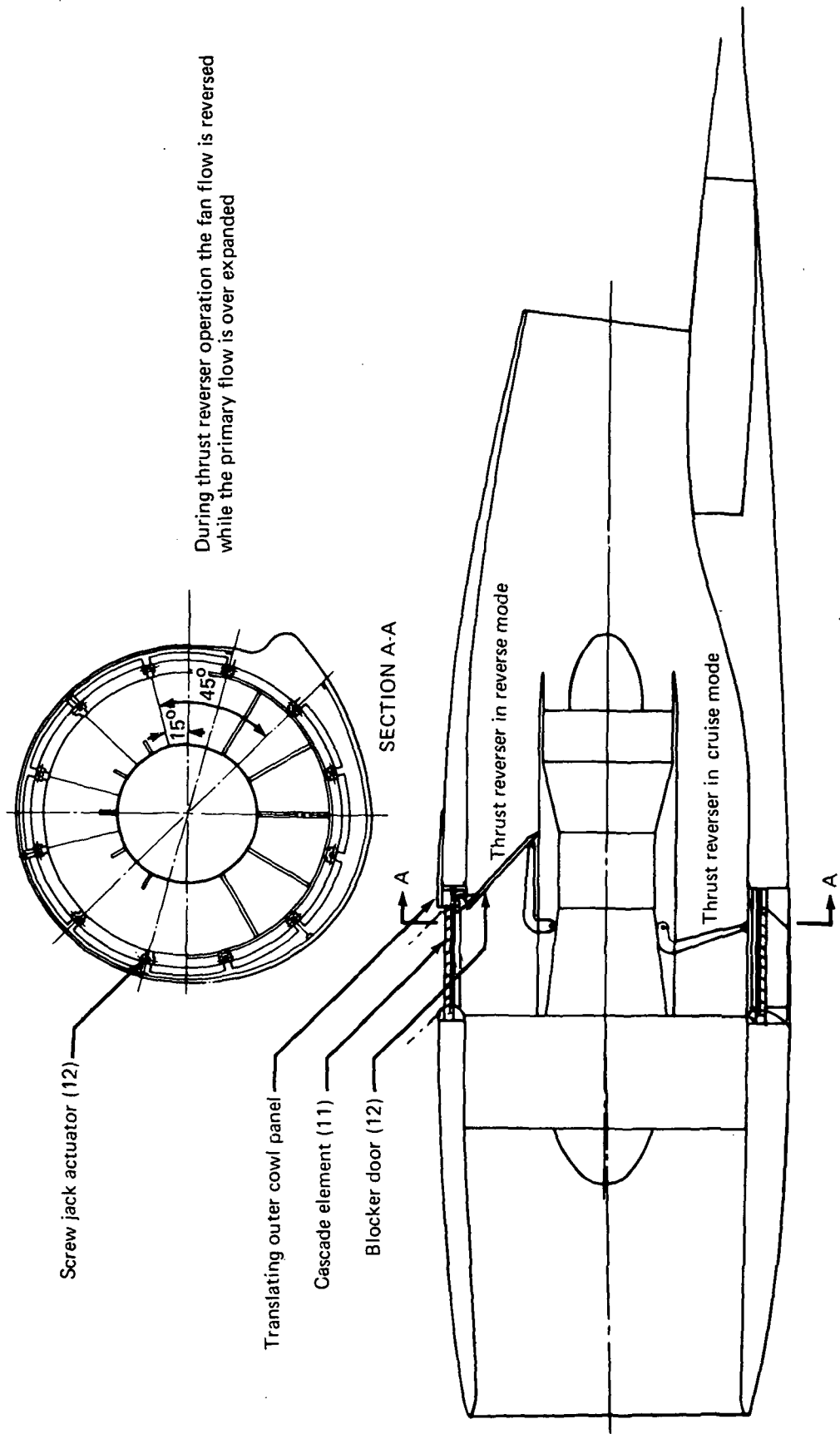


FIGURE 70.—THRUST REVERSER ARRANGEMENT, TWO-ENGINE D-NOZZLE CASE

During thrust reverser operation the fan flow is reversed while the primary flow is over expanded

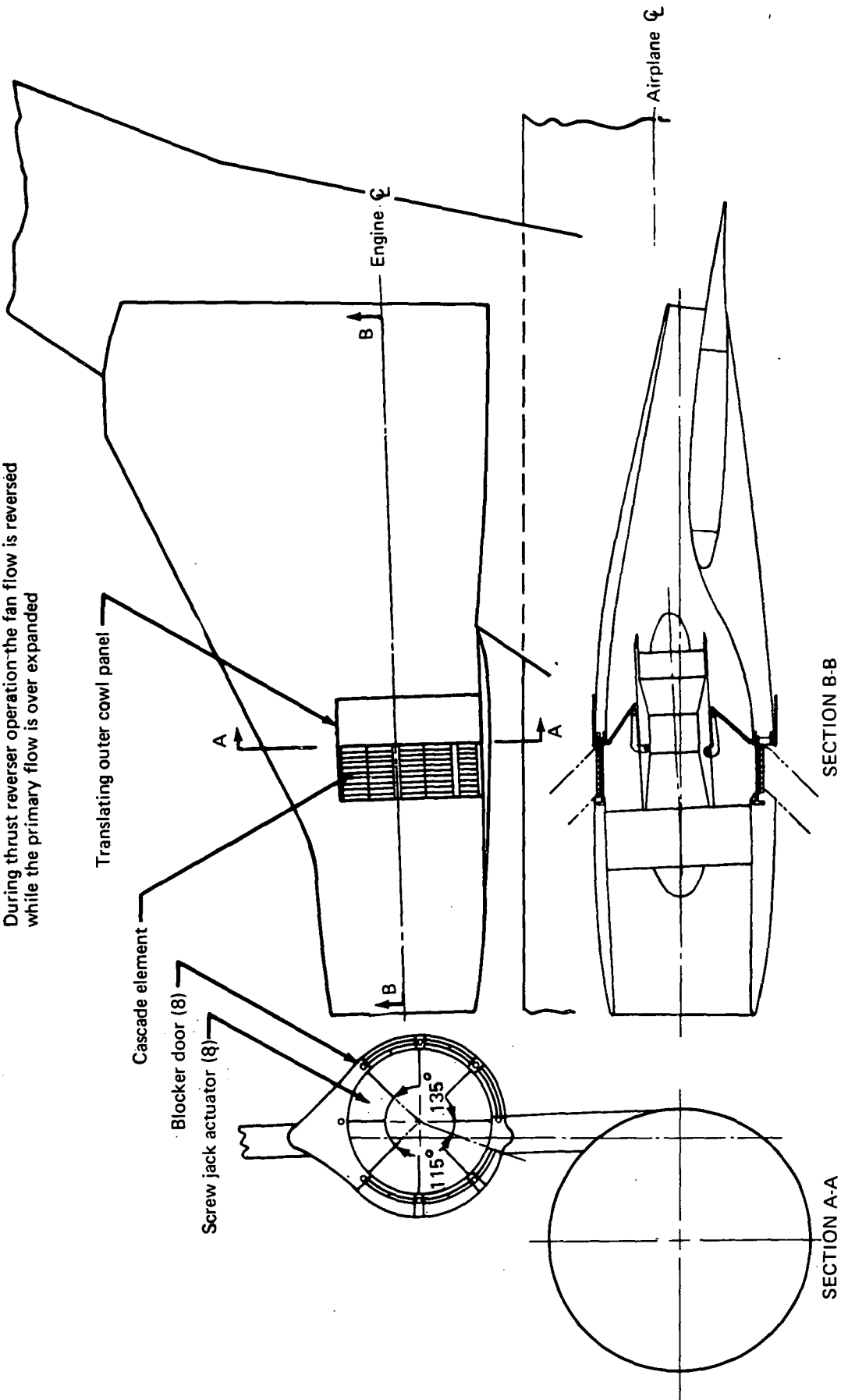


FIGURE 71.—THRUST REVERSER ARRANGEMENT, TWO-ENGINE SPREAD NOZZLE CASE

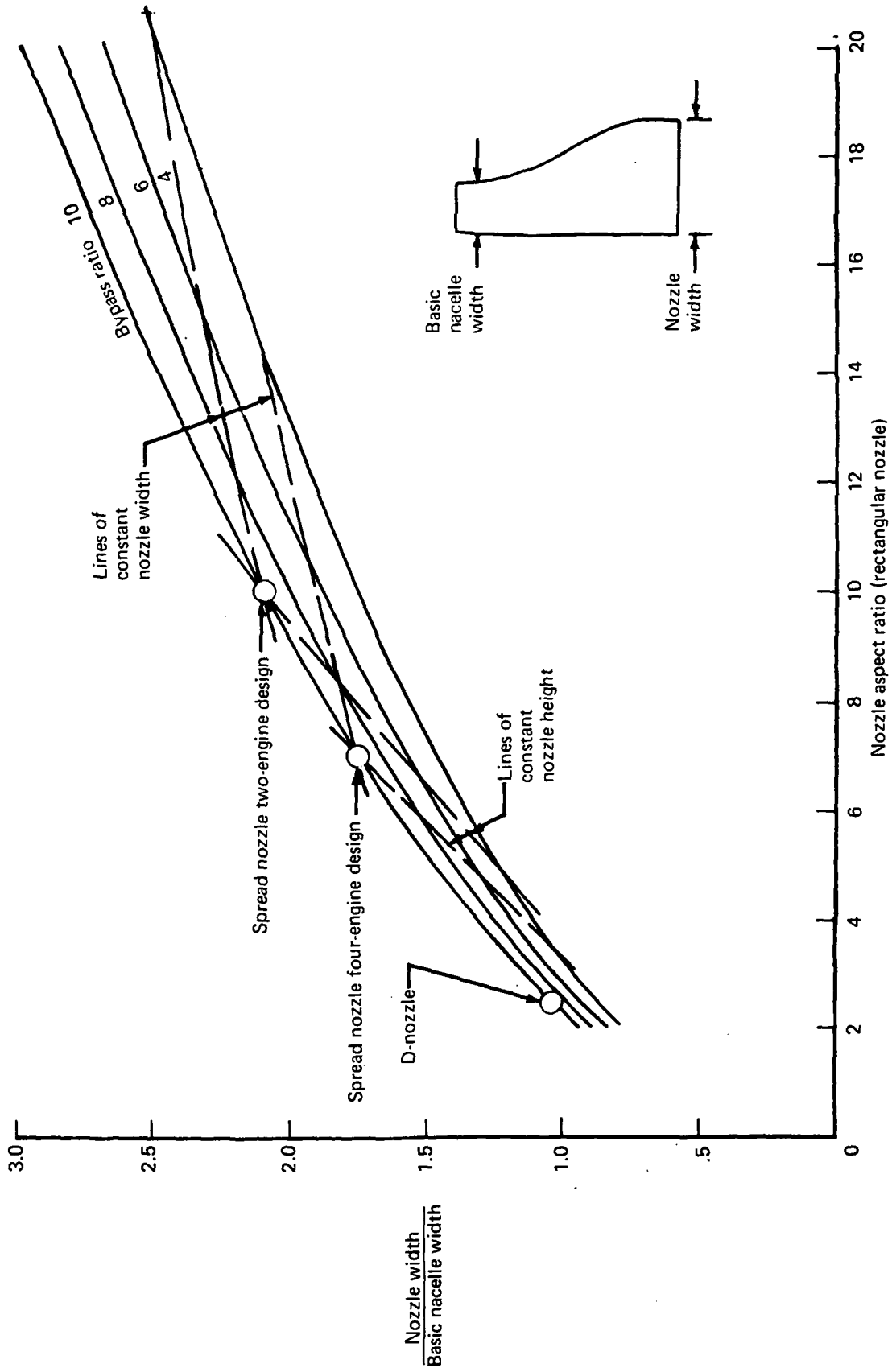


FIGURE 72.—EFFECTS OF BYPASS RATIO AND NOZZLE ASPECT RATIO ON NOZZLE/NACELLE GEOMETRY

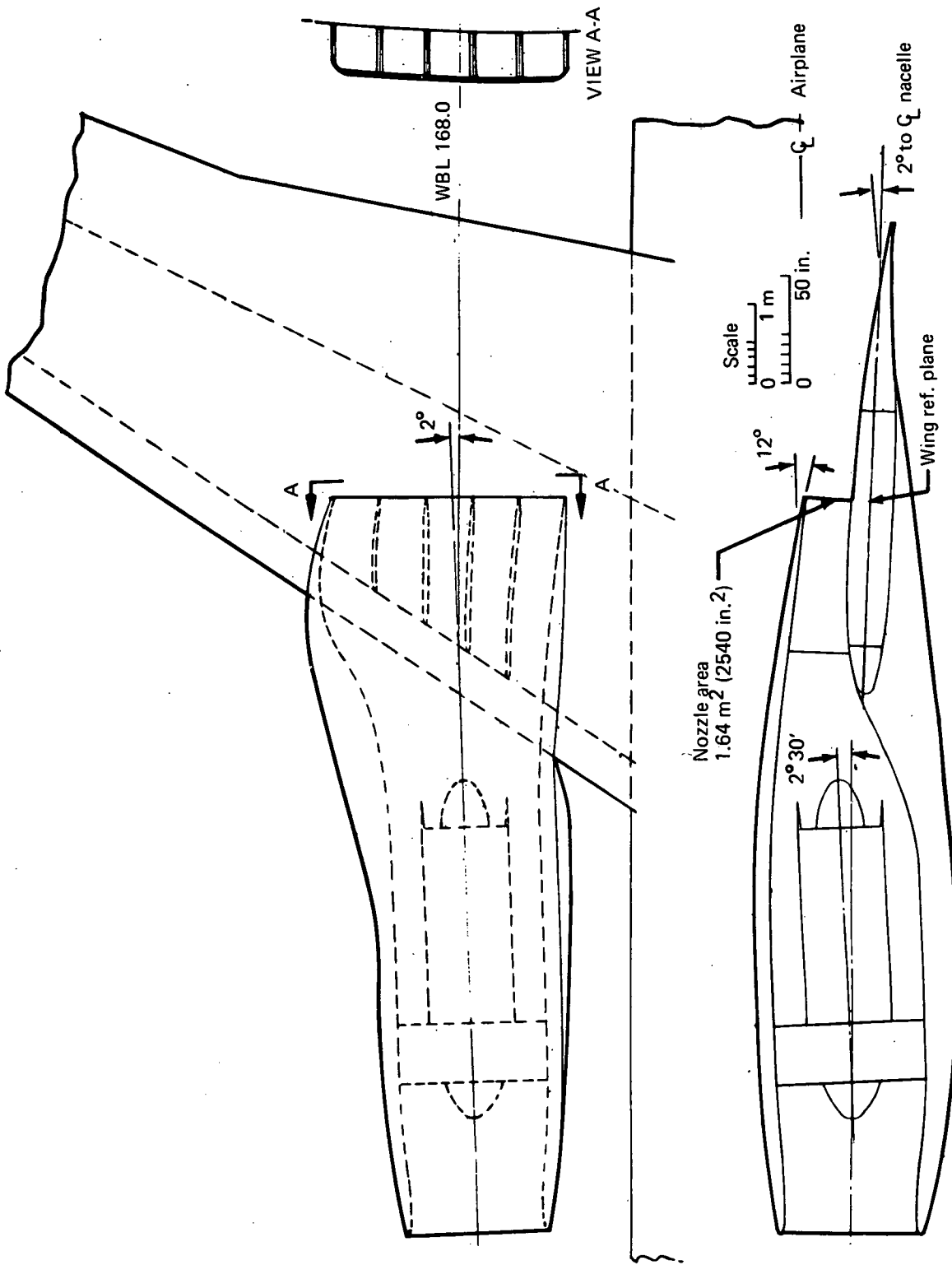


FIGURE 73.—TWIN-ENGINE AIRPLANE, 161 560 N (36 320 LB) ENGINE, BYPASS RATIO = 4,
NOZZLE AR = 5, RECTANGULAR OFFSET NOZZLE

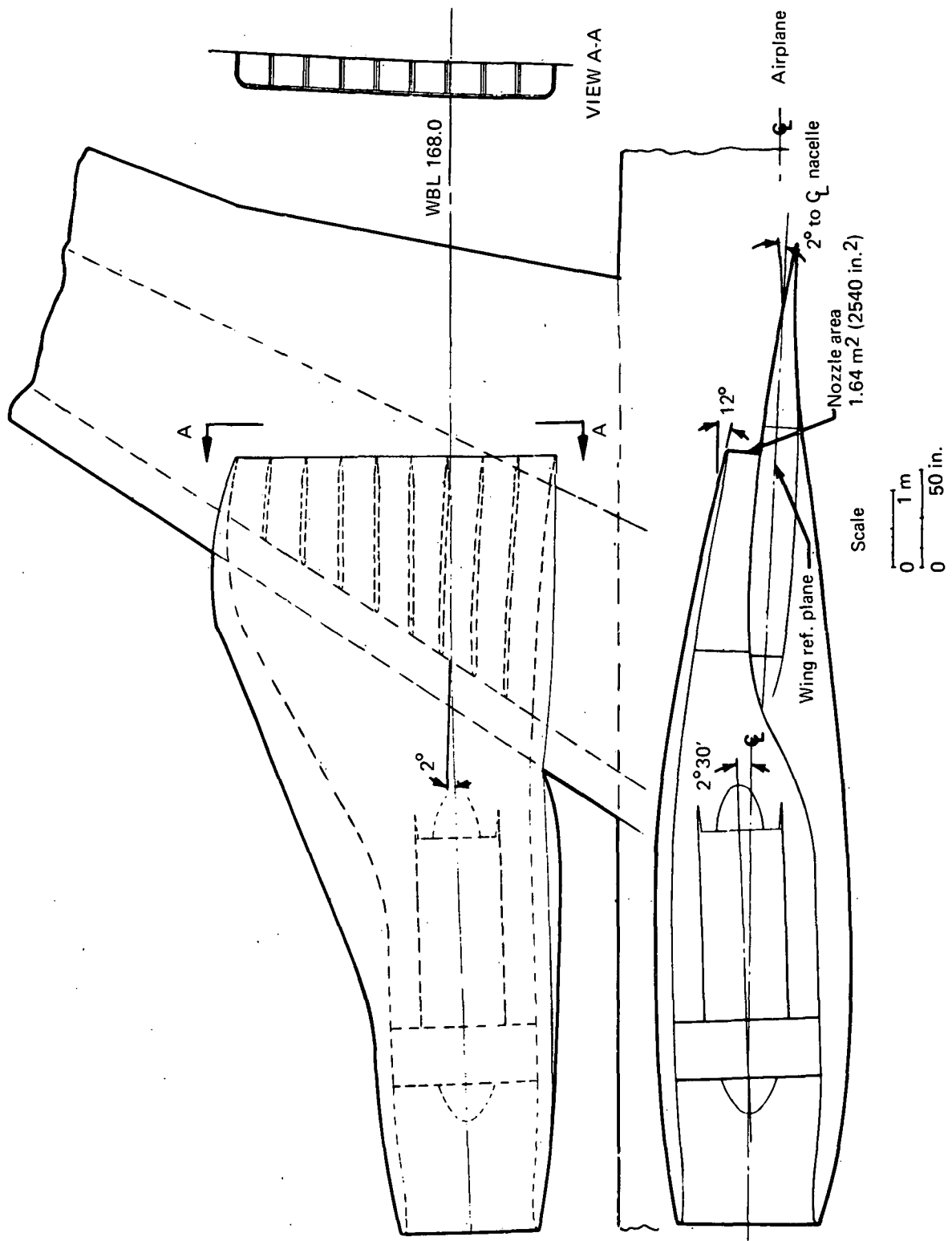


FIGURE 74.—TWIN-ENGINE AIRPLANE, 161 560 N. (36 320 LB) ENGINE, BYPASS RATIO = 4, NOZZLE α = 10, RECTANGULAR OFFSET NOZZLE

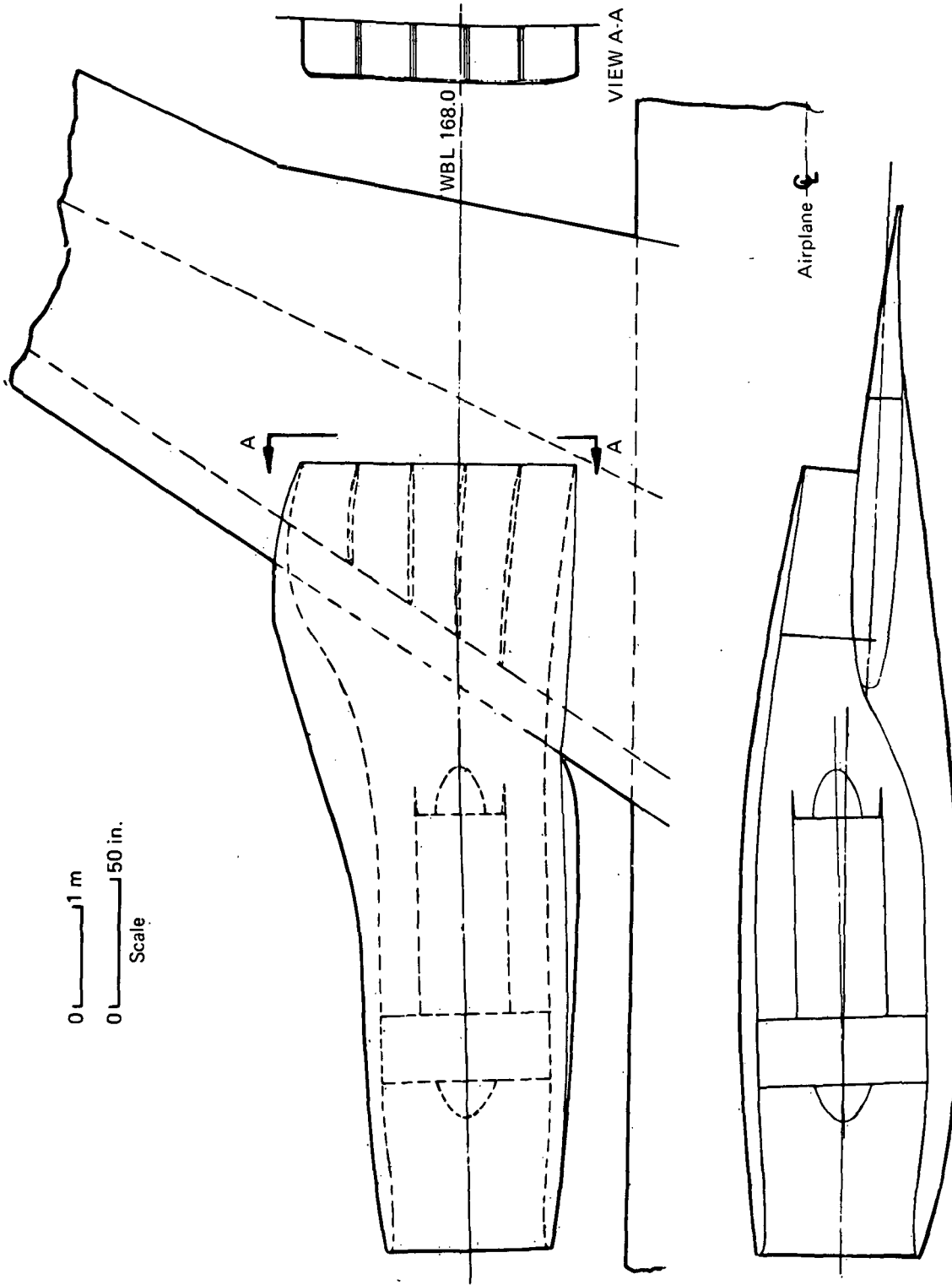


FIGURE 75.—TWIN-ENGINE AIRPLANE, 161 560 N (36 320 LB) ENGINE, BYPASS RATIO = 6,
NOZZLE $\Delta R = 5$, RECTANGULAR OFFSET NOZZLE

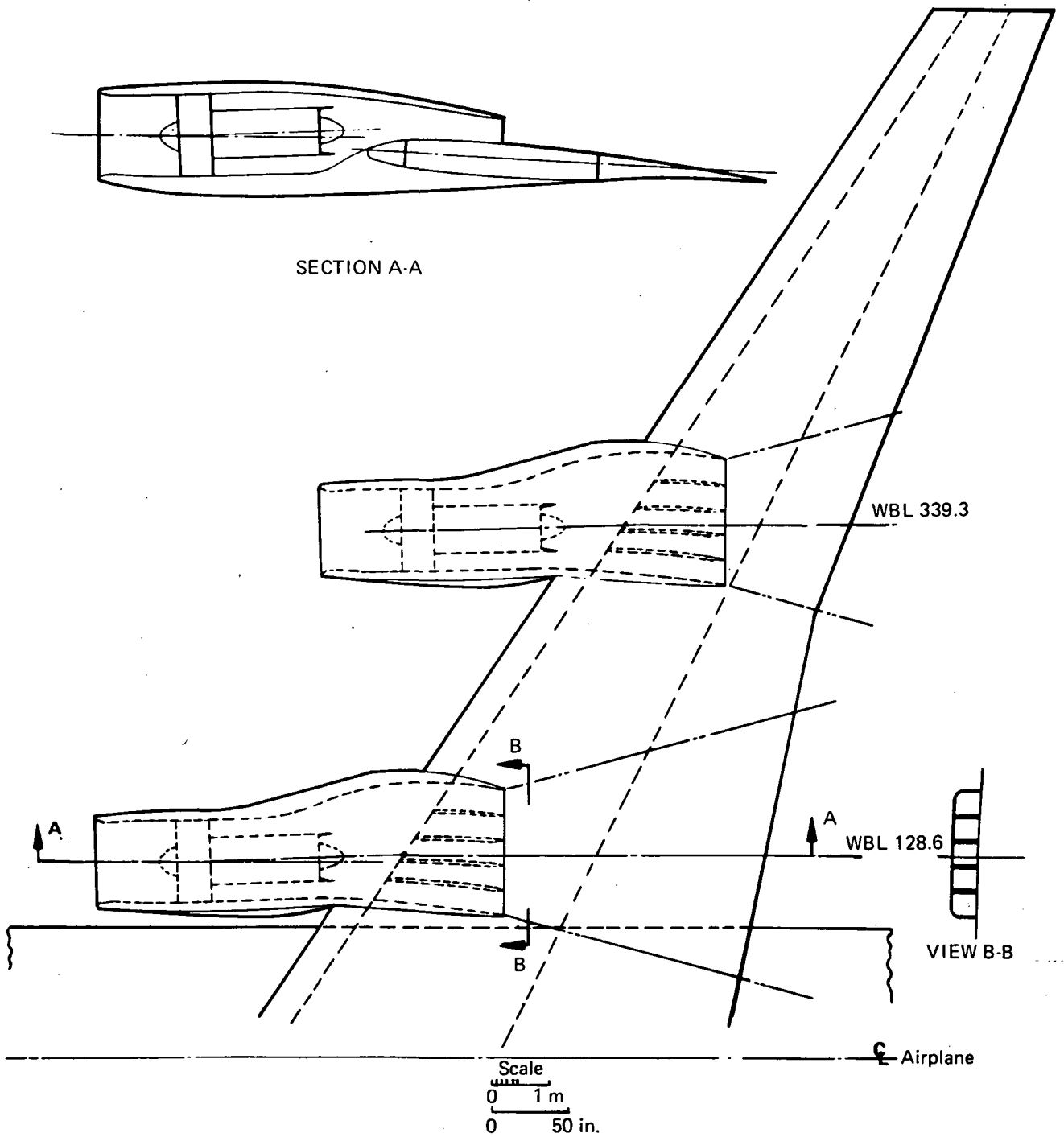


FIGURE 76.—FOUR-ENGINE AIRPLANE, 80 780 N (18 160 LB) ENGINE, BYPASS RATIO = 4, NOZZLE $A=5$, RECTANGULAR OFFSET NOZZLE

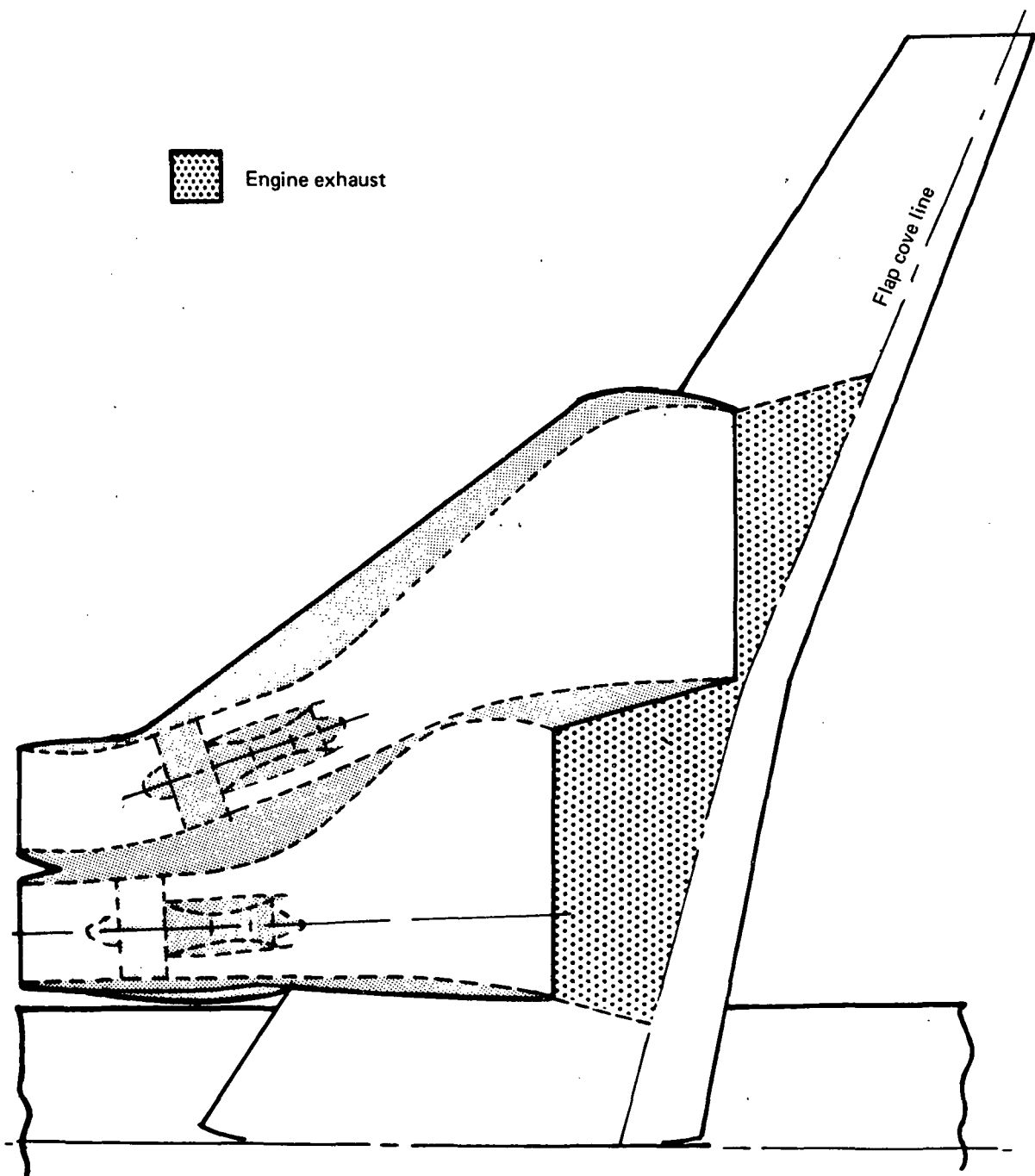


FIGURE 77.—CANDIDATE SPREAD NOZZLE NACELLES FOR FOUR-ENGINE AIRPLANE, CONFIGURATION A

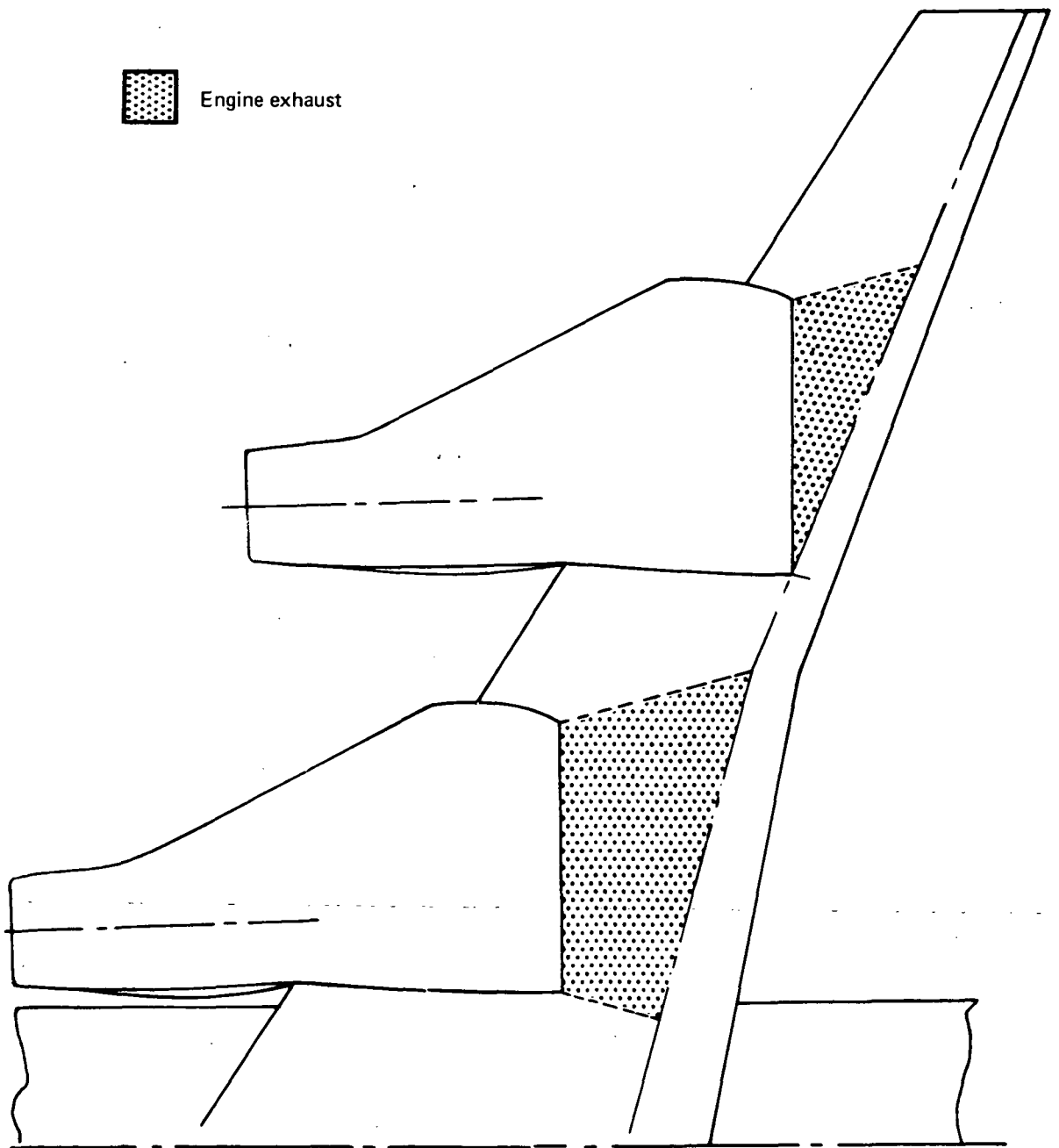


FIGURE 78.—CANDIDATE SPREAD NOZZLE NACELLES FOR FOUR-ENGINE AIRPLANE, CONFIGURATION B

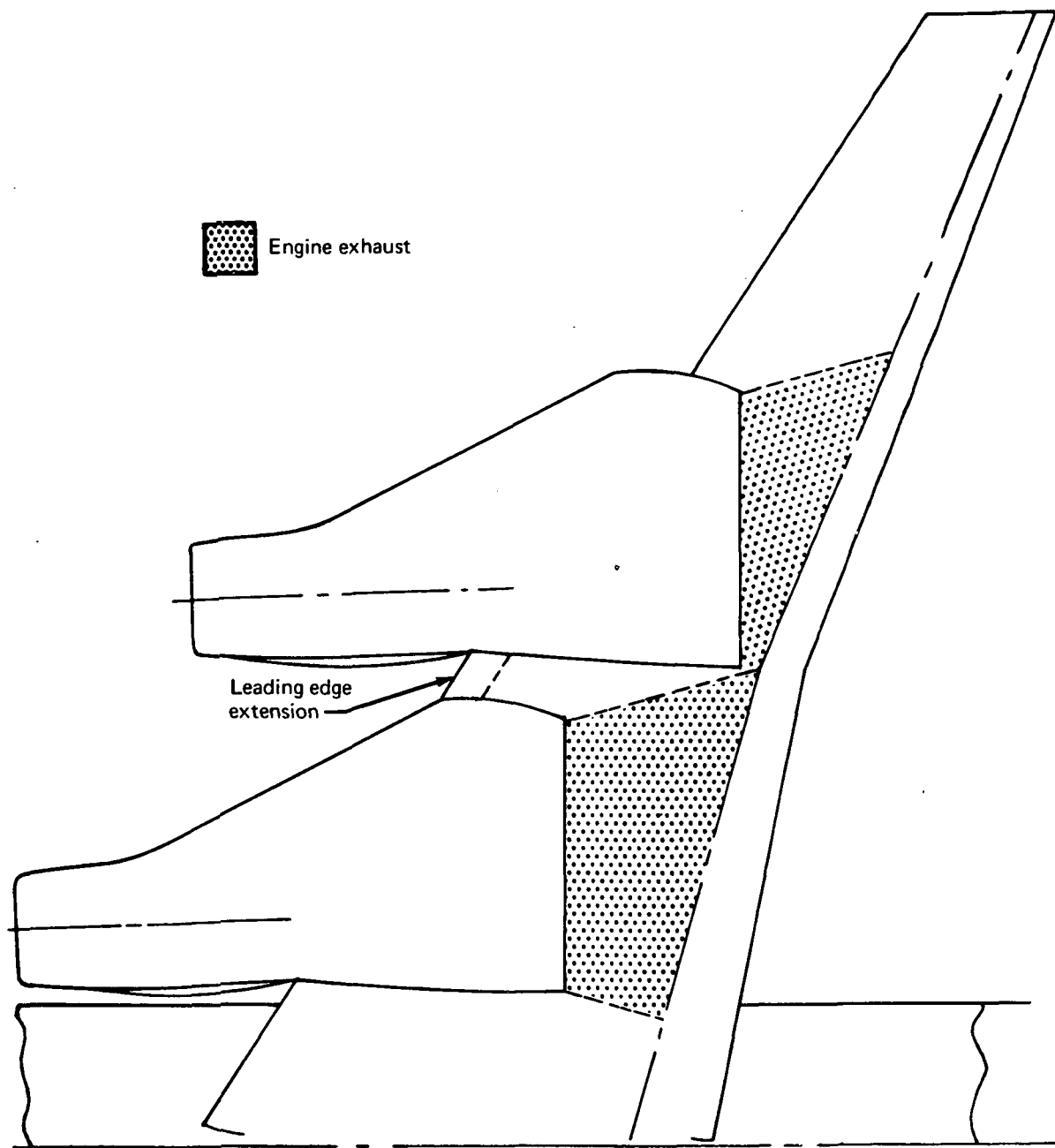


FIGURE 79.—CANDIDATE SPREAD NOZZLE NACELLES FOR FOUR-ENGINE AIRPLANE, CONFIGURATION C

 Engine exhaust

Note: Refer to figure 12 for configuration details

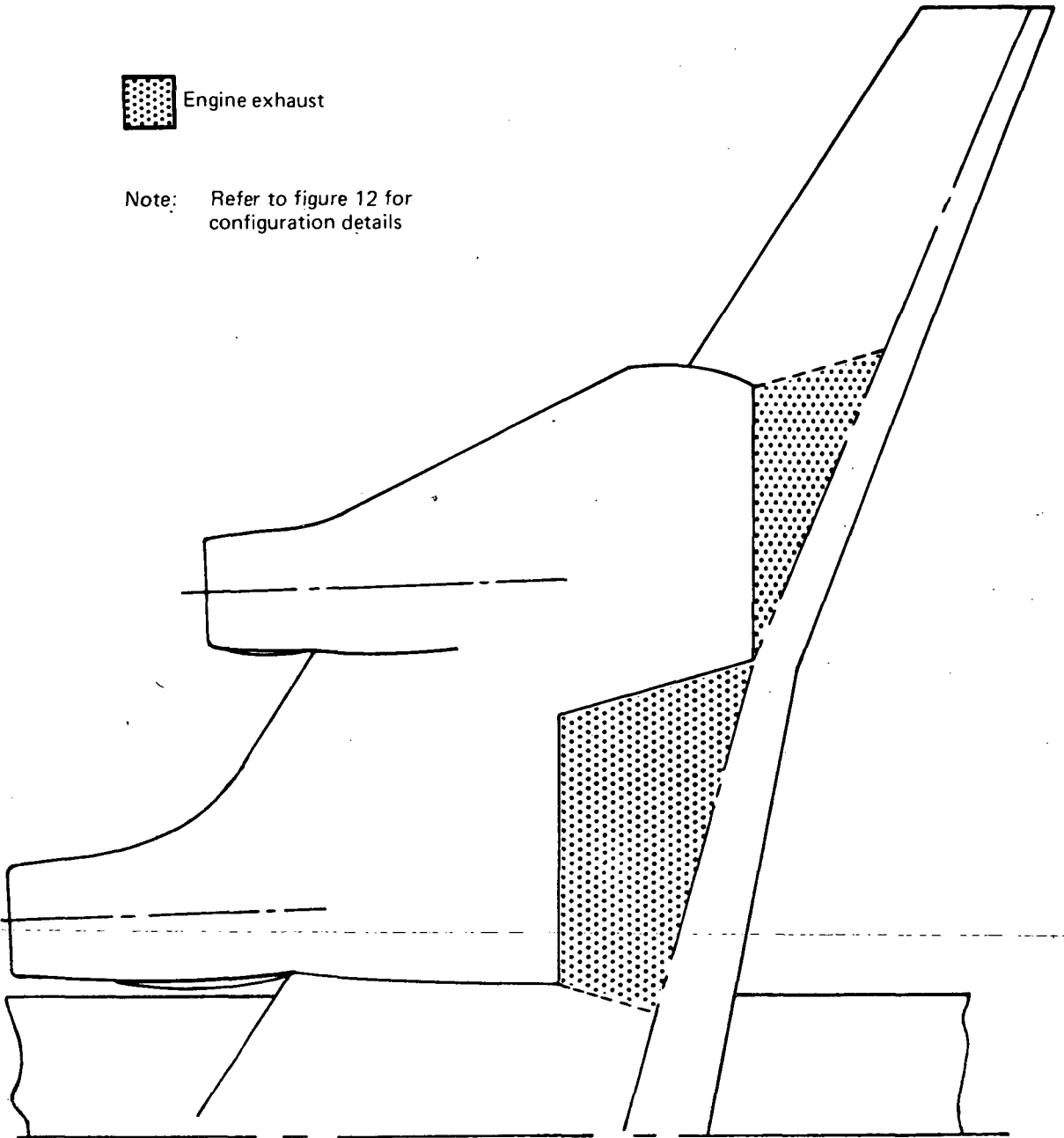


FIGURE 80.—CANDIDATE SPREAD NOZZLE NACELLES FOR FOUR-ENGINE AIRPLANE, CONFIGURATION D

ALTERNATE NO. 1
RELAXED RULE: NO. 1

 Engine exhaust

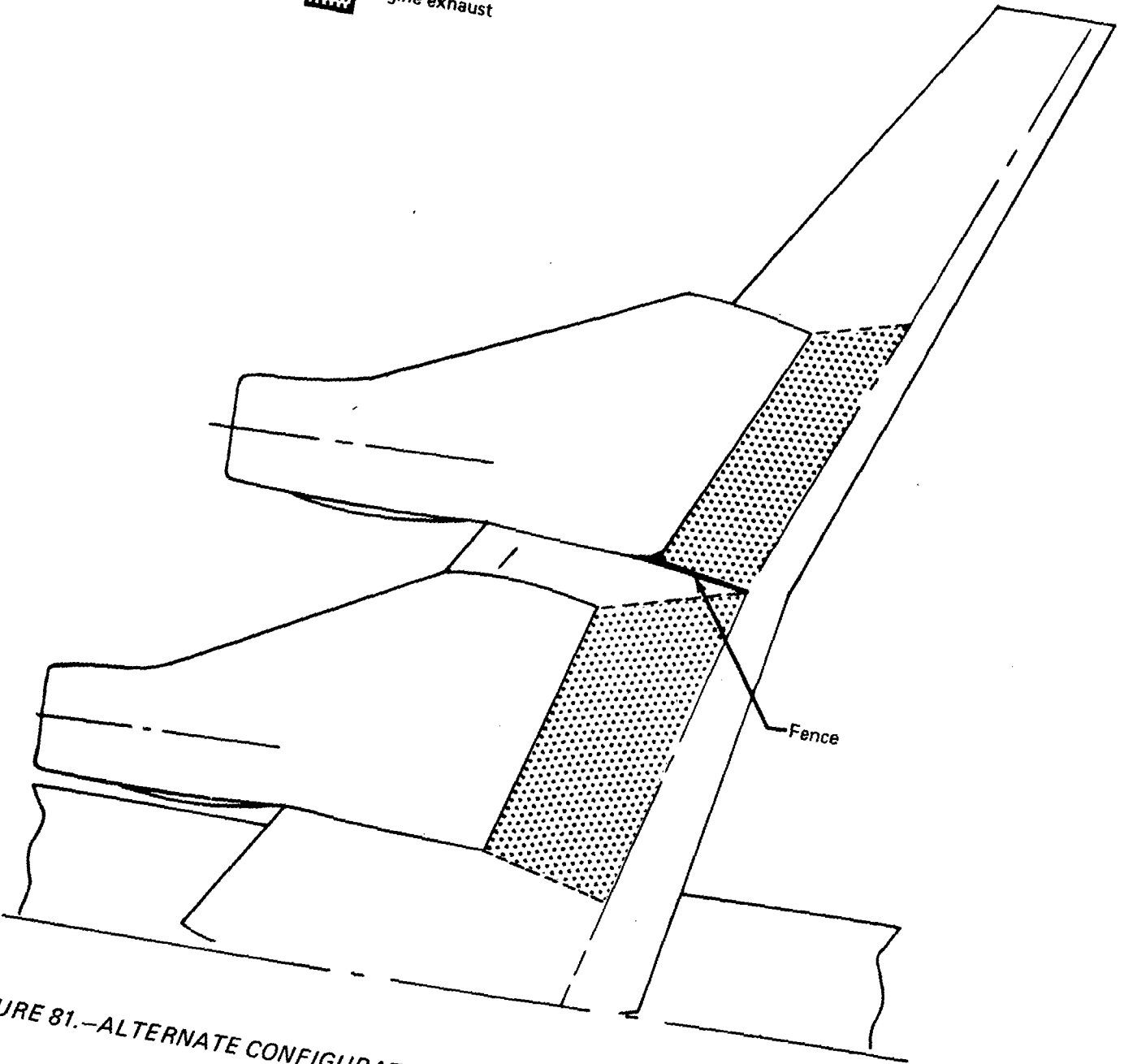


FIGURE 81.—ALTERNATE CONFIGURATION NO. 1, FOUR-ENGINE SPREAD NOZZLE CASE

ALTERNATE NO. 2
RELAXED RULE: NO. 2

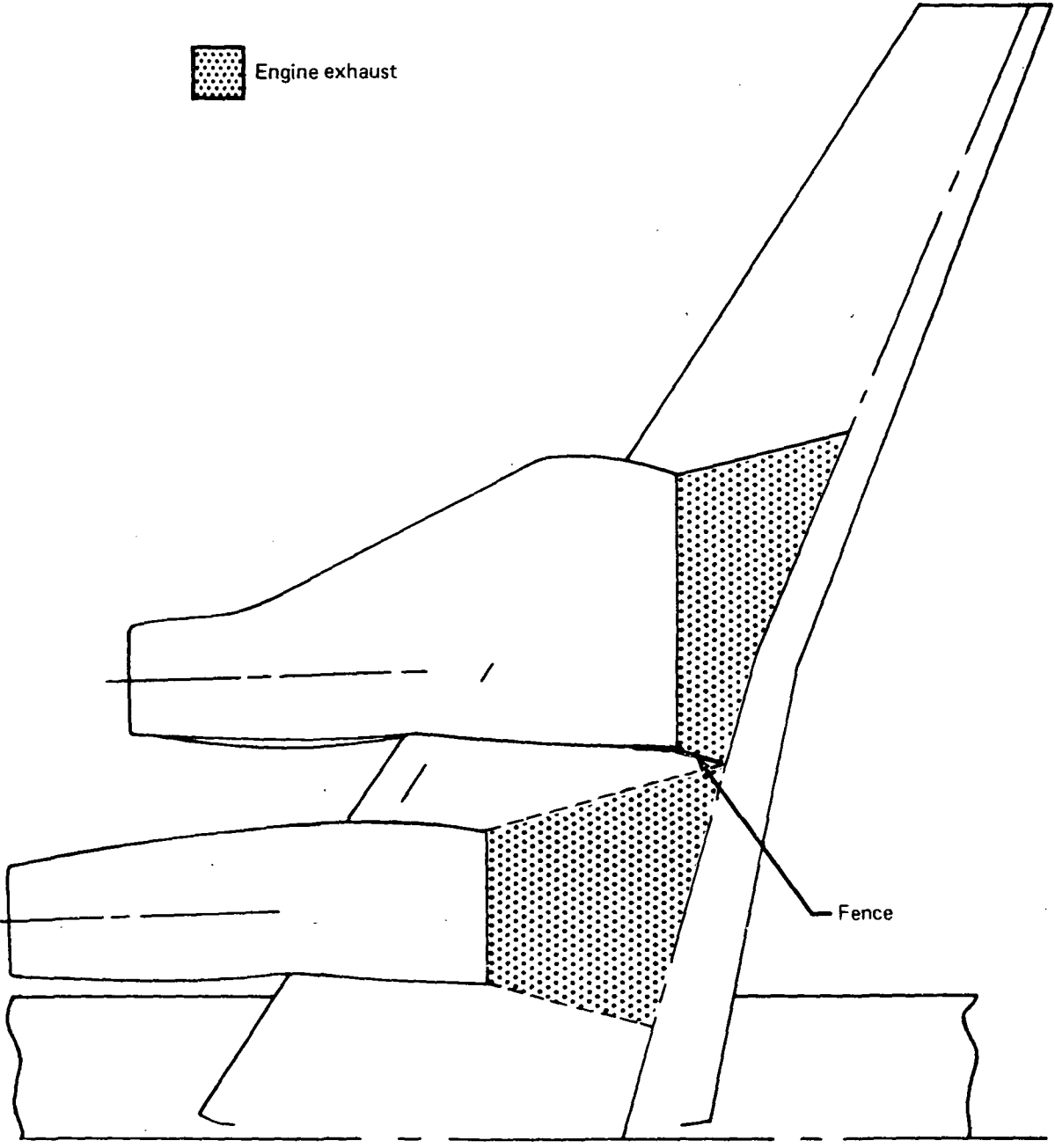


FIGURE 82.—ALTERNATE CONFIGURATION NO. 2, FOUR-ENGINE SPREAD NOZZLE CASE

ALTERNATE NO. 3
RELAXED RULE: NOS. 1 AND 2

 Engine exhaust

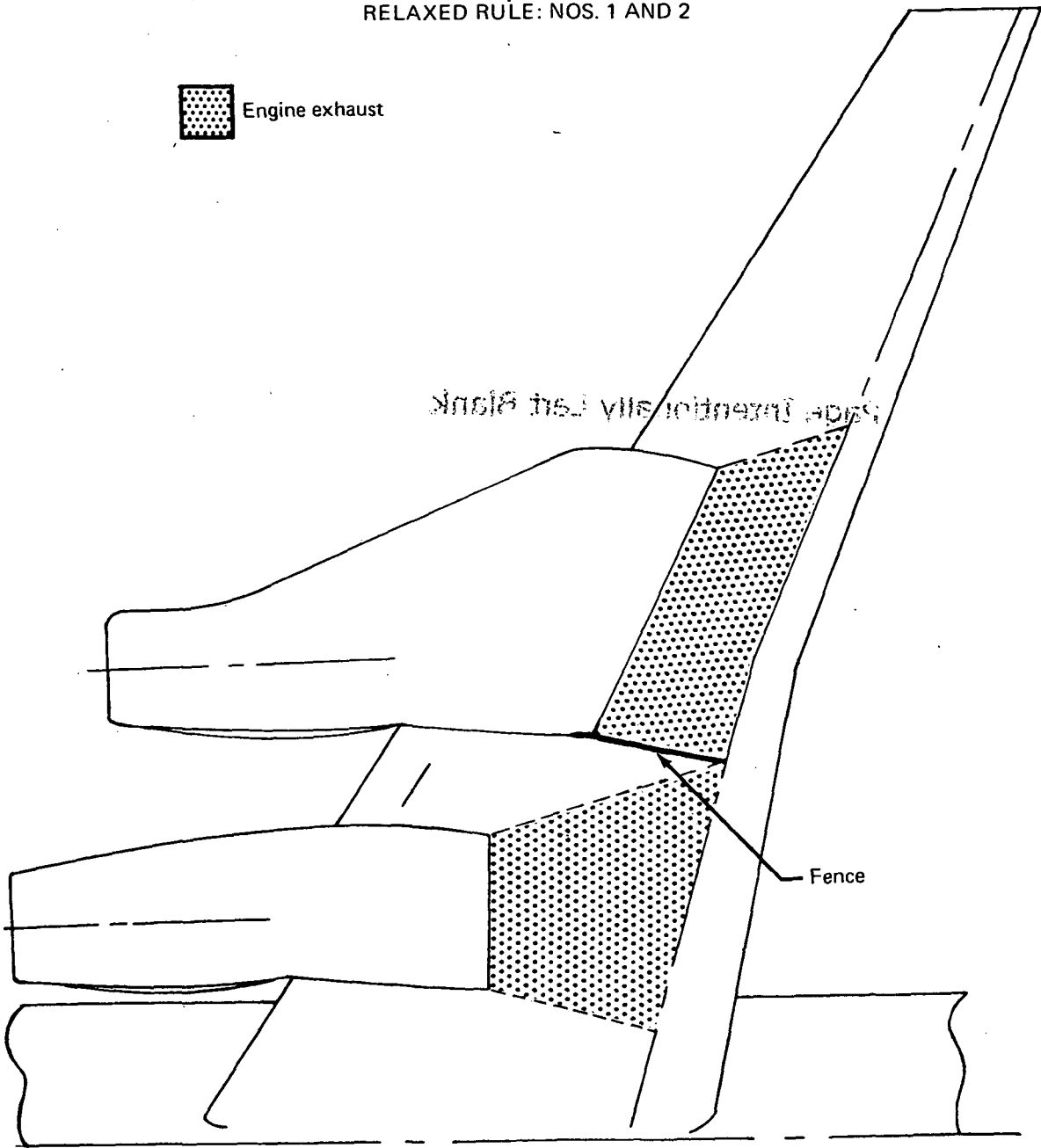


FIGURE 83.—ALTERNATE CONFIGURATION NO. 3, FOUR-ENGINE SPREAD NOZZLE CASE



POSTMASTER: If Undeliverable (Section 158
Postal Manual) Do Not Return

"The aeronautical and space activities of the United States shall be conducted so as to contribute . . . to the expansion of human knowledge of phenomena in the atmosphere and space. The Administration shall provide for the widest practicable and appropriate dissemination of information concerning its activities and the results thereof."

—NATIONAL AERONAUTICS AND SPACE ACT OF 1958

NASA SCIENTIFIC AND TECHNICAL PUBLICATIONS

TECHNICAL REPORTS: Scientific and technical information considered important, complete, and a lasting contribution to existing knowledge.

TECHNICAL NOTES: Information less broad in scope but nevertheless of importance as a contribution to existing knowledge.

TECHNICAL MEMORANDUMS: Information receiving limited distribution because of preliminary data, security classification, or other reasons. Also includes conference proceedings with either limited or unlimited distribution.

CONTRACTOR REPORTS: Scientific and technical information generated under a NASA contract or grant and considered an important contribution to existing knowledge.

TECHNICAL TRANSLATIONS: Information published in a foreign language considered to merit NASA distribution in English.

SPECIAL PUBLICATIONS: Information derived from or of value to NASA activities. Publications include final reports of major projects, monographs, data compilations, handbooks, sourcebooks, and special bibliographies.

TECHNOLOGY UTILIZATION PUBLICATIONS: Information on technology used by NASA that may be of particular interest in commercial and other non-aerospace applications. Publications include Tech. Briefs, Technology Utilization Reports and Technology Surveys.

Details on the availability of these publications may be obtained from:

SCIENTIFIC AND TECHNICAL INFORMATION OFFICE

NATIONAL AERONAUTICS AND SPACE ADMINISTRATION

Washington, D.C. 20546